

See discussions, stats, and author profiles for this publication at: <https://www.researchgate.net/publication/49699461>

# Low Symmetry Phthalocyanines and Their Analogues

ARTICLE *in* CHEMICAL REVIEWS · FEBRUARY 2011

Impact Factor: 46.57 · DOI: 10.1021/cr9003049 · Source: PubMed

---

CITATIONS

125

READS

3,571

## 2 AUTHORS:



John Mack

Rhodes University

98 PUBLICATIONS 2,320 CITATIONS

[SEE PROFILE](#)



Nagao Kobayashi

Tohoku University

529 PUBLICATIONS 11,326 CITATIONS

[SEE PROFILE](#)

# Dye-Sensitized Solar Cells

Anders Hagfeldt,<sup>\*,†,‡,||</sup> Gerrit Boschloo,<sup>†</sup> Licheng Sun,<sup>‡,||</sup> Lars Kloo,<sup>‡</sup> and Henrik Pettersson<sup>†,⊥</sup>

Department of Physical and Analytical Chemistry, Uppsala University, Box 259, SE-751 05 Uppsala, Sweden, Department of Chemistry, KTH - Royal Institute of Technology, Teknikringen 30, SE-100 44 Stockholm, Sweden, State Key Laboratory of Fine Chemicals, DUT-KTH Joint Education and Research Centre on Molecular Devices, Dalian University of Technology (DUT), Dalian 116012, China, and Swerea IVF AB, Box 104, SE-431 22 Mölndal, Sweden

Received October 30, 2009

## Contents

1. Introduction	6596	5.1.2. ZnO	6615
2. Sun, Energy, and Solar Cells	6598	5.1.3. Other Metal Oxides	6616
3. Overview of Performance, Materials, and Operational Principles	6599	5.2. Dyes	6616
4. Operational Principles	6602	5.2.1. Metal Complexes	6617
4.1. Overview of the Different Electron-Transfer Processes	6602	5.2.2. Porphyrins and Phthalocyanines	6620
4.1.1. Reactions 1 and 2: Electron Injection and Excited State Decay	6603	5.2.3. Organic Dyes	6623
4.1.2. Reaction 3: Regeneration of the Oxidized Dyes	6603	5.2.4. The Anchoring of the Dye on the Oxide Surface	6631
4.1.3. Reaction 4: Electron Transport through the Mesoporous Oxide Film	6603	5.2.5. Combining Sensitzers	6632
4.1.4. Reactions 5 and 6: Recombination of Electrons in the Semiconductor with Oxidized Dyes or Electrolyte Species	6603	5.2.6. Summary: Development of Dyes for DSC	6632
4.1.5. Reaction 7: Reduction of Electron Acceptors in the Electrolyte at the Counter Electrode	6603	5.3. Electrolytes and Hole Conductors	6633
4.2. Energetics	6603	5.3.1. Liquid Redox Electrolytes	6633
4.2.1. Energy Levels in Semiconductors	6604	5.3.2. Gel and Polymer Electrolytes	6634
4.2.2. Energy Levels of Redox Systems in Solution	6605	5.3.3. Ionic Liquid Electrolytes	6635
4.2.3. Energy Levels of Excited Molecules	6606	5.3.4. Additives	6636
4.3. Photoinduced Electron Injection vs Direct Recombination - Reactions 1 and 2	6607	5.3.5. Alternative Redox Couples	6636
4.3.1. Electron Injection Studies on Model Systems: Dyes Adsorbed on TiO <sub>2</sub>	6607	5.3.6. Solid Organic Hole Conductors	6637
4.3.2. Injection and DSC Device Efficiency	6608	5.3.7. Inorganic Solid Hole Conductors	6638
4.4. Regeneration of the Oxidized Dyes: Reaction 3	6609	5.4. Surface Passivation of Dye-Sensitized TiO <sub>2</sub>	6638
4.5. Electron Transport in Mesoporous Semiconductor Electrodes: Reaction 4	6610	5.5. Counter Electrodes	6639
4.6. Recombination of Electrons in the Semiconductor with Oxidized Dyes or Electrolyte Species: Reactions 5 and 6	6612	5.5.1. Platinized Conducting Glass	6639
4.7. Transport of the Redox Mediator and Reactions at the Counter Electrode: Reaction 7	6613	5.5.2. Carbon Materials	6639
5. Materials Development	6613	5.5.3. Conducting Polymers	6639
5.1. Nanostructured Metal Oxide Electrodes	6613	5.5.4. Cobalt Sulfide	6639
5.1.1. TiO <sub>2</sub>	6614	5.6. Tandem Cells and p-Type DSCs	6639
* To whom correspondence should be addressed. E-mail: Anders.Hagfeldt@fki.uu.se.		6. Characterization Techniques	6641
† Uppsala University.		6.1. Efficiency Measurements, I–V, IPCE, and APCE	6641
‡ Royal Institute of Technology.		6.2. Electrochemical Methods	6642
Dalian University of Technology (DUT).		6.2.1. Cyclic Voltammetry, Differential Pulse Voltammetry, and Square Wave Voltammetry	6642
⊥ Swerea IVF AB.		6.2.2. Electrochemical Impedance Spectroscopy	6642
		6.2.3. Spectroelectrochemistry	6642
		6.3. Photoelectrochemical Methods	6642
		6.3.1. Electron Transport Measurements	6642
		6.3.2. Electron Lifetime Measurements	6643
		6.3.3. Electron Concentration Measurements	6643
		6.3.4. Measurements of the Electron Quasi-Fermi Level	6644
		6.3.5. Charge Collection Efficiency and Diffusion Length	6644
		6.3.6. Photoinduced Absorption Spectroscopy	6644
		7. Module Development/DSC Modules	6645
		7.1. Module Designs and Performance	6645
		7.1.1. Sandwich Z-Interconnected Modules	6645
		7.1.2. Sandwich W-Interconnected Modules	6645
		7.1.3. Sandwich Current-Collecting Modules	6646

\* To whom correspondence should be addressed. E-mail: Anders.Hagfeldt@fki.uu.se.

† Uppsala University.

‡ Royal Institute of Technology.

|| Dalian University of Technology (DUT).

⊥ Swerea IVF AB.

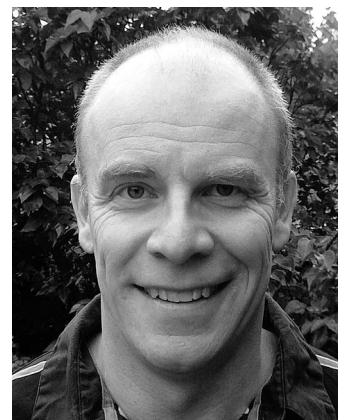
7.1.4. Monolithic Serial-Connection Modules	6647
7.1.5. Monolithic Current-Collecting Modules	6647
7.2. Accelerated and Outdoor Module Testing	6647
7.3. Manufacturing Processes	6648
7.4. Discussion: Future Outlook for the Different DSC Module Designs	6649
8. Future Outlook	6650
9. Acknowledgments	6651
10. Appendix. Content Added after ASAP Publication	6651
11. Note Added after ASAP Publication	6652
12. References	6652

## 1. Introduction

At the end of last century, the possibility to use devices based on molecular components for the construction of a robust large-scale solar electricity production facility seemed utopic. But the seminal paper by O'Regan and Grätzel in 1991<sup>1</sup> spurred researchers to take on the challenge. With the development of dye-sensitized solar cells (DSCs),<sup>2</sup> conventional solid-state photovoltaic technologies are now challenged by devices functioning at a molecular and nanolevel. Record efficiencies of up to 12% for small cells and about 9% for minimodules, promising stability data, passing, for example, the critical 1000 h stability test at 80 °C with a durable efficiency of 8–9%, and means of energy-efficient production methods have been accomplished. The prospect of low-cost investments and fabrication are key features. DSCs perform also relatively better compared with other solar cell technologies under diffuse light conditions and at higher temperatures. DSCs offer the possibilities to design solar cells with a large flexibility in shape, color, and transparency. Integration into different products opens up new commercial opportunities.

Besides the exciting possibilities of using DSCs for solar energy application, the riddles of the device are as thrilling. How does it work? DSCs should according to the photovoltaic textbooks in the early 1990s simply not work. The paradigm was to use highly pure semiconductor materials avoiding defects and interfaces and to rely on a built-in electrical field to separate photogenerated electron–hole pairs. DSCs, in contrast, were based on a huge internal interface prepared in a simple laboratory environment without strict demands on the purity of the materials. It was a mystery how the DSC could work in the absence of a built-in electric field. The initial research developed a relatively simple picture of how DSCs operate, reviewed in this journal in 1995.<sup>3</sup> The basic characteristics and conceptual models, reviewed in several recent articles,<sup>4–11</sup> have been reasonably successful to describe various reactions and interactions. With time, however, the chemical complexity of the DSC device has become more and more evident. The DSC is a good example of a molecular system where the function of the overall device is better than predicted from the sum of the properties of its components.<sup>12</sup> There are complex interactions between the device components, in particular, at the oxide/dye/electrolyte interface, but the interactions also depend on external variables such as solar irradiation, temperature, and device working conditions. Also inherent in the devices are multiscaling properties, both in time and in length, which need to be characterized and handled for the optimization of the overall device performance.

DSC research groups have been established around the world with biggest activities in Europe, Japan, Korea, China,



**Anders Hagfeldt** is professor in Physical Chemistry and the Dean of Chemistry at Uppsala University. He obtained his Ph.D. in 1993 at Uppsala University and was a postdoctoral fellow with Prof. Michael Grätzel (1993–1994) at EPFL, Switzerland. His research focuses on physical chemical characterization of mesoporous electrodes for different types of optoelectronic devices, specifically dye-sensitized solar cells. He has about 200 scientific publications and 8 patent applications. He is a member of the Royal Swedish Academy of Engineering Sciences (IVA), Stockholm, and a visiting professor at the Royal Institute of Technology, Stockholm, at Dalian University of Technology, China, and at the Institute for Materials Research and Engineering in Singapore. He is the director of Center for Molecular Devices.



**Gerrit Boschloo** obtained his Ph.D. in 1996 at Delft University of Technology (The Netherlands). He held postdoctoral positions at University College Dublin (Ireland) with Prof. D. J. Fitzmaurice and at Uppsala University (Sweden) with Prof. Anders Hagfeldt. After a period as a researcher at the Royal Institute of Technology in Stockholm, he currently holds a position as an Associate Professor at the Department of Physical and Analytical Chemistry, Uppsala University. His main research interest is advanced photoelectrochemical characterization of dye-sensitized solar cells and nanostructured semiconductors. He is author of more than 70 peer-reviewed articles.

and Australia. The field is growing fast, which can be illustrated by the fact that about two or three research articles are being published every day. In Figure 1, a simple and limited literature search illustrates the growth of the number of research papers and patents over the last years.

The industrial interest in DSCs is strong with large multinational companies such as BASF, Bosch, and Corus in Europe and Toyota, Sharp, Panasonic, Sony, Fujikura, and Samsung in Asia. A large volume production line has been set up in the company G24i, Wales. Research companies such as Dyesol, Australia, Solaronix, Switzerland, and Peccell, Japan, are expanding, focusing on selling material components and equipment.

The principle of DSCs has also become a part of the core chemistry and energy science teaching and research. Text



**Licheng Sun** obtained his Ph.D. in 1990 in Dalian University of Technology (DUT), China. After postdoctoral stays of one year (1992–1993) with Dr. Helmut Görner in Max-Planck-Institut für Strahlenchemie, Mülheim an der Ruhr, Germany, and two years (1993–1995 as Alexander von Humboldt fellow) with Prof. Dr. Harry Kurreck in Institut für Organische Chemie, Freie Universität Berlin, he went to Stockholm first as an Assistant Professor (1995–1999) in Department of Chemistry, Royal Institute of Technology (KTH), and then Associate Professor (1999–2004) in Department of Organic Chemistry, Stockholm University. He moved back to KTH as a full Professor in Molecular Devices in 2004. He is now also a distinguished professor in DUT. His research interests focus on solar energy conversion at the molecular level including bioinspired systems for catalytic water oxidation and hydrogen production, artificial photosynthesis, dye-sensitized solar cells, supramolecular photochemistry, and light-driven water splitting. He has published more than 200 peer-reviewed papers.



**Henrik Pettersson** is project leader at Swerea IVF AB, a research institute providing applied R&D to bring new technologies and new methods into practical applications. He has been involved in the development of dye-sensitized solar cells for more than 15 years, specializing in module technologies, process methods, up-scaling, and reliability testing. Prior to joining Swerea IVF AB, he worked for Ekologisk Energi AB, one of the first companies to work on dye-sensitized solar cells, and for four years for Professor Michael Grätzel at EPFL in Switzerland.



**Lars Kloo** received his Ph.D. in Inorganic Chemistry at Lund University, Sweden, in 1990 and moved to his current position as Professor in Inorganic Chemistry at the Royal Institute of Technology (KTH) in Stockholm in 1998. During 1991–1995, he was in shorter or longer periods visiting scientist in other laboratories in the U.K., U.S.A., and New Zealand. He has been involved in DSC research for about 10 years with a main focus on electrolytes, in particular ionic liquids, and more recently the electrolyte–electrode interaction. Apart from photoelectrochemical solar cells, his research interests also embrace fundamental aspects of inorganic synthesis, cluster chemistry, and computational biological chemistry.

books have sections or chapters dealing with DSC.<sup>13,14</sup> Laboratory kits have been developed for educational purposes under the slogan “make your own solar cell”. Not only energy science but also photochemistry, photoelectrochemistry, materials science, and transition metal coordination chemistry have significantly benefitted from DSC research.

The challenge to review the DSC research field is the speed of publications of new research data. With the risk of missing or leaving out interesting work, as well as studies of

importance for the development of the field, we aim to cover the DSC research in a broad sense. We will, however, limit ourselves to sensitization by molecular dyes and will not discuss sensitization by semiconductor quantum dots. This topic was recently reviewed elsewhere.<sup>15,16</sup>

After some brief notes on solar energy in general and DSC in particular (sections 2 and 3), we go through the operational

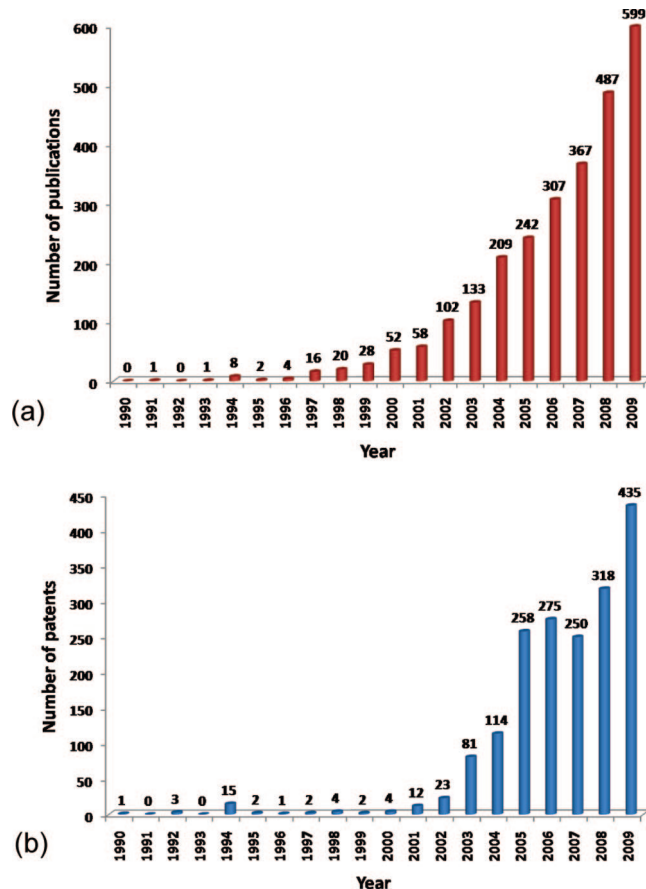


**Figure 1.** Number of publications published per year obtained from a simple and limited literature search using the keywords “dye-sensitized” and “solar”: (a) number of research articles (data source, ISI Web of Knowledge); (b) number of patent families (data source, esp@cenet).

principles of DSC (energetics and kinetics) in section 4. The development of material components is treated in section 5 and some specific experimental techniques to characterize DSC in the following section. Section 7 deals with the current status of module development, and finally we end up with a brief future outlook.

## 2. Sun, Energy, and Solar Cells

It is clear that access to economically viable renewable energy sources is essential for the development of a globally sustainable society. The mean global energy consumption rate was 13 TW in the year 2000. Assuming a kind of “business-as-usual” scenario with rather optimistic but reasonable assumptions of population growth and energy consumption, the projection is 28 TW in 2050 for the global energy demand.<sup>17,18</sup> Solar energy, besides fusion, has the largest potential to satisfy the future global need for renewable energy sources.<sup>19</sup> From the  $1.7 \times 10^5$  TW of solar energy that strikes the earth’s surface, a practical terrestrial global solar potential value is estimated to be about 600 TW. Thus, using 10% efficient solar farms, about 60 TW of power could be supplied.

The sun emits light with a range of wavelengths from the ultraviolet and visible to the infrared. It peaks in the visible, resembling the spectrum of a blackbody at a temperature of 5760 K. It is, however, influenced by atmospheric absorption and the position of the sun. Ultraviolet light is filtered out by ozone, and water and CO<sub>2</sub> absorb mainly in the infrared making dips in the solar spectrum at 900, 1100, 1400, and 1900 nm (H<sub>2</sub>O) and at 1800 and 2600 nm (CO<sub>2</sub>). When skies are clear, the maximum radiation strikes the earth’s surface when the sun is directly overhead, having the shortest path length through the atmosphere. The path length is called the *air mass* (AM) and can be approximated by  $AM = 1/\cos \varphi$ , where  $\varphi$  is the angle of elevation of the sun. The standard solar spectrum used for efficiency measurements of solar cells is AM 1.5 G (global), giving that  $\varphi = 42^\circ$ . This spectrum is normalized so that the integrated irradiance (the amount of radiant energy received from the sun per unit area per unit time) is 1000 W m<sup>-2</sup>. The irradiance varies depending on the position of the sun, orientation of the Earth, and sky conditions. One also distinguishes sunlight in direct or diffuse light. The direct component can be concentrated, which increases the solar cell efficiency by increasing cell voltage outputs. Diffuse light arises by scattering of the sunlight in the atmosphere. This fraction is around 15% on average<sup>20</sup> but larger at higher latitudes and in regions with a significant amount of cloud cover. Materials with rough surfaces such as DSCs are relatively better suited for diffuse light than perfectly flat surfaces and are less sensitive to movements of the sun.

The AM 1.5 G solar radiation spectrum can be found from different sources.<sup>21</sup> The spectrum is shown in Figure 2 as the irradiance of the sun as a function of wavelength.

In the diagram, we also indicate the maximum current (short-circuit condition) for a solar cell device converting all incident photons below the absorption onset wavelength into electric current (see ref 22). For example, the maximum short-circuit current ( $J_{sc}$ ) for a solar cell with an absorption onset of 800 nm is 26 mA cm<sup>-2</sup>. The overall solar-to-electrical energy conversion efficiency,  $\eta$ , for a solar cell is given by the photocurrent density measured at short-circuit

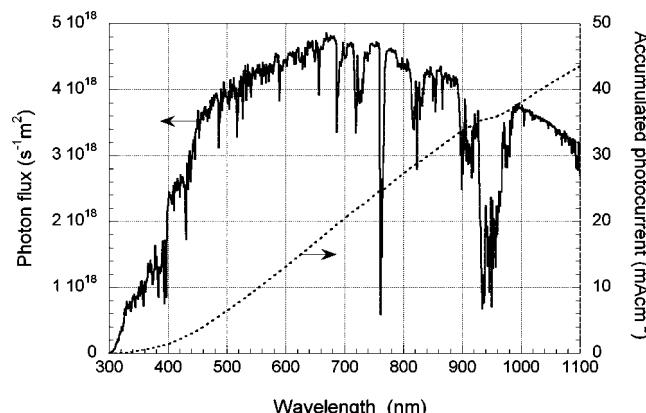


**Figure 2.** Photon flux of the AM 1.5 G spectrum at 1000 W m<sup>-2</sup> (ASTM G173-03), and calculated accumulated photocurrent.

( $J_{sc}$ ), the open-circuit photovoltage ( $V_{oc}$ ), the fill factor of the cell (FF), and the intensity of the incident light ( $P_{in}$ ).

$$\eta = \frac{J_{sc} V_{oc} FF}{P_{in}} \quad (1)$$

The fill factor can assume values between 0 and less than 1 and is defined by the ratio of the maximum power ( $P_{max}$ ) of the solar cell per unit area divided by the  $V_{oc}$  and  $J_{sc}$  according to

$$FF = P_{max}/(J_{sc} V_{oc}) \quad (2)$$

The maximum power is obtained as the product of the photocurrent and photovoltage at the voltage where the power output of the cell is maximal. Another fundamental measurement of the performance of a solar cell is the “external quantum efficiency”, which in the DSC community is normally called the incident photon to current conversion efficiency (IPCE). The IPCE value corresponds to the photocurrent density produced in the external circuit under monochromatic illumination of the cell divided by the photon flux that strikes the cell. From such an experiment the IPCE as a function of wavelength can be calculated from

$$IPCE = \frac{J_{sc}(\lambda)}{e\Phi(\lambda)} = 1240 \frac{J_{sc}(\lambda) [\text{A cm}^{-2}]}{\lambda [\text{nm}] P_{in}(\lambda) [\text{W cm}^{-2}]} \quad (3)$$

where  $e$  is the elementary charge. IPCE values provide practical information about the monochromatic quantum efficiencies of a solar cell.

Solar cell production has grown at about 30% per annum over the past 15 years. The conventional solar cells of today, the first generation solar cells, are based on silicon. The estimated total installed capacity in 2007 was 7.8 GW.<sup>23,24</sup> Most of this was grid-connected with a price of around \$7 per peak Watt (W<sub>p</sub>). A selling price of \$2/W<sub>p</sub>, which would correspond to a production cost of about \$0.5/W<sub>p</sub>, would make PV competitive with electricity production from fossil fuels. Additional 2.26 GW was installed in 2007 alone (a 50% increase over the preceding year) and 90% of that was installed in four countries: Germany, Spain, Japan, and the U.S.A. In 2008, the worldwide photovoltaic installations increased by 6.0 GW. However, the photovoltaic (PV) industry is largely dependent on governmental subsidies. Silicon-based systems make up around 90% of the current PV market. The production cost is presently around \$3/W<sub>p</sub>.

but is highly dependent on the price of the silicon material. China is now the world leader in producing crystalline silicon (c-Si) based PV cells and modules with a capacity of over 2.3 GW/year. The International Energy Agency (IEA) have estimated the energy payback time of c-Si PV modules, incorporated as a grid-connected roof-top installation, as between 1.5 and 2 years.<sup>25</sup>

The second generation solar cells, for example, amorphous silicon, CIGS, and CdTe, are based on thin film technologies. They are becoming a competitive class of PVs, doubling production from 2006 to 2007. The advantages of thin film solar cells include the ease of manufacture permitting a reduction of the production cost to about \$1/W<sub>p</sub>, a wider range of applications with attractive appearance, and possibilities of using flexible substrates. The most established thin-film technology is amorphous silicon (a-Si).<sup>26</sup> The efficiencies are lower than c-Si, but it has other advantages such as a lower temperature coefficient for power loss. The cost is only slightly lower than that of c-Si mainly because of expensive manufacturing equipment. After an initial efficiency loss, the so-called Staebler–Wronski effect, stable laboratory efficiencies of 13.5% and module efficiencies around 5–6% have been achieved. For CdTe laboratory efficiencies of 16.7% and module efficiencies of 10.9% have been reported. The company First Solar has announced a production cost below \$1/W<sub>p</sub> for their CdTe solar modules. The drawbacks include the toxicity and low abundance of the materials, temperature-dependent efficiencies, and only an average light tolerance. Nonetheless, CdTe is a highly interesting technology for future PVs. Another such technology is CIGS (copper indium gallium diselenide). CIGS systems are capable of high efficiencies (19.9% in the lab,<sup>27</sup> 16.7% in submodules,<sup>28</sup> and 13.5% in modules.<sup>29</sup> They are very durable, and the materials cost can be kept low even though indium is rare. Since the bandgap can be tuned, they are also suitable for tandem cells. Several plants with 10–50 MW capacity are now installed globally.

Both first and second generation solar cells are based on single junction devices. Calculated thermodynamic efficiency limits in single junction solar cells (31%) assume that absorption of an individual photon results in the formation of a single electron–hole pair and that all photon energy in excess of the energy gap is lost as heat. This so-called Shockley–Queisser limit can be overcome by the use of various types of so-called third generation solar cell devices.<sup>30</sup> In principle, sunlight can be converted to electricity at an efficiency close to the Carnot limit of 95%. Various schemes to achieve efficiencies above 31% include tandem cells, hot carrier cells, multiexciton generation, multiband cells, and thermophotovoltaics.<sup>30</sup> The goal for the third generation solar cells is to deliver electricity at a large scale competitive price, that is, less than \$0.5/W<sub>p</sub>. This means very effective solar cells that are produced by techniques that permit facile mass production. The impact on economics if such concepts could be implemented would be enormous, making PVs one of the cheapest options for future energy production.

DSC can be considered to be a technology between the second and third generation solar cells. It has the potential to become a third generation technology utilizing the nanoscale properties of the device. In the present stage, the technology offers the following selling points:

- low production cost and particularly interesting much lower investment costs compared with conventional PV technologies

- design opportunities, such as, transparency and multi-color options (building integration, consumer products, etc.)
- flexibility
- lightweight
- feedstock availability to reach terawatt scale
- short energy payback time (<1 year)
- enhanced performance under real outdoor conditions (relatively better than competitors at diffuse light and higher temperatures)
- bifacial cells capture light from all angles
- outperforms competitors for indoor applications

### 3. Overview of Performance, Materials, and Operational Principles

The “Bob Beaman like”-increase in efficiency for DSC type solar cells reported in the famous 1991 *Nature* paper by O’Regan and Grätzel was bewildering. The use of a mesoporous semiconductor electrode with a high internal surface area led to a paradigm shift in the fields of photoelectrochemistry and photovoltaics in general. Attempts to develop dye-sensitized photoelectrochemical cells had been made before,<sup>5,31–33</sup> but the basic problem was the belief that only smooth semiconductor surfaces could be used. The light-harvesting efficiency for a monomolecular layer of dye sensitizer, even for phthalocyanines and porphyrins, which have among the highest extinction coefficients known, absorb far less than 1% of the AM 1.5 G spectrum.<sup>34</sup> Attempts to harvest more light by using multilayers of dyes were in general unsuccessful. Indications of the possibilities to increase the roughness of the semiconductor surface so that a larger number of dyes could be adsorbed directly to the surface and simultaneously be in direct contact with a redox electrolyte had also been reported before 1991. For example, Matsumura et al.<sup>35</sup> and Alonso et al.<sup>36</sup> used sintered ZnO electrodes to increase the efficiency of sensitization by rose bengal and related dyes. But the conversion yields from solar light to electricity remained well below 1% for these systems. In addition, the dyes used in these systems were unstable. Grätzel, Augustynski, and co-workers presented results on dye-sensitized fractal-type TiO<sub>2</sub> electrodes with high surface area in 1985.<sup>37</sup> For DSC, there was an order-of-magnitude increase when O’Regan and Grätzel in 1991 reported efficiencies of 7–8%.<sup>1</sup> With regards to stability, a turnover number of  $5 \times 10^6$  was measured for the sensitizer (a trimeric ruthenium complex<sup>38,39</sup>). This was followed up by the introduction of the famous N3 dye (structure **2** in Table 1) giving efficiencies around 10%.<sup>40</sup>

Since the initial work in the beginning of the 1990s, a wealth of DSC components and configurations have been developed. Perhaps a key concept for the future success of DSC in this regard is “diversity”. At present, several thousands of dyes have been investigated, as well as hundreds of electrolyte systems and numerous types of mesoporous films with different morphologies and compositions. Whereas nature has over billions of years developed highly sophisticated molecular systems that give life on earth, chemists are at present facing the intriguing challenge of developing technologies based on complex molecular interactions that can assist in keeping the earth livable. Such technologies are expected to progress rapidly, be it through design of new materials based on fundamental insights or by statistical, combinatorial approaches. For DSC at present, in the official table of world record efficiencies for solar cells, the record

**Table 1. Collection of Some Representative Ru-Complex Photosensitizers**

Dye	Structure	Dye	Structure	Dye	Structure	Dye	Structure
1		2(N3)		21		22	
3		4(N719)		23		24	
5		6(Z907)		25		26	
7		8		27		28(C101)	
9		10		29		30	
11		12		31		32	
13		14		33(C103)		34(JK56)	
15		16(K9)		35		36	
17		18		37		38	
19		20		39		40	

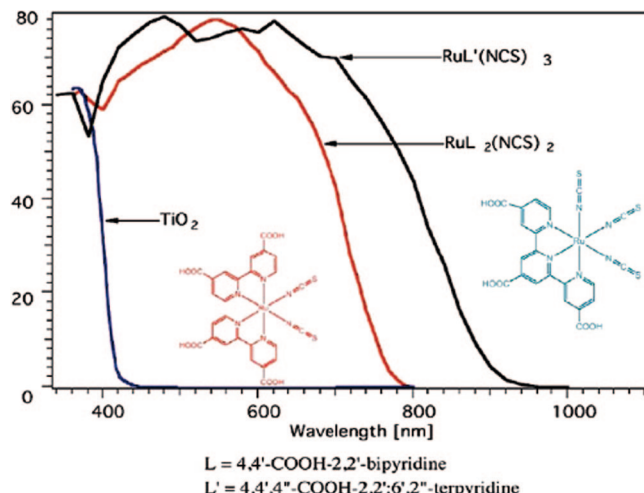


**Figure 3.** Incident photon to current conversion efficiency as a function of the wavelength for the standard ruthenium sensitizers N3 (red line), the black dye N749 (black curve), and the blank nanocrystalline TiO<sub>2</sub> film (blue curve). The chemical structures of the sensitizers are shown as insets. Reprinted with permission from ref 22. Copyright 2009 American Chemical Society.

is held by the Sharp company in Japan at  $10.4\% \pm 0.3\%$ .<sup>41</sup> A criterion to qualify for these tables is that the solar cell area is at least  $1\text{ cm}^2$ . For smaller cells, a certified conversion efficiency of 11.1% has been reached using the black dye as sensitizer.<sup>42</sup>

Early on in DSC research, the classical dyes N3 and its salt analogue N719 (structure 4 in Table 1) and the black dye (N749, structure 3 in Table 1) were developed. The certified record efficiencies are obtained with these dyes, and their IPCE spectra are shown together with the molecular structures of the dyes in Figure 3.<sup>22</sup> The IPCE values are close to 80% for both sensitizers across the visible part of the solar spectrum. The N3 dye starts to absorb light at around 800 nm, whereas the photocurrent onset is red-shifted for the black dye to 900 nm. As seen from Figure 3, however, the IPCE increases only gradually from the absorption onset to shorter wavelengths due to relatively low extinction coefficients of these sensitizers.

There is thus much to be gained by developing sensitizers with high extinction coefficients particularly in the near-IR region of the solar spectrum. The highest photocurrent densities of the black dye under AM 1.5 G condition is close to  $21\text{ mA cm}^{-2}$ ,<sup>42,43</sup> which can be compared with the theoretical maximum photocurrent of  $33\text{ mA cm}^{-2}$  from Figure 2 for a dye with an absorption threshold of 900 nm. Improving the solar light absorption in the 650–950 nm domain (note the dip in the solar irradiance spectrum at 950 nm, Figure 2) would then be one of the main directions to take aiming for DSC efficiencies above 15%. The other direction is to increase the photovoltage by replacing the conventionally used  $\text{I}^-/\text{I}_3^-$  redox couple with a system having a more positive redox potential. These are key challenges facing present DSC research and will be further discussed below.

During the last 2–3 years, the advent of heteroleptic ruthenium complexes furnished with an antenna function has taken the performance of the DSC to a new level. Two examples of these dyes are Z991 and C101, structures 21 and 28, respectively, in Table 1. Compared with the classical DSC Ru dyes, their extinction coefficients are higher and the spectral response is shifted to the red. The solar cell

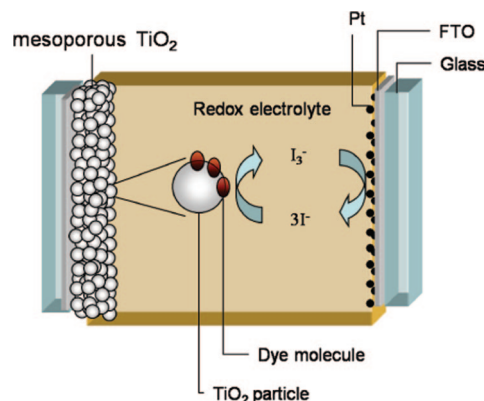


**Figure 4.** Schematic overview of a dye-sensitized solar cell.

efficiency of these types of sensitizers has increased continuously over the last 2 years, and at present efficiencies of 12% have been reported.<sup>22</sup> There are sometimes arguments that DSCs have not developed much since the breakthrough in the early 1990s. The record efficiencies reached a plateau at 10–11%, and the most efficient devices have remained essentially unchanged from its original concepts. It is, however, a complex system. The realization of the need to handle complexities with the plethora of material components to explore make the 12% efficiency now reached with one of the new classes of dyes a strong indicator for further progress in efficiency performance. Another essential performance indicator is long-term stability. Here, the progress during the last 15 years has been steady, and accelerated durability tests have been passed with higher and higher efficiencies. Most of the earlier work has been reviewed.<sup>44–46</sup> As an example of recent results, the C101 sensitizer maintains outstanding stability at efficiency levels over 9% under light soaking at  $60^\circ\text{C}$  for more than 1000 h.<sup>47</sup> This is achieved by the molecular engineering of the sensitizer but also very importantly by the use of robust and nonvolatile electrolytes, such as ionic liquids, and adequate sealing materials. Good results on overall system endurance have been reported for several years, and these results are presently being confirmed under real outdoor conditions. Because of the direct relevance to the manufacturing of commercial products, little work is published on these issues, and it is, for example, difficult to find information on processing issues, as well as sealing materials and methods. The industrial development and commercialization of DSCs was the topic of the DSC-IC 3 conference in Nara, Japan, April 2009. Many encouraging results were presented giving confidence that the DSCs can match the stability requirements needed to sustain outdoor operation for many years. Still, many research and development activities need to be performed, and in particular, more data on outdoor field tests is required. One important research topic is to develop protocols for accelerated long-term stability tests relevant to DSC technologies.

A schematic of the interior of a DSC showing the principle of how the device operates is shown in Figure 4.

The typical basic configuration is as follows: At the heart of the device is the mesoporous oxide layer composed of a network of TiO<sub>2</sub> nanoparticles that have been sintered together to establish electronic conduction. Typically, the film thickness is ca.  $10\text{ }\mu\text{m}$  and the nanoparticle size 10–30 nm in diameter. The porosity is 50–60%. The mesoporous layer is deposited on a transparent conducting oxide (TCO) on a

glass or plastic substrate. The most commonly used substrate is glass coated with fluorine-doped tin oxide (FTO). Attached to the surface of the nanocrystalline film is a monolayer of the charge-transfer dye. Photoexcitation of the latter results in the injection of an electron into the conduction band of the oxide, leaving the dye in its oxidized state. The dye is restored to its ground state by electron transfer from the electrolyte, usually an organic solvent containing the iodide/triiodide redox system. The regeneration of the sensitizer by iodide intercepts the recapture of the conduction band electron by the oxidized dye. The  $I_3^-$  ions formed by oxidation of  $I^-$  diffuse a short distance ( $<50\ \mu m$ ) through the electrolyte to the cathode, which is coated with a thin layer of platinum catalyst, where the regenerative cycle is completed by electron transfer to reduce  $I_3^-$  to  $I^-$ . To have some numbers for typical materials and relative concentrations of the different species in the mesoporous system under normal working conditions (1 sun illumination), we refer to the recent paper by O'Regan and Durrant.<sup>11</sup>

- Under working conditions there are about 10 electrons per  $TiO_2$  particle.
- More than 90% of electrons in  $TiO_2$  are trapped and <10% in the conduction band.
- There are  $\sim 10\,000$  adsorption sites for  $H^+$  on an 18 nm (diameter)  $TiO_2$  particle.
- A  $TiO_2$  particle (18 nm) has  $\sim 600$  dye molecules on the surface.
- Each dye molecule absorbs a photon once per second.
- The flux of electron injection into the  $TiO_2$  particle is  $\sim 600\ s^{-1}$ .
- Under working conditions, about 1 dye per 150  $TiO_2$  particles is in its oxidized state.
- The total volume fraction of the solutes in the electrolyte is  $\sim 10-20\%$ .
- In the pore volume around the  $TiO_2$  particle, there will be  $\sim 1000\ I^-$  and  $200\ I_3^-$  ions.
- The concentration of iodine,  $I_2$ , is  $<1\ \mu M$ , that is, about one free iodine per 10 000  $TiO_2$  particles.

For a DSC cell to be durable for more than 15 years outdoors, the required turnover number is  $10^8$ , which may be satisfied by the ruthenium complexes mentioned above.<sup>48</sup> The voltage generated under illumination corresponds to the difference between electrochemical potential of the electron at the two contacts, which generally for DSC is the difference between the Fermi level of the mesoporous  $TiO_2$  layer and the redox potential of the electrolyte. Overall, electric power is generated without permanent chemical transformation.

The basic electron transfer processes in a DSC, as well as the potentials for a state-of-the-art device based on the N3 dye adsorbed on  $TiO_2$  and  $I^-/I_3^-$  as redox couple in the electrolyte, are shown in Figure 5.

Besides the desired pathway of the electron transfer processes (processes 2, 3, 4, and 7) described above, the loss reactions 1, 5, and 6 are indicated. Reaction 1 is direct recombination of the excited dye reflected by the excited state lifetime. Recombination of injected electrons in the  $TiO_2$  with either oxidized dyes or acceptors in the electrolyte is numbered as 5 and 6, respectively. In principle, electron transfer to  $I_3^-$  can occur either at the interface between the nanocrystalline oxide and the electrolyte or at areas of the anode contact (usually a fluorine-doped tin oxide layer on glass) that are exposed to the electrolyte. In practice, the second route can be suppressed by using a compact blocking layer of oxide deposited on the anode by spray pyrolysis.<sup>49,50</sup>

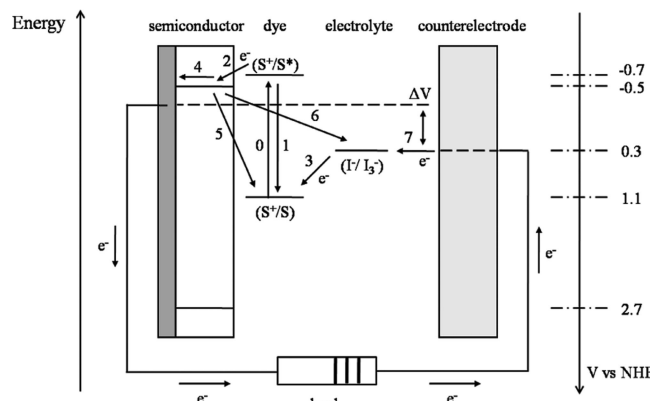


**Figure 5.** Simple energy level diagram for a DSC. The basic electron transfer processes are indicated by numbers (1–7). The potentials for a DSC based on the N3 dye,  $TiO_2$ , and the  $I^-/I_3^-$  redox couple are shown.

Blocking layers are necessary for DSCs that utilize one-electron redox systems such as cobalt complexes<sup>51–53</sup> or for cells using solid organic hole-conducting media.<sup>54,55</sup>

As mentioned above, hundreds of alternatives to the components used in conventional DSCs have been investigated. As for the sensitizers, Ru-complexes have since the early days given the best results. These dyes have recently been reviewed by Robertson.<sup>56</sup> Osmium and iron complexes and other classes of organometallic compounds such as phthalocyanines and porphyrins have also been developed. Metal-free organic dyes are catching up, showing efficiencies close to 10% with the use of indoline dyes.<sup>57,58</sup> Moreover, chemically robust organic dyes showing promising stability results have recently been developed by several groups.<sup>59–62</sup> Organic dyes for DSCs have been reviewed by Bäuerle and co-workers.<sup>63</sup> With regards to the hole-conducting medium, electrolytes based on the  $I^-/I_3^-$  redox couple have been the preferred choice. Organic nitrile-based solvents give the highest efficiencies, whereas gelification of the solvent or ionic liquids is used for the best stability, compromising somewhat the efficiency. However, the  $I^-/I_3^-$  couple is not necessarily unique. Successful results have also been achieved with other redox systems such as cobalt-based systems,<sup>52</sup>  $SCN^-/(SCN)_3^-$  and  $SeCN^-/(SeCN)_3^-$ ,<sup>64–66</sup> and organic systems based on TEMPO<sup>67</sup> and TDP.<sup>68</sup> Interesting development has been made for solid-state DSCs using organic hole conductors<sup>69</sup> and inorganic p-type semiconductors such as  $CuI$ <sup>70</sup> and  $CuSCN$ .<sup>71</sup> Recent overviews for photoanode materials are found in refs 72–74. The preferred oxides are so far  $TiO_2$ ,  $ZnO$ ,  $SnO_2$ , and  $Nb_2O_5$ . Different morphologies based on nanoparticles, nanofibers and tubes, and core–shell structures have been developed. In this review, we will overview works on  $TiO_2$  and  $ZnO$ . Different counter electrode (cathode) materials will also be reviewed. The most common counter electrode is a platinized conducting glass, but also carbon materials and conducting polymers have been developed.

#### 4. Operational Principles

##### 4.1. Overview of the Different Electron-Transfer Processes

The much simplified picture of the energetics and kinetics for a working DSC device that emerged in the early research<sup>3</sup>

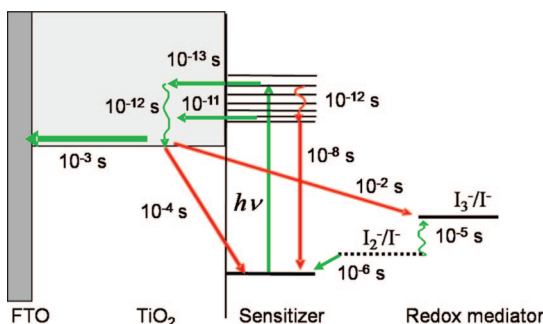


**Figure 6.** Overview of processes and typical time constants under working conditions (1 sun) in a Ru-dye-sensitized solar cell with iodide/triiodide electrolyte. Recombination processes are indicated by red arrows.

is still useful as an introduction of working principles. The chemical complexity of the device must, however, be understood and mastered to improve our ability to identify predictive materials and optimized structure/function relationships.<sup>11</sup> The present level of understanding of the energetics and kinetics is discussed in the following sections. The reader is also referred to the article by Ardo and Meyer<sup>7</sup> for a recent review.

Our starting point is the simplified picture for which typical energetic data were presented in Figure 5. With reference to the different reactions in Figure 5, the kinetic data for the different electron transfer processes taking place at the oxide/dye/electrolyte interface for state-of-the-art DSCs are summarized in Figure 6.

#### 4.1.1. Reactions 1 and 2: Electron Injection and Excited State Decay

One of the most astounding findings in DSC research is the ultrafast injection from the excited Ru-complex in the  $\text{TiO}_2$  conduction band, reaction 2. Although the detailed mechanism of the injection process is still under debate, it is generally accepted that a fast femtosecond component is observed for this type of sensitizer directly attached to an oxide surface.<sup>75–78</sup> For DSC device performance, the time scales of the injection process should be compared with decay of the excited state of the dye to the ground state, reaction 1. This is given by the excited state lifetime of the dye, which for typical Ru-complexes used in DSCs is 20–60 ns.<sup>4</sup> Interestingly, Durrant and co-workers have observed a much slower electron injection in a *complete* DSC device with halftimes around 150 ps. This would then be slow enough for kinetic competition between electron injection and excited state decay of the dye with potential implications for the overall DSC performance.<sup>79</sup>

#### 4.1.2. Reaction 3: Regeneration of the Oxidized Dyes

The interception of the oxidized dye by the electron donor, normally  $\text{I}^-$ , is in the microsecond time domain. For a turnover number, that is, the cycle life of the sensitizer in the DSC device, to be above  $10^8$ , which is required for a DSC lifetime of 20 years in outdoor conditions, the lifetime of the oxidized dye must be >100 s if the regeneration time is 1  $\mu\text{s}$ . This is achieved by the best-performing Ru-complexes.<sup>80</sup>

#### 4.1.3. Reaction 4: Electron Transport through the Mesoporous Oxide Film

When the dye-sensitized mesoporous solar cell was first presented, perhaps the most puzzling phenomenon was the highly efficient charge transport through the nanocrystalline  $\text{TiO}_2$  layer. The mesoporous electrodes are very much different compared with their compact analogues because (i) the inherent conductivity of the film is very low, (ii) the small size of the individual colloidal particles does not support a built-in electrical field, and (iii) the oxide particles and the electrolyte-containing pores form interpenetrating networks whose phase boundaries produce a junction of huge contact area. These films may be viewed as an ensemble of individual particles through which electrons can percolate by hopping from one crystallite to the next. The charge transport mechanisms in DSC are still under keen debate today. How are the electrons moving? What and where are the traps? These are some of the questions being discussed.

#### 4.1.4. Reactions 5 and 6: Recombination of Electrons in the Semiconductor with Oxidized Dyes or Electrolyte Species

The kinetics of the back-electron-transfer reaction from the conduction band to the oxidized sensitizer follow a multiexponential time law, occurring on a microsecond to millisecond time scale depending on electron concentration in the semiconductor and thus the light intensity.

Recombination of electrons in  $\text{TiO}_2$  with acceptors in the electrolyte is normally referred to as the electron lifetime. Lifetimes observed with the  $\text{I}^-/\text{I}_3^-$  are very long (1–20 ms under one sun light intensity) compared with other redox systems used in DSC, explaining the success of this redox couple.

#### 4.1.5. Reaction 7: Reduction of Electron Acceptors in the Electrolyte at the Counter Electrode

Counter electrodes for DSCs with  $\text{I}^-/\text{I}_3^-$  electrolytes can be rather easily prepared by deposition of a thin catalytic layer of platinum onto a conducting glass substrate. Best performance and long-term stability has been achieved with nanoscale Pt clusters. Charge transfer resistances of less than  $1 \Omega \text{ cm}^2$  can be achieved.<sup>81</sup>

### 4.2. Energetics

The positions of the energy levels at the oxide/dye/electrolyte interface are fundamentally important to the function of the DSC. This is conventionally drawn as a simplified schematic energy level diagram as in Figure 5. Standard measurements of energy levels for semiconductors, redox couples, and dyes in solutions or adsorbed to surfaces can be found in many textbooks, for example, see refs 13 and 82, and will not be described in this section. In chapter 6 we review specific electrochemical and spectroelectrochemical experiments within the DSC *tool-box* approach, that is, to obtain data of the energy levels at the oxide/dye/electrolyte interface from *in situ* measurements.

Care needs to be taken in using an energy level diagram like the one depicted in Figure 5 for interpretation and analyses of the actual energetic situation in a DSC. The indicated values may be taken from measurements of the individual components, excluding effects due to adsorption

of the dye and electrolyte species to the oxide surface. The ordinate in Figure 5 may present internal energy and not free energy. The charge carriers have significant configurational entropy arising from the number of accessible energy states, which can be very different in the different phases. Sometimes the energy levels of the dye are reported as HOMO/LUMO levels, obtained, for example, from electronic structure calculations, which involve several approximations.

Figure 5 also represents an “interface” between physics and chemistry. In solid-state physics and electrochemistry, one normally uses the energy scale with vacuum as reference for the former and the potential scale with the standard hydrogen electrode (SHE) or normal hydrogen electrode (NHE) as reference for the latter. The electrochemical potential of electrons in a semiconductor is normally referred to in energy as the Fermi level,  $E_F$ , and in an electrolyte solution, it is often referred to in potential as the redox potential,  $U_{\text{redox}}$ . At equilibrium, the electrochemical potentials (or the Fermi levels) of the semiconductor and electrolyte will be equal. The difference of the potential of the NHE versus an electron in vacuum cannot be measured with thermodynamic rigor,<sup>82</sup> but an estimate is given in ref 13 relating the energy,  $E_{F,\text{redox}}$ , and the potential,  $U_{\text{redox}}$ , of any redox couple by

$$E_{F,\text{redox}} [\text{eV}] = -(4.6 \pm 0.1) - eU_{\text{redox}} [\text{V}] \quad (4)$$

where  $e$  is the elementary charge. With this value, the standard potentials of other redox couples can be expressed on the absolute scale.

#### 4.2.1. Energy Levels in Semiconductors

In nondegenerate semiconductors, the equilibrium Fermi level is given by

$$E_F = E_c + k_B T \ln \left( \frac{n_c}{N_c} \right) \quad (5)$$

where  $E_c$  is the energy at the conduction band edge,  $k_B T$  is the thermal energy,  $n_c$  is the density of conduction band electrons, and  $N_c$  is the effective density of conduction band states. With respect to vacuum,  $E_c$  is given by the electron affinity  $E_A$ .

However, these values are very sensitive to the environment, and measurements of absolute and relative energies in vacuum must be carefully interpreted and analyzed in terms of their relevance to DSCs. In the field of semiconductor electrochemistry, the standard approach of determining the so-called flatband potential of a semiconductor,  $U_{fb}$ , which estimates the work function of the semiconductor in contact with the specific electrolyte, is Mott–Schottky analysis of capacitance data.<sup>13</sup> This approach is based on the potential-dependent capacitance of a depletion layer at the semiconductor surface. For a DSC such behavior is not expected to be observed for the ~20 nm anatase nanocrystals that are expected to be fully depleted; see ref 4 and references therein. Instead, cyclic voltammetry and spectroelectrochemical procedures have been used to estimate  $E_c$ . These methods also give information of the density of states (DOS) of the semiconductor.

For a recent review on the measurements of  $E_c$  and the density of states in mesoporous TiO<sub>2</sub> films, see ref 7. Fitzmaurice reviewed the first spectroelectrochemical mea-

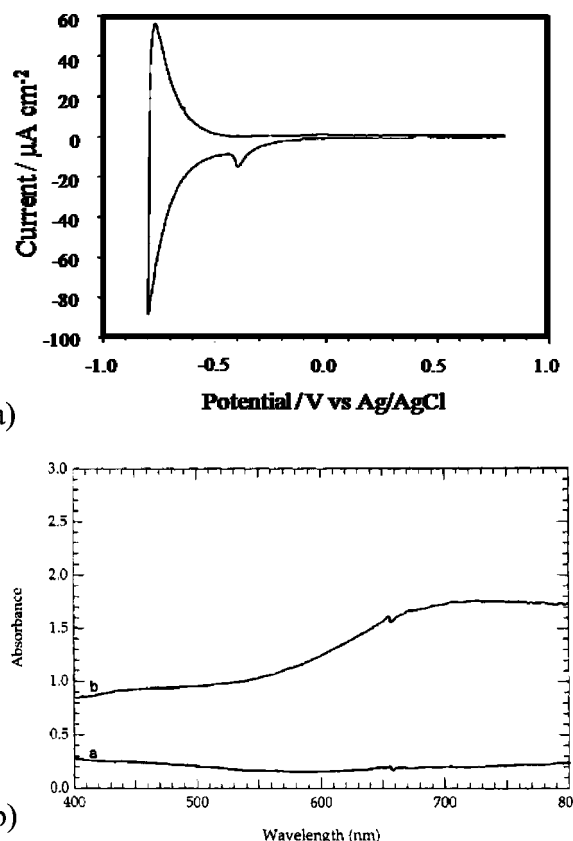


**Figure 7.** (a) Cyclic voltammogram of a nanostructured TiO<sub>2</sub> electrode in aqueous LiClO<sub>4</sub> (0.2 M), pH 6.2. Scan rate 5 mV s<sup>-1</sup>. Reprinted with permission from ref 84. Copyright 1999 American Chemical Society. (b) Spectroelectrochemistry of lithium ion insertion in a mesoporous TiO<sub>2</sub> electrode. The UV-vis spectrum changes during electrochromic switching from essentially colorless at a reverse bias of -0.64 V vs Ag/AgCl (sat. KCl in water) to an intense blue color following Li<sup>+</sup> insertion at a forward bias of -1.64 V. Reprinted with permission from ref 3. Copyright 1995 American Chemical Society.

surements of  $E_c$  for transparent mesoporous TiO<sub>2</sub> electrodes.<sup>83</sup> Using an accumulation-layer model to describe the potential distribution within the TiO<sub>2</sub> nanoparticle at negative potentials and assuming that  $E_c$  remains fixed as the Fermi level is raised into accumulation conditions, Fitzmaurice and co-workers estimated  $E_c$  values in organic and aqueous electrolytes. At present, there is an extensive compilation of data that shows that  $E_c$  is not that well-defined. Many electrochemical and spectroelectrochemical studies indicate that mesoporous TiO<sub>2</sub> films possess a tailing of the DOS (trap states) rather than an abrupt onset from an ideal  $E_c$ . Nevertheless, the  $E_c$  values estimated in the early work by Fitzmaurice and co-workers are still used today to, at least qualitatively, discuss, for example, the energy level matching between the conduction band edge of the oxide and the excited state of the dye.

The cyclic voltammogram of a mesoporous TiO<sub>2</sub> film in an aqueous electrolyte is shown in Figure 7a.<sup>84</sup>

The large reversible peak was indicative of filling and emptying the TiO<sub>2</sub> DOS, whereas the smaller cathodic prepeak was assigned to the filling of deep trap states. Thus, cyclic voltammetry with the use of a reference electrode gives us indications of the position of the energy levels in the semiconductor, although determination of, for example,  $E_c$ , estimated from the onset of the cathodic current, is rather inaccurate. The electrons in the TiO<sub>2</sub> inferred from electro-

chemical measurements have spectroscopic signatures as well. Because the band gap energy of anatase  $\text{TiO}_2$  is 3.2 eV, its ground state UV-vis absorption spectrum shows a threshold at 385 nm. At a reverse bias applied to the mesoporous  $\text{TiO}_2$  in a spectroelectrochemical cell, there will thus be essentially no coloration in the visible part of the spectrum. The example in Figure 7b is reprinted from an early work of lithium ion insertion studies of mesoporous  $\text{TiO}_2$  for electrochromic applications.<sup>85</sup> The small attenuation of light at this potential ( $-0.64$  V vs  $\text{Ag}/\text{AgCl}$ ) is due to light scattering. Changing the potential to  $-1.64$  V in a stepwise fashion leads to intercalation of  $\text{Li}^+$  and the appearance of an intensely dark blue coloration ( $\text{Ti}^{3+}$  states) as shown in Figure 7b.

In the original work of Fitzmaurice and co-workers,<sup>83</sup> the  $E_c$  of  $\text{TiO}_2$  was estimated from the absorption changes as a function of applied potential in the same way as that shown in Figure 7b. The electrons in the mesoporous  $\text{TiO}_2$  film, in the conduction band, or in trap states, have been studied to a great extent since the early work in the beginning of the 1990s. For further reading on the different experimental and theoretical methods applied for these investigations and on the electronic and optical properties of electrons in  $\text{TiO}_2$ , the reader is referred to ref 7 and references therein. Spectroelectrochemical studies as described above have also been applied to other mesoporous semiconductor electrodes such as  $\text{ZnO}$ <sup>86,87</sup> and  $\text{NiO}$ .<sup>88</sup> It can be noted that, based on the studies described above, mesoporous  $\text{TiO}_2$  films have been developed for electrochromic display applications using surface-attached viologens as chromophores<sup>89</sup> and for secondary  $\text{Li}^+$  batteries.<sup>90,91</sup>

The position of the conduction band edge depends in the first place on surface charge and in the second on adsorbed dipolar molecules. The pH dependence of  $E_c$  for mesoporous  $\text{TiO}_2$  films in aqueous solutions follows a Nernstian behavior with a shift of 59 meV/pH unit due to protonation/deprotonation of surface titanol groups on  $\text{TiO}_2$ ; see refs 7 and 92 and references therein. In nonaqueous solutions,  $E_c$  can be widely tuned by the presence of cations. This effect is greatest with cations possessing a large charge-to-radius ratio. For example,  $E_c$  has been reported to be  $-0.8$  V vs NHE in 0.1 M  $\text{LiClO}_4$  acetonitrile electrolyte and approximately  $-1.8$  V when  $\text{Li}^+$  was replaced by  $\text{TBA}^+$ .<sup>93</sup> This large variation can be explained by surface adsorption of the cation or insertion processes into the anatase lattice being coupled to electron accumulation.<sup>7</sup> This cation-dependent shift in  $E_c$  is used to promote photoinduced electron injection from the surface-bound sensitizer. For this to occur,  $E_c$  must be at a lower energy than the excited state of the sensitizer,  $E_{\text{F},\text{redox}}^*(\text{S}^*/\text{S}^+)$ . In contrast, one would like  $E_c$  to be at as high energy as possible to achieve a high photovoltage, see Figure 5. Thus, there is a compromise for the position of  $E_c$  in order to attain an efficient electron injection while maintaining a high photovoltage. Additives in the electrolyte are normally used to fine-tune the energy level matching of  $E_c$  and  $E_{\text{F},\text{redox}}^*(\text{S}^*/\text{S}^+)$ . The effect of the additive, most often 4-*tert*-butylpyridine (TBP) is used, can be studied by measuring shifts of  $E_c$  depending on surface charge and by measuring the electron lifetime. The shift of  $E_c$  is measured by charge extraction methods as described in detail in section 6.3.3. The determination of electron lifetimes is presented in section 6.3.2.

Addition of TBP to the redox electrolyte gives a significant improvement of DSC efficiencies, mainly because of an

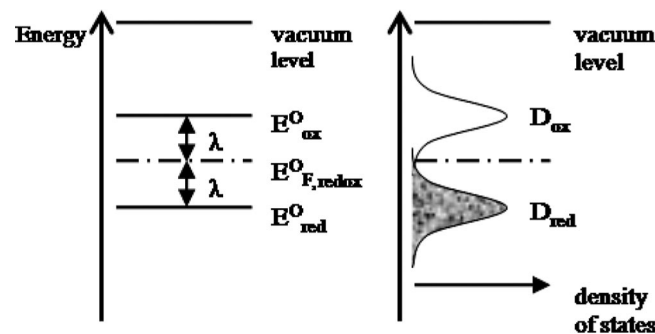


**Figure 8.** (a) Electron energies of a redox system using vacuum as a reference level.  $E_{\text{red}}^0$  = occupied states,  $E_{\text{ox}}^0$  = empty states,  $E_{\text{F},\text{redox}}^0$  = Fermi level of the redox couple. (b) Corresponding distribution functions. Adapted from ref 95, Copyright 1985, with permission from Elsevier.

increase in the open-circuit photovoltage,  $V_{\text{oc}}$ . In ref 94,  $V_{\text{oc}}$  increased by 0.26 V on addition of 0.5 M TBP in the electrolyte. Through analyses of charge extraction and electron lifetime data, it was concluded that  $E_c$  is shifted 0.16 eV toward higher energies with the addition of TBP. The additional 0.1 V was attributed to longer lifetimes of the  $\text{TiO}_2$  electrons, and thus higher concentration, under open-circuit conditions.

#### 4.2.2. Energy Levels of Redox Systems in Solution

The electrochemical potential of electrons, or the redox potential or Fermi level, for a one-electron redox couple is given by the Nernst equation and can be written in the energy scale as<sup>95</sup>

$$E_{\text{F},\text{redox}} = E_{\text{F},\text{redox}}^0 - k_B T \ln \left( \frac{c_{\text{ox}}}{c_{\text{red}}} \right) \quad (6)$$

where  $E_{\text{F},\text{redox}}^0$  is the formal redox energy including nonideality effects,  $c_{\text{ox}}$  and  $c_{\text{red}}$  are the concentrations of the oxidized and reduced species of the redox system, and  $k_B$  is the Boltzmann constant. Besides the Fermi energy, we also need a description of the energy states being empty or occupied by electrons. The electronic energies of a redox system are shown in Figure 8 and are based on the fluctuating energy level model originally developed by Marcus<sup>96</sup> and applied to the semiconductor/electrolyte interface by Gerischer.<sup>13,97,98</sup>

In this energy scale,  $E_{\text{red}}^0$  corresponds to the energy position of occupied electron states and  $E_{\text{ox}}^0$  to the empty states. They differ from the Fermi level,  $E_{\text{F},\text{redox}}^0$  by the so-called reorganization energy,  $\lambda$ . The reorganization energy is the energy involved in the relaxation process of the solvation shell around the reduced species following transfer of an electron to the vacuum level. For the reverse process, that is, electron transfer from vacuum to the oxidized species, there is an analogous relaxation process. It is normally assumed that  $\lambda$  is equal for both processes. The electron states of a redox system are not discrete energy levels but are distributed over a certain energy range due to fluctuations in the solvation shell surrounding the molecule. This is indicated by the distribution of energy states around  $E_{\text{red}}^0$  and  $E_{\text{ox}}^0$ , Figure 8b.  $D_{\text{red}}$  is the density of occupied states (in relative units) represented by the reduced component of the redox system, and  $D_{\text{ox}}$  is the density of empty states represented by the oxidized component. Assuming a harmonic oscillation of the solvation shell, the distribution curves,  $D_{\text{red}}$  and  $D_{\text{ox}}$ , are described by Gaussian functions:

$$D_{\text{red}} = D_{\text{red}}^0 \exp \left[ -\frac{(E - E_{\text{F,redox}}^0 - \lambda)^2}{4k_B T \lambda} \right] \quad (7)$$

$$D_{\text{ox}} = D_{\text{ox}}^0 \exp \left[ -\frac{(E - E_{\text{F,redox}}^0 + \lambda)^2}{4k_B T \lambda} \right] \quad (8)$$

$D_{\text{red}}^0$  and  $D_{\text{ox}}^0$  are normalizing factors such that  $\int_{-\infty}^{\infty} D(E) dE = 1$ . The half-width of the distribution curves is given by

$$\Delta E_{1/2} = 0.53\lambda^{1/2} \text{ eV} \quad (9)$$

Accordingly, the widths of the distribution function depend on the reorganization energy, which is of importance for the kinetics of electron transfer processes at the oxide/dye/electrolyte interface. Typical values of  $\lambda$  are in the range from a few tenths of an electronvolt up to 2 eV. In Figure 8b, the concentration of reduced and oxidized species are equal ( $D_{\text{red}} = D_{\text{ox}}$ ). Changing the concentration ratio varies the Fermi level of the redox couple ( $E_{\text{F,redox}}^0$ ) according to the Nernst equation, which can be graphically illustrated as different amplitudes of the distribution functions.

The energy levels at the dye/oxide interface can be measured using photoelectron spectroscopy. The valence level spectra from unsensitized, as well as sensitized, nanostructured TiO<sub>2</sub> electrodes can be directly derived from such measurements. Figure 9 shows the density of states in the valence region for derivatized nanostructured TiO<sub>2</sub> films using the organic D5 dye (structure 123 in Table 5), the N3 and N719 dyes, and the black dye.<sup>99,100</sup> The HOMO orbitals of the complexes can clearly be distinguished above the valence band edge of the semiconductor. Their positions fit well with the energy requirements for efficient electron regeneration. Comparing the HOMO energy level of the dyes, we note that the D5 dye is about 0.2 eV lower than N3 and N719, which are another 0.2 eV lower compared with the black dye.

#### 4.2.3. Energy Levels of Excited Molecules

Reduction of a sensitizer molecule, S, occurs by electron transfer from an electron donor to an unoccupied level of S giving the reduction potential of the molecule with a Fermi level in the energy scale  $E_{\text{F,redox}}^0(S^-/S)$ . Oxidation of S occurs by an electron transfer from the lower lying occupied state to a suitable acceptor molecule. The Fermi level of the oxidation potential of S is  $E_{\text{F,redox}}^0(S/S^+)$ . The energy difference between these two redox levels can only roughly be taken as the difference of the lowest unoccupied (LUMO) and highest occupied (HOMO) states in the molecule. An excited sensitizer is more easily reduced or oxidized, because of the excitation energy  $\Delta E^*$  stored in the molecule.

The Fermi levels of excited molecules can be estimated by adding or subtracting  $\Delta E^*$  from the redox energy level of the molecule in the ground state. The stored excitation energy  $\Delta E^*$  corresponds to the energy of the 0–0 transition between the lowest vibrational levels in the ground and excited states, that is,  $\Delta E^* = \Delta E_{0-0}$ . We obtain

$$E_{\text{F,redox}}^*(S^*/S^+) = E_{\text{F,redox}}(S/S^+) + \Delta E_{0-0}(S/S^*) \quad (10)$$

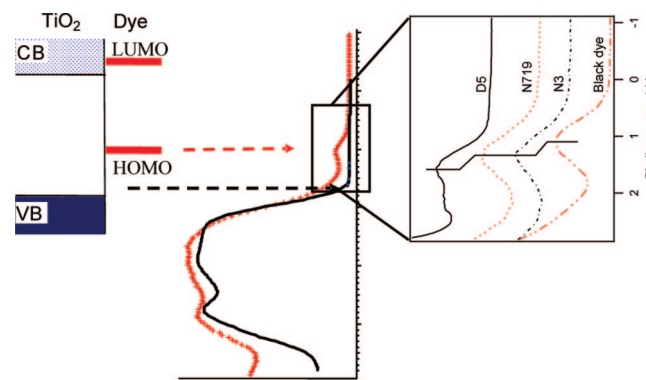


**Figure 9.** Valence band (VB) spectrum of a nanostructured TiO<sub>2</sub> film sensitized with the organic dye D5 (structure 123 in Table 5), N719, N3, and the black dye. A schematic energy level diagram indicating the conduction band (CB) and VB levels of the semiconductor and the HOMO and LUMO levels of the dye are also shown.

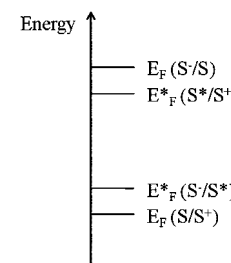


**Figure 10.** A schematic diagram of the relative positions of the Fermi levels of a redox system in its ground and excited states. Adapted from ref 95, Copyright 1985, with permission from Elsevier.

$$E_{\text{F,redox}}^*(S^-/S^*) = E_{\text{F,redox}}(S^-/S) - \Delta E_{0-0}(S/S^*) \quad (11)$$

From these equations, it may be illustrative to schematically indicate the relative positions of the Fermi levels of a redox system in its ground and excited states, Figure 10.

Introducing the corresponding distribution functions of the occupied and empty states for the most relevant reaction in DSC, we arrive at a more complete energy level diagram compared with Figure 5 and obtain the so-called Gerischer diagram for an excited-state electron injection from surface-bound sensitizers into the DOS of the mesoporous TiO<sub>2</sub> film, Figure 11.

In Figure 11, the distribution functions of the empty and occupied states for the ground state and excited state are drawn with equal areas indicating that the concentrations of the different species are the same. Differences in concentration will lead to different Fermi levels,  $E_{\text{F,redox}}(S/S^+)$  and  $E_{\text{F,redox}}^*(S^*/S^+)$ , and thus different driving forces for electron injection and for regeneration of the oxidized dyes by the electrolyte. The actual concentrations of the different species indicated in Figure 11 in a DSC device will depend on several factors such as the Fermi levels of the semiconductor and electrolyte, dye loading, extinction coefficients, and light intensity.

Since the sensitizer is adsorbed at the oxide surface in a DSC, the measurements to determine the energy levels as indicated in Figure 11 should be made *in situ*, that is, the oxidation potential of S and the excitation energy  $\Delta E_{0-0}$  should be determined for the sensitizer anchored to the semiconductor. Previous studies have shown that molecules anchored to mesoporous TiO<sub>2</sub>, ZrO<sub>2</sub>, or Al<sub>2</sub>O<sub>3</sub> films can be reversibly oxidized in standard electrochemical cells provided

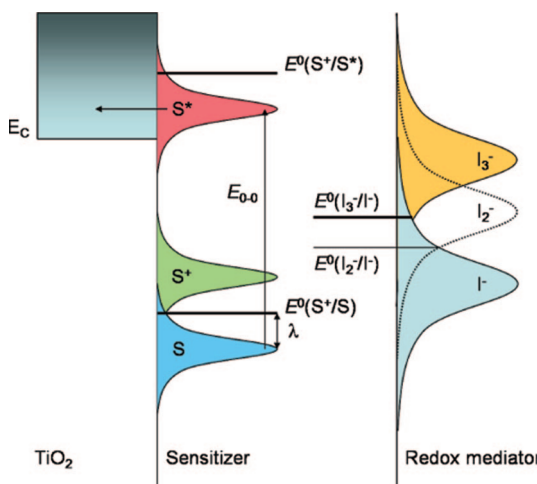


**Figure 11.** Gerischer diagram of the dye-sensitized solar cell with iodide/triiodide electrolyte. The level of the unstable reaction intermediate diiodide ( $I_2^-$ ) is indicated. Adapted from ref 7, reproduced by permission of the Royal Society of Chemistry, and ref 95, Copyright 1985, with permission from Elsevier.

that the surface coverage exceeds a percolation threshold.<sup>101–103</sup> Such a mechanism was presented by Bonhôte et al. for phosphonated triarylamines adsorbed on mesoporous  $TiO_2$ , which displayed reversible electrochemistry as well as electrochromic behavior.<sup>101</sup> In the review of Ardo and Meyer,<sup>7</sup> the literature on the studies of this lateral hole hopping process through the adsorbed molecular layer in mesoporous films is summarized. Zaban et al. found that the redox potential of a number of dye molecules adsorbed at  $TiO_2$  was dependent on pH of the aqueous electrolyte or on the cations present in nonprotic electrolytes.<sup>104</sup> This effect was attributed to dye molecules being located within the ionic double layer at the semiconductor oxide/solution interface.

$\Delta E_{0-0}$  can be estimated by the photoluminescence (PL) onset or from the intersection of the absorption and PL spectra. If difficulties arise in measuring the PL spectrum another way to estimate  $\Delta E_{0-0}$  is from the absorption onset of the dyes adsorbed on the oxide at a certain percentage (e.g., 10%) of the full amplitude at the absorption maximum. For the classical  $RuL_2(NCS)_2$  (N3) dye, the reported values are  $U_{\text{redox}}^0(S/S^+) = 1.1$  V (vs NHE) in acetonitrile,  $\Delta E_{0-0} = 1.75$  eV giving  $U_{\text{redox}}^*(S^*/S^+) = -0.65$  V vs NHE.<sup>40</sup> The reorganization energy for N3 in the ground state has been estimated to 0.35 eV.<sup>105</sup> The importance of the reorganization energy of the different redox species in a DSC device is at present not well understood. For the ultrafast electron injection process from the photoexcited dye to the semiconductor, which occurs on the femtosecond time scale, there may simply be no time for reorganization of the solvation shell. The effects of surface adsorption and other molecular interactions also need to be taken into account.

### 4.3. Photoinduced Electron Injection vs Direct Recombination - Reactions 1 and 2

A unique feature of DSCs compared with other solar cell technologies is that they separate the function of light absorption from charge carrier transport. The charge separation of the photoexcited electron and hole occurs by the ultrafast injection from the excited dye to the semiconductor oxide. For sensitizers like N719 and the black dye, light absorption is of MLCT (metal to ligand charge transfer) character with a contribution from the sulfur atom of the

-NCS group. Thus, the excitation process promotes electrons from the metal center and the sulfur atom to the carboxylated bipyridyl ligand that is directly bound to the semiconductor surface. For state-of-the-art DSCs, excited-state charge separation thus occurs from the  $\pi^*$  orbitals of the organic ligand of the Ru complex to the acceptor states in  $TiO_2$ . The injection process has always been debated. The femto- to picosecond time scale has made it difficult to measure the time constant accurately, and satisfactory mechanistic models are still lacking. Time constants  $<25$  fs have been measured, for example, by Willig and co-workers for injection from the excited state of the N3 dye into  $TiO_2$  under ultrahigh-vacuum conditions.<sup>106</sup> Such a fast process can therefore not involve redistribution of vibrational excitation energy by exchange with phonons in the solid and is thus different from the weak electronic coupling case of Marcus–Levich–Jortner–Gerischer type, see ref 7 and references therein. The lifetime of a molecular vibration is about 160 fs,<sup>7</sup> which implies that injection is occurring before thermal relaxation of the molecular excited state.

#### 4.3.1. Electron Injection Studies on Model Systems: Dyes Adsorbed on $TiO_2$

Generally, it is found that electron injection kinetics into  $TiO_2$  is nonexponential. This is, for example, attributed to the surface heterogeneity of  $TiO_2$ , distribution of sensitizer binding modes and strengths, interactions between the sensitizers, and dye aggregates. The injection can take place from various states in the thermal relaxation pathway, that is, Franck–Condon singlet injection, thermally relaxed excited-state singlet injection, or intersystem crossing to the triplet state(s) followed by injection. The research on the injection process for both organic and transition-metal coordination compounds bound to metal oxides has been extensively reviewed.<sup>7,76,107–114</sup> In this section, we will therefore only briefly summarize the studies on the injection process from excited dyes adsorbed onto oxide surfaces. We will discuss a little more, however, the recent observations that the injection process may be significantly slower, subnanosecond, in *complete* DSC devices.<sup>79,115,116</sup>

Normally, techniques such as femtosecond transient absorption spectroscopy are used to determine the kinetics of the injection process by measuring the absorption changes associated with the formation of the dye cation or injected electron.<sup>112</sup> Besides the ultrafast femtosecond injection,<sup>75–78</sup> a slower picosecond time scale (typically tens of picoseconds) process is observed, resulting in biphasic injection kinetics. The origin of the slower component is discussed as an injection mechanism proceeding via the lower (compared with the singlet) energy triplet excited state. The spin–orbit coupling from the ruthenium heavy atom center gives the time for intersystem crossing to occur as  $\sim 100$  fs.<sup>117</sup> Wenger et al. reported that the slower picosecond components vanished upon employing a lower surface-coverage film or sonicating the dyeing solution.<sup>118</sup> Under such conditions, only an ultrafast component ( $<20$  fs) for injection remained. The injection kinetics, and the proportion of singlet versus triplet injection, have been studied as a function of excitation wavelength,<sup>111,119–121</sup> solvent,<sup>122,123</sup> pH,<sup>121,124</sup> inclusion of cationic potential determining ions,<sup>115,125</sup>  $TiO_2$  Fermi level,<sup>126,127</sup> bridging units, and distance dependence between the dye and the  $TiO_2$  surface.<sup>40,128</sup> How these external parameters influence the injection process for a given system (dye and oxide)

is thus understood at a detailed level and is elegantly reviewed by Ardo and Meyer.<sup>7</sup>

### 4.3.2. Injection and DSC Device Efficiency

For an efficient DSC device, it is not important that the injection process is ultrafast. It is important that the quantum efficiency for injection is high. The electron injection efficiency is defined as follows:

$$\varphi_{\text{inj}} = \frac{k_{\text{inj}}}{k_{\text{inj}} + k_1} \quad (12a)$$

where  $k_{\text{inj}}$  and  $k_1$  are the rate constants for electron injection and decay (radiative and nonradiative) of the excited dye, respectively. For efficient injection,  $k_{\text{inj}}$  should be about 100 times larger than  $k_1$ . If  $k_{\text{inj}}$  is much larger, there is “kinetic redundancy”, as discussed by Durrant and co-workers.<sup>116,129</sup> It may, for example, be beneficial for the performance of the DSC device to slow down the electron injection by increasing  $E_c$ . On one hand, this should lead to an increase in  $V_{\text{oc}}$ . On the other hand, this will lead to a decrease in driving force for electron injection ( $\Delta E_{\text{inj}}$ ), that is, the energy difference between the injecting electron state of the dye (normally the excited state,  $E_{\text{F,redox}}(\text{S}^*/\text{S}^+)$ ) and the acceptor states in  $\text{TiO}_2$  (normally the conduction band,  $E_c$ ), and a decrease in energetic overlap between injecting and accepting states. This may result in a decrease in  $\varphi_{\text{inj}}$  and  $J_{\text{sc}}$ . Optimization of a DSC device is achieved by maximizing the electrical power output, that is, the product of current and voltage, which will be a compromise. For recently developed metal-free organic dyes, it was highlighted that the dye excited state needs to be sufficiently high in energy to allow high injection efficiencies.<sup>130–133</sup>

The observation that part of the injection dynamics in complete DSC devices appears to be on the 100 ps time scale opens up the possibility to use single pulse techniques like single-photon counting.<sup>134</sup> This greatly simplifies the experiments and importantly makes it possible to use laser light intensities commensurate with solar irradiation. Thus, injection processes can be studied on complete DSC devices under normal solar cell working conditions. With the use of noninjecting control samples, such as  $\text{ZrO}_2$ , a time resolution of ~60 ps is obtained for the single-photon counting experiments.<sup>134</sup>

**4.3.2.1. Effect of Driving Force,  $\Delta E_{\text{inj}}$ .** As described above  $E_c$  depends on surface charge, and frequently additives and cations in the electrolyte, such as TBP and  $\text{Li}^+$ , have been used to enhance device performance. The influence of such additives on the injection process in complete DSCs and their correlation with device performance is at present one of the most important topics in fundamental DSC research.<sup>7,79,115,116,135</sup> As an example, the difference in injection times between the N3 dye and its salt analogue N719, replacing two of the four protons on the carboxylic groups with  $\text{TBA}^+$  counterions, is illustrative. Durrant and co-workers found that N719 had a 30-fold slower rate of injection as compared with N3.<sup>124</sup> They suggested that the labile protons from the carboxylic acid binding groups of N3 lowered the  $E_c$ , leading to an increase in  $\Delta E_{\text{inj}}$  and promoting more favorable energetics for injection. To check this, Lian and co-workers pretreated  $\text{TiO}_2$  films coated with N3 in aqueous buffer solutions at pH 2–8.<sup>121</sup> After removing weakly bound and desorbed sensitizers, biphasic kinetics as described above was observed, and injection yields were

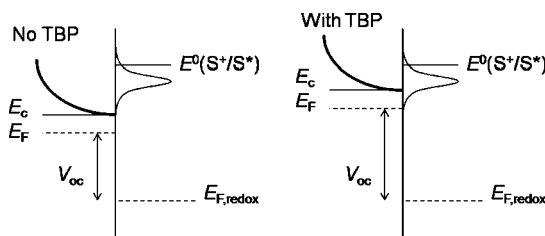


**Figure 12.** Energy scheme of the different conduction band edge ( $E_c$ ) positions in the presence and absence of TBP. This causes a variation in overlap between the dye excited states and  $\text{TiO}_2$  conduction band states. Adapted from ref 133, reprinted by permission of the PCCP Owner Societies.

found to be pH dependent decreasing with higher pH. Moreover, as the pH was raised from 2 to 8, there was a decrease in the rate of the slower component and the ratio of the faster-to-slower components to injection. Interestingly, even though the injection is slower for N719 compared with N3, the energy conversion efficiency is observed to be higher for N719.<sup>116</sup> This occurs because protons shift  $E_c$  to a lower energy and can thus lower the  $V_{\text{oc}}$ . In a very recent work, Koops et al.<sup>79</sup> measured injection half-times for the N719 dye ( $t_{1/2}$ ) ranging from <60 ps for 0.1 M  $\text{Li}^+$  and 0 M TBP (injection yield of 0.97) to  $550 \pm 120$  ps for 0 M  $\text{Li}^+$ , 0.5 M TBP (injection yield of 0.7). The variation of complete DSC device performance with electrolyte composition agreed with what is normally observed, that is, more “basic” electrolytes (low  $\text{Li}^+$  and high TBP concentrations) reduce the photocurrent but increase the voltage. They measured the relative difference in the  $\text{TiO}_2$  conduction band potential for the different electrolytes by charge extraction measurements and found that a 100 meV shift in  $E_c$  correlated with a 2-fold increase in injection half-time. The difference in injection yield between the electrolytes resulted in a linear relationship of the injection yield versus DSC photocurrent, indicating that electron injection losses can be a key determinant of device photocurrent efficiency.

A schematic energy level diagram of the effect of TBP treatment with respect to accessible states in the  $\text{TiO}_2$  for injection from an excited dye is shown in Figure 12.

**4.3.2.2. Effect of Distance.** The distance between the dye and the acceptor,  $\text{TiO}_2$ , will affect the injection dynamics.

Asbury et al. found a slower injection for Re complexes when  $\text{CH}_2$  spacer groups were introduced between the bipyridine ligand and the carboxylic acid binding groups.<sup>136</sup> Galoppini and co-workers designed and synthesized several series of dyes with spacers between the anchoring group and the actual chromophore. Results were found to depend strongly on the nature of the spacer. For Ru dyes with rigid conjugated *p*-phenylene ethynylene spacers, electron transfer reactions (injection and recombination) were found to be nearly independent of spacer length.<sup>137,138</sup> For perylene dyes with carboxylic acid or phosphonic acid binding groups, introduction of saturated  $\text{CH}_2$  spacer groups led to a decrease in injection rate constants.<sup>139</sup>

The effect of distance has also been studied by introducing an insulating layer such as  $\text{Al}_2\text{O}_3$  between dye and the metal oxide. Guo et al. found a systematic decrease in injection rate with the number of application cycles for  $\text{Al}_2\text{O}_3$  deposition.<sup>140</sup> Antila et al. found that addition of  $\text{Al}_2\text{O}_3$  layers slows electron injection from the singlet excited state of N3 and decreases the overall injection efficiency.<sup>141</sup> Injection from the triplet state injection was also suppressed.

**4.3.2.3. Effect of Quasi-Fermi Level (Electron Concentration) in the  $\text{TiO}_2$ .** The quasi-Fermi level and filling of

DOS in the TiO<sub>2</sub> can be manipulated by an applied potential and illumination. Tachibana et al. showed that the application of an electrical bias of −700 mV vs Ag/AgCl to N3/TiO<sub>2</sub> films in the presence of a redox-inactive electrolyte retards the injection rate 25-fold.<sup>126</sup> This was assigned to an increase in electron concentration within the TiO<sub>2</sub> reducing the density of unoccupied states available for electron injection. For the N719/TiO<sub>2</sub> DSC, only a relatively small dependence of the half-time,  $t_{1/2}$ , and injection yield on applied bias was observed.<sup>79</sup> With an application of −1070 mV in the dark to the DSC, which gives a significantly higher electron concentration compared with open-circuit conditions and solar irradiation,  $t_{1/2}$  increased from 180 to 230 ps with a corresponding decrease in injection yield from 0.83 to 0.76. These observations indicate that for the N719/TiO<sub>2</sub> DSC system, the injection yield is relatively insensitive to electron density in the TiO<sub>2</sub> film over the operating range of the device and that bias-dependent loss of injection yield does not impact DSC device performance. Care must of course be taken for the generalization of these observations to other DSC systems. As pointed out by Koops et al. the observations are consistent with the relatively low electron densities injected into the TiO<sub>2</sub> film (~10 electrons per nanoparticle under solar irradiation) with a high dielectric constant of TiO<sub>2</sub> resulting in negligible electron–electron repulsion.

A model to explain the nonexponential nature of the injection kinetics given by Durrant and co-workers is based on local inhomogeneities in the density of acceptor states.<sup>142</sup> In this model, the rate constant for electron injection is proportional to the number of accessible electronic states in the TiO<sub>2</sub> material, which has a density of acceptor states increasing exponentially with energy, with additional local energy inhomogeneities in the order of 150 meV.

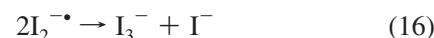
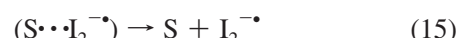
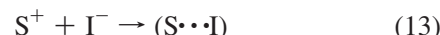
#### 4.4. Regeneration of the Oxidized Dyes: Reaction 3

After photoinduced electron injection from the dye into the conduction band of TiO<sub>2</sub>, the dye is in its oxidized state and must be reduced by an electron donor in the electrolyte for regeneration. A lower limit for the regeneration time is given by diffusion-limited kinetics. In nonviscous electrolytes, the diffusion rate constant,  $k_{\text{diff}}$ , is in the range 10<sup>9</sup>–10<sup>10</sup> M<sup>−1</sup> s<sup>−1</sup>. For an electron donor concentration in electrolyte concentration ≥0.1 M, a lower limit for the regeneration time ( $(k_{\text{diff}} \times \text{donor concentration})^{-1}$ ) of some nanoseconds is calculated. It is useful to define the regeneration efficiency,  $\varphi_{\text{reg}}$ , which gives the probability that an oxidized dye is regenerated by an electron donor in the electrolyte rather than by recombination with an electron in the TiO<sub>2</sub>:

$$\varphi_{\text{reg}} = \frac{k_{\text{reg}}}{k_{\text{reg}} + k_{\text{rec}}} \quad (12b)$$

Here,  $k_{\text{reg}}$  is the rate constant for regeneration, and  $k_{\text{rec}}$  is the (pseudo-) first-order rate constant for electron–oxidized dye recombination.

The standard electron donor (reductant) in DSCs is iodide. For many types of sensitizer, very high  $\varphi_{\text{reg}}$  values, approaching unity, have been found with iodide. Upon reduction of the oxidized dye, the diiodide radical, I<sub>2</sub><sup>−•</sup>, is formed,<sup>143–145</sup> which is subsequently converted into triiodide. The reduction of the oxidized sensitizer (S<sup>+</sup>) by iodide follows most likely the following reaction mechanism:



The first step is most likely a one-electron transfer reaction between S<sup>+</sup> and I<sup>−</sup>. The oxidation of iodide to free iodine radical (I<sup>•</sup>) is, however, unlikely for energetic reasons:  $U^0(\text{I}^{\bullet}/\text{I}^-)$  is +1.33 V vs NHE in aqueous solutions<sup>146</sup> and has been reported to +1.23 V vs NHE in acetonitrile,<sup>147</sup> which is more positive than the  $U^0(\text{S}^+/\text{S})$  of most of the dyes that are used as sensitizers in DSCs. The redox potential of the iodine radical bound to the dye (S···I) will be less positive in potential, and the formation of a (S···I) complex is therefore a likely first step in the dye regeneration. Addition of a second iodide leads to the formation of a (S···I<sub>2</sub><sup>−•</sup>) complex, which can dissociate into ground-state dye S and I<sub>2</sub><sup>−•</sup>. Finally, I<sub>2</sub><sup>−•</sup> disproportionates under the formation of triiodide and iodide. The second-order rate constant for this reaction is 2.3 × 10<sup>10</sup> M<sup>−1</sup> s<sup>−1</sup> in acetonitrile.<sup>148</sup>

Evidence for the formation of intermediate dye–iodide complexes comes from nanosecond laser spectroscopy studies. Clifford et al. observed the formation of a (S···I) complex for the oxidized sensitizer *cis*-Ru(dcbpy)<sub>2</sub>(CN)<sub>2</sub> with iodide.<sup>149</sup> Fitzmaurice et al. proposed the formation of a (S···I<sub>2</sub><sup>−•</sup>) complex in the case of a Ru(dcbpy)<sub>3</sub><sup>2+</sup> sensitizer.<sup>150</sup> Quantum chemical calculations confirm that formation of such complexes is energetically favorable in the case of *cis*-Ru(dcbpy)<sub>2</sub>(NCS)<sub>2</sub>.<sup>151</sup> A very similar mechanism of reduction is also deduced for organic dyes based on quantum chemical calculations. For the most common sensitizer *cis*-Ru(dcbpy)<sub>2</sub>(NCS)<sub>2</sub>, the half-time for regeneration in the presence of about 0.5 M iodide in the electrolyte is in the range of 100 ns to 10 μs.<sup>149,152–155</sup> Regeneration kinetics depends strongly on the precise composition of the electrolyte. Pelet et al. found that the nature of the cation of the iodide salt has a significant effect on regeneration.<sup>153</sup> Rapid regeneration occurs in the presence of cations that adsorb onto the TiO<sub>2</sub> surface, such as Li<sup>+</sup> and Mg<sup>2+</sup>, whereas much slower regeneration was found with TBA<sup>+</sup> ions. This effect was attributed to the resulting higher local iodide concentration near the TiO<sub>2</sub> surface when positive charge is adsorbed.

A large number of sensitizers are efficiently regenerated by iodide, as follows from their good solar cell performance. Most of these sensitizers have oxidation potentials that are similar to or more positive than that of the standard sensitizer Ru(dcbpy)<sub>2</sub>(NCS)<sub>2</sub> ( $U^0 = +1.10$  V vs NHE). Because the redox potential of the iodide/triiodide electrolyte with organic solvent is about +0.35 V vs NHE, the driving force  $\Delta G^0$  for regeneration of Ru(dcbpy)<sub>2</sub>(NCS)<sub>2</sub> is 0.75 eV. It is of interest to estimate how much driving force is needed. Kuciauskas et al.<sup>154</sup> investigated regeneration kinetics of a series of Ru and Os complexes and found that Os(dcbpy)<sub>2</sub>(NCS)<sub>2</sub> with a  $\Delta G^0 = 0.52$  eV is not (or is very slowly) regenerated by iodide, while Os(dcbpy)<sub>2</sub>(CN)<sub>2</sub> ( $\Delta G^0 = 0.82$  eV) is regenerated. The black dye, Ru(tcterpy)(NCS)<sub>3</sub>, with  $\Delta G^0 = 0.60$  eV, shows rapid regeneration.<sup>145</sup> Clifford et al.<sup>149</sup> studied regeneration in a series of Ru sensitizers and found that Ru(dcbpy)<sub>2</sub>Cl<sub>2</sub> with  $\Delta G^0 = 0.46$  eV gave slow regeneration (>100 μs), leading to a low regeneration efficiency. The results suggest that 0.5 to 0.6 eV driving force

is needed for regeneration of Ru complex sensitizers in iodide/triiodide electrolyte. The need for such a large driving force comes probably from the fact that the initial regeneration reaction involves the  $I^-/I_3^-$  redox couple, having a more positive potential than  $I^-/I_3^-$ .

Rapid regeneration kinetics of the oxidized dye by iodide ( $t_{1/2} \approx 10 \mu s$ ) was also observed for sensitizers such as chlorophyll derivates<sup>156</sup> and a porphyrin (ZnTPPC).<sup>144</sup> The driving force for this reaction is  $\geq 0.5$  eV for these dyes. No regeneration was observed for a naphthalocyanine dye ( $\Delta G^0 = 0.1$  eV)<sup>157</sup> and a squarilium dye ( $\Delta G^0 = 0.35$  eV),<sup>158</sup> although a small photocurrent was observed for the latter dye in a DSC. For two very similar small organic donor-conjugated chain-acceptor dyes having  $\Delta G^0$  values for regeneration by iodide of 0.48 and 0.16 eV, respectively, efficient dye regeneration was found for the first but not the latter.<sup>159</sup> Effective regeneration seems therefore to occur when the oxidation potential of a sensitizer is about 0.5 V more positive than the  $I_3^-/I^-$  redox potential. An exception to this has, however, recently been reported by Wenger et al.<sup>160</sup>

Efficient regeneration of oxidized dye molecules can be obtained with bromide instead of iodide, provided that the oxidation potential of the dye is sufficiently positive. Ferrere et al. showed that a perylene dye attached to  $SnO_2$  yielded 30% IPCE and  $3.2 \text{ mA cm}^{-2}$  photocurrent in the presence of a  $Br^-/Br_3^-$  redox electrolyte.<sup>161</sup> Wolfbauer et al. tested  $I^-$ ,  $I_3^-$ ,  $SCN^-$ ,  $Br^-$ , and ferrocene as electron donors for Ru(dcbpy)<sub>2</sub>(NCS)<sub>2</sub>-sensitized  $TiO_2$ .  $SCN^-$  and  $Br^-$  yielded photocurrents less than 2% of that generated by iodide, while  $I_3^-$  and ferrocene yielded no photocurrent.<sup>162</sup> Oskam et al. compared the pseudohalides selenocyanate ( $SeCN^-$ ) and thiocyanate ( $SCN^-$ ) with iodide in DSCs based on Ru(dcbpy)<sub>2</sub>(NCS)<sub>2</sub>-sensitized  $TiO_2$ .<sup>163</sup> In the presence of  $SeCN^-$ , most oxidized dye was regenerated within  $5 \mu s$ , which was much slower than in the presence of iodide under the same conditions. Regeneration of the oxidized dye by  $SCN^-$  was negligible. The  $SeCN^-/(SeCN)_3^-$  redox couple was later successfully applied in an ionic liquid electrolyte for DSCs by Wang et al.<sup>164</sup> Fast regeneration of the Z907 dye (structure 6 in Table 1) was obtained due to the high concentration of the reductant in the ionic liquid. The reaction mechanism for dye regeneration using (pseudo)halides should be essentially identical to that of iodide, in particular, when considering the inner-sphere mechanism proceeding via the  $SCN^-$  ligands of the ruthenium dye proposed by Privalov et al.<sup>165</sup>

Fast regeneration kinetics are also found for the one-electron redox mediators. Cobalt(II)-bis[2,6-bis(1'-butylbenzimidazol-2'-yl)pyridine] ( $Co(dbipb)_2^{2+}$ ) gave regeneration times of some microseconds and regeneration efficiencies of more than 0.9.<sup>166,167</sup> Ferrocene and phenothiazine gave rapid regeneration, while cobalt(II) bis(4,4'-di-*tert*-butyl-2,2'-bipyridine) was slow.<sup>168</sup> Interestingly, mixtures of this Co complex with ferrocene and phenothiazine were efficient in dye-sensitized solar cells, suggesting that a mix of redox mediators can be a viable approach in DSCs.<sup>168</sup>

Very rapid dye regeneration was observed in the case of the solid state DSCs where the redox electrolyte is replaced by the solid hole conductor 2,2',7,7'-tetrakis-(*N,N*-di-*p*-methoxyphenyl-amine)-9,9'-spirobifluorene (spiro-MeOTAD). Bach et al. found that hole injection from the oxidized Ru(dcbpy)<sub>2</sub>(SCN)<sub>2</sub> dye to the spiro-MeOTAD proceeds over a broad time scale, ranging from less than 3 ps to a few nanoseconds.<sup>169</sup>

## 4.5. Electron Transport in Mesoporous Semiconductor Electrodes: Reaction 4

The mesoporous semiconductor electrode consists of numerous interconnected nanocrystals. Because these particles are typically not electronically doped (the doping density of dense  $TiO_2$  films annealed in air at 500 °C was determined to  $10^{17} \text{ cm}^{-3}$ ,<sup>170</sup> which is negligible for nanoparticles) and surrounded by ions in the electrolyte, they will not have an internal electrical field and will not display any significant band bending. Electrons photojected into the nanoparticles from the dye molecules are charge compensated by ions in the electrolyte. Photocurrent will be detected in the external circuit once the electrons are transferred into the conducting substrate. The gradient in electron concentration appears to be the main driving force for transport in the mesoporous  $TiO_2$  film, that is, electron transport occurs by diffusion.<sup>171–173</sup>

Because the electrons in the mesoporous  $TiO_2$  are charge compensated by ions in the electrolyte, the diffusion processes of electrons and ions will be coupled through a weak electric field. This will affect transport of charge carriers. The measured electron diffusion is described by the ambipolar diffusion model:<sup>174,175</sup>

$$D_{\text{amb}} = \frac{n + p}{(n/D_p) + (p/D_n)} \quad (17)$$

$D_{\text{amb}}$  is the ambipolar diffusion coefficient,  $n$  and  $p$  are the concentrations of negative and positive charge carriers (corresponding to electron and cation concentration in the DSC), and  $D_p$  and  $D_n$  are the diffusion coefficients of positive and negative charge carriers. The basic validity of this model for electron transport in electrolyte-permeated mesoporous  $TiO_2$  was demonstrated by Yanagida and co-workers using laser-induced transient photocurrent experiments.<sup>176,177</sup> They found, however, a significant cation effect on electron transport, an effect that was attributed to differences in the specific adsorption of the cations. In DSCs under operating conditions, the concentration of cations in the electrolyte ( $\sim 3 \times 10^{20} \text{ cm}^{-3}$ ) is much higher than the electron concentration in  $TiO_2$  ( $\sim 10^{18} \text{ cm}^{-3}$  at 1 sun operating conditions), so electron transport should not be much affected by ion mobility and type of ions. Nevertheless, significant effects on  $D_{\text{eff}}$  depending on the type of cation have been observed.<sup>178</sup> Different anions show negligible effect on electron transport.<sup>179</sup> The additive 4-*tert*-butylpyridine was found to decrease electron transport times in DSC with LiI-based electrolytes.<sup>94,178,180</sup> The type of dye does not seem to affect electron transport in the mesoporous  $TiO_2$ .<sup>181</sup>

In contrast to the notion that electron transport occurs by diffusion, it is observed that the electron transport depends on the incident light intensity, becoming more rapid at higher light intensities.<sup>182,183</sup> This can be explained by a diffusion coefficient that is light-intensity dependent or, more correctly, dependent on the electron concentration and Fermi level in the  $TiO_2$ . The measured value of the diffusion coefficient is orders of magnitude lower than that determined for single-crystalline  $TiO_2$  anatase ( $\sim 0.4 \text{ cm}^2 \text{ s}^{-1}$ ).<sup>184</sup> These observations are usually explained using a multiple trapping (MT) model.<sup>183,185–188</sup> In this model, electrons are considered to be mostly trapped in localized states below the conduction band, from which they can escape by thermal activation, see Figure 13.

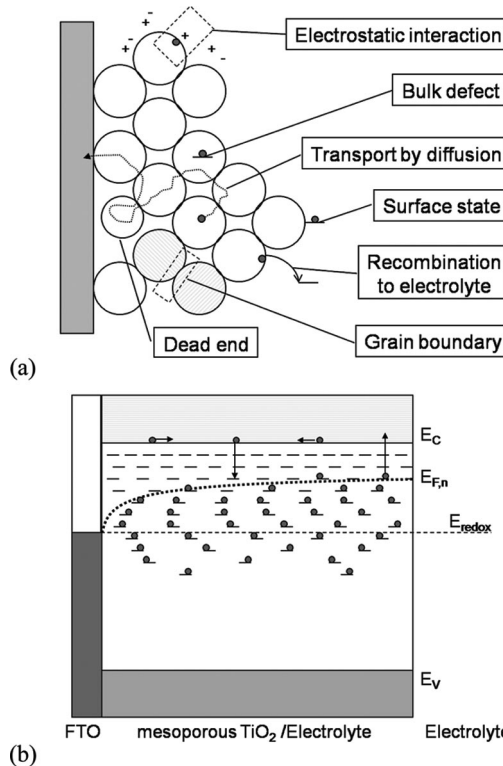


**Figure 13.** (a) Overview of the electron transport process in the electrolyte-infiltrated mesoporous  $\text{TiO}_2$  electrode of a dye-sensitized solar cell, showing the possible origins of the relatively slow diffusion. Traps can be located at the  $\text{TiO}_2$ /electrolyte interface, in the bulk of the  $\text{TiO}_2$  particles, or at grain boundaries, while electrostatic interactions between electrons and ions in the electrolyte cause ambipolar diffusion but possibly also trapping. (b) Schematic diagram of the mesoporous  $\text{TiO}_2$  electrode in the DSC under short-circuit conditions in the multiple trapping model. The electrode is treated as an effective medium with a distribution of localized energy states located below the conduction band edge. Most electrons are trapped; transport takes place when electrons are thermally detrapped and move in the conduction band, before trapping again.

Experiments suggest that the density and energetic location of such traps is described by an exponentially decreasing tail of states below the conduction band.<sup>185,187</sup> When electron transport is studied using small-modulation methods (see section 6.3.1), a chemical diffusion coefficient ( $D_n$ ) is determined. With a quasi-static approximation in the MT model, the following expression was derived for  $D_n$ :<sup>186,188</sup>

$$D_n = \left(1 + \frac{\partial n_t}{\partial n_c}\right)^{-1} D_0 \quad (18)$$

where  $n_t$  and  $n_c$  are the concentrations of trapped and conduction band electrons, respectively, and  $D_0$  is the diffusion coefficient of conduction band electrons.

Conductivity studies of mesoporous  $\text{TiO}_2$  in inert electrolyte showed that under conditions of strong electron accumulation (>20 electrons in 20 nm  $\text{TiO}_2$  particle), the measured  $D_n$  reaches a constant value.<sup>189</sup> Reported mobility values in this regime vary between 0.01 and 0.05  $\text{cm}^2 \text{V}^{-1} \text{s}^{-1}$ ,<sup>189,190</sup> corresponding to  $D_n$  of  $2 \times 10^{-4}$  to  $1.3 \times 10^{-3} \text{ cm}^2 \text{ s}^{-1}$ . More recently, it was confirmed by impedance spectroscopy that at sufficiently negative applied potentials,  $D_n$  becomes constant; a value of  $6 \times 10^{-5} \text{ cm}^2 \text{ s}^{-1}$  was determined.<sup>191</sup> The observation of a constant  $D_n$  may be the result of unpinning of the conduction band at high electron densities.

The precise nature and location of the traps in the mesoporous  $\text{TiO}_2$  is a subject of discussion. In a spectro-electrochemical study, Boschloo and Fitzmaurice could distinguish deeply trapped electrons, ca. 0.5 eV below the conduction band edge, having an absorption maximum at about 400 nm, from conduction band electrons (or shallowly trapped electrons) that give a very broad absorption spectrum without a clear maximum, as well as a bleach at wavelengths below 380 nm.<sup>192</sup> The deep traps are located at the semiconductor/electrolyte interface, as follows from the strong pH dependence of the trap density,<sup>193</sup> and can most likely be attributed to a surface defect, such as a surface oxygen vacancy.<sup>194</sup> These deep traps do not appear to be involved in electron transport in DSCs.

The traps that are involved in electron transport in DSCs can be located either in the bulk, at grain boundaries, or at the  $\text{TiO}_2$ /electrolyte interface. The density of trap states will scale differently with nanoparticle size depending on their location. Frank and co-workers performed transport and recombination studies of DSCs prepared from differently sized  $\text{TiO}_2$  particles and could conclude from the scaling factor of the roughness factor with trap density and electron diffusion coefficient that traps are located on the surface of the  $\text{TiO}_2$  (surface states).<sup>195,196</sup> It is evident from these studies that an increase in particle size (i.e., a decrease in roughness factor) leads to a decrease in trap state density and an increase in electron diffusion coefficient. Intercalation of  $\text{Li}^+$  ions into  $\text{TiO}_2$  was found to occur in DSCs with  $\text{Li}^+$ -containing electrolyte under open-circuit conditions with high illumination.<sup>197</sup> This was found to lead to an increased trap density near the surface and to a decrease in  $D_n$  and increase of electron lifetime.

The origin of the electron traps remains obscure at present: they could correspond to trapping of electrons at defects in the bulk or surface regions of the mesoporous oxide or to Coulombic trapping due to local field effects through interaction of electrons with the polar  $\text{TiO}_2$  crystal or with cations of the electrolyte.<sup>198–200</sup>

Other experiments point to the importance of grain boundaries for electron transport in DSCs. No light-intensity dependence was found in DSCs prepared using single-crystalline  $\text{ZnO}$  nanorods (without grain boundaries), while it is observed in  $\text{ZnO}$  nanoparticle-based DSCs.<sup>201</sup>  $\text{TiO}_2$  nanoparticles in a mesoporous electrode can be preferentially oriented along their crystal faces by means of application of an electrical field prior to their connection by sintering.<sup>202</sup> It was found that this leads to faster electron transport in the mesoporous film, which was attributed to a higher degree of ordering. Such ordering would also decrease the number of grain boundaries.

Electron transport in the mesoporous  $\text{TiO}_2$  electrode is also influenced by the network geometry of the film. Benkstein et al. performed simulations and experiments on random networks with different porosities built from spherical  $\text{TiO}_2$  nanoparticles.<sup>203</sup> The average coordination number of the particles decreases with increasing porosity. This leads to more dead ends (particles with only one neighbor), from less than 1% in a 50% porous film to 31% in a 75% porous film. The percolation threshold was found at the critical porosity of 76%. The path of the electrons becomes increasingly tortuous in more porous films, leading to slower electron transport to the conducting substrate. Differences in porosity in this study were obtained by changing the concentration of poly(ethylene glycol) in the  $\text{TiO}_2$  paste. Similar results

were obtained in compressed  $\text{TiO}_2$  (using Degussa P25 nanoparticles) films, where the porosity was controlled by changing the pressure during preparation.<sup>204</sup>

#### 4.6. Recombination of Electrons in the Semiconductor with Oxidized Dyes or Electrolyte Species: Reactions 5 and 6

During their relatively slow transport through the mesoporous  $\text{TiO}_2$  film constituted of nanometer-sized particles, electrons are always within only a few nanometers distance of the semiconductor/electrolyte interface. Recombination of electrons with either oxidized dye molecules or acceptors in the electrolyte is therefore a possibility. The recombination of electrons with oxidized dye molecules competes with the regeneration process, which usually occurs on a time scale of about 1  $\mu\text{s}$ . The electron transfer from nanocrystalline  $\text{TiO}_2$  to oxidized dye molecules has been studied in detail using nanosecond laser spectroscopy.<sup>115,149,152,154,205–209</sup> This process proceeds over a time scale from nano- to milliseconds and does not follow simple first-order kinetics. The driving force for the electron transfer is usually on the order of 1.5 eV, which is larger than reorganization energies expected for bound sensitizers. Recombination kinetics are therefore expected to lie in the Marcus inverted region, where electron transfer is thermally activated and an increase in driving force leads to a decrease in transfer rate constant.<sup>210</sup>

In separate investigations, the groups of Meyer<sup>115,205</sup> and Durrant<sup>206,209</sup> showed that recombination kinetics were hardly affected by differences in driving force for similar types of dye, and it was proposed that the kinetics were determined by diffusion-limited encounters between electrons in  $\text{TiO}_2$  and oxidized dye molecules. Meyer and co-workers used equal-concentration second-order kinetics in their analysis, an approach that is appropriate for electron transfer between mobile species in solution, and obtained good fits using a summation of two second-order recombination processes, where the determined rate constants were independent of initial reactant concentration.<sup>115,205</sup> Durrant and co-workers found that transient absorption ( $\Delta A$ ) kinetics for recombination was well approximated by a stretched exponential function:  $\Delta A(t) = \Delta A(0) \exp[-(t/\tau)^\alpha]$ .<sup>207,211</sup> Nelson et al. showed that a model where electron–oxidized dye recombination is limited by multiple trapping events of the electron in the  $\text{TiO}_2$  gives rise to stretched exponential decay, when trap states are exponentially distributed in energy.<sup>211</sup> The stretched exponential dispersion parameter  $\alpha$  is related to the exponential distribution of trap states in the  $\text{TiO}_2$ . Experimental data showed that  $\alpha$  depends both on electrolyte composition<sup>211</sup> and on the nature of the dye.<sup>206</sup> In the special case where the back reaction to the oxidized dye is extremely slow, due to an increased distance between electron and acceptor, single-exponential decay was found.<sup>212</sup>

In other work, clear dependence of recombination kinetics on driving force was found. Hupp and co-workers investigated a series of phosphonated ruthenium bipyridyl complexes differing in oxidation potential.<sup>213</sup> These dyes adsorb very strongly onto  $\text{TiO}_2$  and allowed study in aqueous electrolyte over a wide pH range. The measured recombination kinetics was consistent with Marcus normal region behavior: thermally activated electron transfer with rate constants increasing with increasing driving force ( $\Delta G^0$ ). This behavior was attributed to a sequential electron and proton transfer process. No change in kinetics was found when the

$\text{TiO}_2$  conduction band energy was changed by means of pH adjustment, although the driving force is also altered in this way.<sup>213,214</sup> This too was attributed to the sequential process.

In contrast, Lewis and co-workers studied a series of ruthenium and osmium polypyridyl complexes and found recombination kinetics consistent with Marcus inverted region: kinetics become slower with increasing driving force for recombination within the series, while rate constants increased with temperature.<sup>154</sup> From the temperature-dependent recombination studies, activation energies of 0.1–0.2 eV were found, and a reorganization energy of 0.8 eV was determined for  $\text{Ru}(\text{dcbpy})_2(\text{NCS})_2$  as a sensitizer.

The study of Clifford et al. on a series of Ru complexes and porphyrin compounds gave no evident relation between half-decay time and  $\Delta G^0$ .<sup>206</sup> They did, however, find evidence for a distance dependence of the recombination kinetics: an increase in the spatial separation of the dye cation HOMO orbital from the metal oxide surface by 3 Å resulted in a more than 10-fold increase in the recombination half-time, consistent with electron tunneling theory.<sup>206</sup>

In older work by Moser and Grätzel on the recombination reaction on  $\text{TiO}_2$  colloids sensitized with small dye molecules (coumarin, alizarin, and merocyanine), first-order recombination kinetics were found.<sup>215</sup> The back reaction was nearly temperature independent, and reorganization energies of about 0.3 eV were determined. Results were consistent with electron transfer in the Marcus inverted region.

Application of a potential to the mesoporous  $\text{TiO}_2$  electrode has a strong effect on the recombination kinetics.<sup>152,154,171,214</sup> When the electron concentration in the  $\text{TiO}_2$  particles is increased, a strong increase in recombination kinetics is found. Under actual working conditions, electron concentration in the  $\text{TiO}_2$  particles is rather high, and recombination kinetics may compete with dye regeneration.

Recombination of electrons in  $\text{TiO}_2$  with acceptors in the electrolyte has been mainly studied in actual devices by measuring transient response of the open circuit potential ( $V_{\text{oc}}$ ).<sup>216,217</sup> The time constant found in such experiments will be referred to as the electron lifetime. The steady-state value of  $V_{\text{oc}}$  provides also information on the recombination. Under illumination at open circuit, the net rate of electron injection from dyes into the mesoporous oxide is balanced by the net rate of electron transfer to electron acceptors. In most studies, it is assumed that only recombination of electrons with acceptors in the electrolyte occurs, as oxidized molecules are very rapidly regenerated. Recombination can occur both at the interface between the nanocrystalline oxide and the electrolyte and at the part of the conducting substrate that is exposed to the electrolyte. This second route can be suppressed by deposition of a compact blocking layer of the metal oxide onto the conducting substrate.<sup>218</sup>

Lifetimes observed with iodide/triiodide electrolytes are very long (about 1–20 ms under one sun illumination)<sup>217,219,220</sup> in comparison to most other redox mediators, such as ferrocene<sup>221</sup> and TEMPO,<sup>222</sup> and hole conductors, such as  $\text{CuSCN}$ <sup>223</sup> and spiro-MeOTAD.<sup>224–226</sup> Increase of electron concentration in the  $\text{TiO}_2$  always leads to shorter electron lifetimes. No conclusions on the reaction order of the recombination reaction with respect to electrons can, however, be drawn from the electron concentration dependence of the lifetime, since it appears to be close to second order even for obvious one-electron redox couples.<sup>224,227</sup> Recombination kinetics may be dominated by the electron trapping–detrapping mechanism in the  $\text{TiO}_2$  instead.<sup>228</sup>

Alternatively, surface states may be involved in the recombination reaction. Salvador and co-workers demonstrated that a single surface state level as well as a range of levels will give rise to apparent reaction orders that deviate from one.<sup>229</sup>

The electron lifetime is expected to decrease with increasing acceptor concentration, as was observed for triiodide<sup>178,216</sup> and TEMPO<sup>+</sup>.<sup>222</sup> Nakade et al. found, however, that the lifetime was independent of acceptor concentration in the case of a number of Co complexes as mediator.<sup>227</sup>

In a transient absorption spectroscopy study, Green et al. found that recombination of electrons in bare mesoporous TiO<sub>2</sub> with I<sub>2</sub> is 2 orders of magnitude faster than that with I<sub>3</sub><sup>-</sup>.<sup>230</sup> The kinetics appeared to be first order with respect to the I<sub>2</sub> concentration. The I<sub>2</sub><sup>-</sup> intermediate was not observed in their experiment, which may be explained by a process where iodine adsorbs dissociatively on the TiO<sub>2</sub> surface, followed by reduction of bound iodine atoms to iodide.

Dyes adsorbed at the mesoporous TiO<sub>2</sub> electrode will usually affect the reduction reaction of triiodide. There are several reasons: First, adsorption of dye can lead to changes in the position of the conduction band edge of TiO<sub>2</sub>, due to changes in the surface charge. Second, dyes can promote reduction of I<sub>3</sub><sup>-</sup> at TiO<sub>2</sub>. Most organic dyes<sup>181,231</sup> and phthalocyanines<sup>232</sup> give shorter electron lifetimes in DSCs than the standard Ru(dcbpy)<sub>2</sub>(NCS)<sub>2</sub> sensitizer. O'Regan and co-workers proposed that such dyes provide a binding site for iodine near the TiO<sub>2</sub> surface, leading to accelerated recombination.<sup>233,234</sup> They presented evidence for dye–iodine binding mechanism by studying two heteroleptic Ru complexes that differed only by two atoms. By changing two oxygen atoms to two sulfur atoms in equivalent positions (a change from ether to thioether at a side group of one of the bipyridyl ligands), a 2-fold increase in the recombination rate and a 20–30 mV loss in  $V_{oc}$  were found. From literature, it is known that the binding constant between iodine and sulfur in ethylthioether is substantially higher than that between iodine and oxygen in ethylether. The iodine–dye complexation and its role in DSC devices requires further investigation and understanding so that improved dyes can be designed for iodide/triiodide-based DSCs.

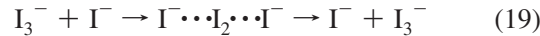
The TiO<sub>2</sub> particle size is expected to have a significant effect on electron lifetime. Zhu et al. found that, at a fixed potential, more dark current is generated using smaller particles for the same thickness of mesoporous film, as expected based on the increased surface area.<sup>196</sup> Nakade et al., however, found a decrease in lifetime for increasing particle size.<sup>235</sup> They plotted lifetimes for different films as a function of generated short-circuit photocurrent per volume TiO<sub>2</sub>, rather than comparing lifetime at the same  $V_{oc}$ .

#### 4.7. Transport of the Redox Mediator and Reactions at the Counter Electrode: Reaction 7

Transport of the redox mediator between the electrodes is mainly driven by diffusion. Typical redox electrolytes have a high conductivity and ionic strength so that the influence of the electric field and transport by migration is negligible. In viscous electrolytes, such as ionic liquids, diffusion coefficients can be too low to maintain a sufficiently large flux of redox components, which can limit the photocurrent of the DSC.<sup>236</sup> Transport of the redox mediator in the electrolyte gives rise to a diffusion impedance, which acts as a series resistance in the solar cell. The diffusion impedance depends on the diffusion coefficient and concentration of the redox mediator and on the distance between

the electrodes.<sup>237</sup> Han et al. optimized dye-sensitized solar cells with the help of impedance spectroscopy measurements and achieved a value for the diffusion resistance as low as 0.7 Ω cm<sup>2</sup> by minimizing the distance between the working and counter electrodes, while a separation of 20 μm led to a value of 2 Ω cm<sup>2</sup>.<sup>238</sup>

In the case of the iodide/triiodide electrolyte, an alternative type of charge transport can occur when high mediator concentrations are used, the Grotthus mechanism. In this case, charge transport corresponds to formation and cleavage of chemical bonds:



In viscous electrolytes, such as ionic liquid based electrolytes, this mechanism can contribute significantly to charge transport in the electrolyte.<sup>236,239–241</sup>

In amorphous hole conductors that replace the electrolyte in solid-state DSCs, charge transport takes place through hole hopping. In the most investigated molecular hole conductor for DSCs, spiro-MeOTAD, mobility is increased 10-fold by the addition of a Li salt.<sup>242</sup> Fabregat et al. determined the resistance in an illuminated spiro-MeOTAD solid-state DSC by impedance spectroscopy and found a resistance on the order of 100 Ω cm<sup>2</sup> under illumination.<sup>226</sup> Although this value appears to be unrealistically high, it points to the fact that resistance in the hole transporting layer can be a problem in solid-state DSCs.

At the counter electrode in standard DSCs, triiodide is reduced to iodide:



The counter electrode must be catalytically active to ensure rapid reaction and low overpotential. Pt is a suitable catalyst for reaction 20, as iodine (triiodide) dissociates to iodine atoms (iodine atoms and iodide) upon adsorption, enabling a rapid one-electron reduction. The charge transfer reaction at the counter electrode leads to a series resistance in the DSC, the charge transfer resistance  $R_{CT}$ . An overpotential  $\eta$  is needed to drive reaction 20 at a certain current density  $J$ . At small overpotentials,  $\eta$  is linear with  $J$  and a charge transfer resistance can be defined,  $R_{CT} = \eta/J = RT/nFJ_0$ , where  $n = 2$  for reaction 20 and  $J_0$  is the exchange current density. Ideally,  $R_{CT}$  should be  $\leq 1$  Ω cm<sup>2</sup> to avoid significant losses. A poor counter electrode will affect the current–voltage ( $I$ – $V$ ) characteristics of the DSC by lowering the fill factor.

## 5. Materials Development

### 5.1. Nanostructured Metal Oxide Electrodes

The key to the breakthrough for DSCs in 1991<sup>1</sup> was the use of a mesoporous TiO<sub>2</sub> electrode, with a high internal surface area, to support the monolayer of a sensitizer. Typically, the increase of surface area by using mesoporous electrodes is about a factor 1000 in DSCs. TiO<sub>2</sub> still gives the highest efficiencies, but many other metal oxide systems have been tested, such as ZnO, SnO<sub>2</sub>, and Nb<sub>2</sub>O<sub>5</sub>. Besides these simple oxides, ternary oxides, such as SrTiO<sub>3</sub> and Zn<sub>2</sub>SnO<sub>4</sub>, have been investigated, as well as core–shell structures, such as ZnO-coated SnO<sub>2</sub>. For recent reviews on the development of nanostructured metal oxide electrodes for DSC, the reader is referred to refs 72–74 and 243.

During the last years, large efforts have been paid to optimize the morphology of the nanostructured electrode and a large range of nanostructures has been tested, spanning from random assemblies of nanoparticles to organized arrays of nanotubes and single-crystalline nanorods. These studies are motivated by the expectation of an improved and directed charge transport along the rods and tubes and by an improved pore filling of hole conductor materials for solid-state DSC. General reviews for preparation techniques and structures are, for example, Chen et al. for  $\text{TiO}_2$ <sup>244</sup> and Ozgur et al. for  $\text{ZnO}$ .<sup>245</sup> Here we will give a short overview on the development of nanostructured  $\text{TiO}_2$ ,  $\text{ZnO}$ , and other metal oxides for DSCs.

### 5.1.1. $\text{TiO}_2$

$\text{TiO}_2$  is a stable, nontoxic oxide, which has a high refractive index ( $n = 2.4\text{--}2.5$ ) and is widely used as a white pigment in paint, toothpaste, sunscreen, self-cleaning materials, and food (E171). Several crystal forms of  $\text{TiO}_2$  occur naturally: rutile, anatase, and brookite. Rutile is the thermodynamically most stable form. Anatase is, however, the preferred structure in DSCs, because it has a larger bandgap (3.2 vs 3.0 eV for rutile) and a higher conduction band edge energy,  $E_c$ . This leads to a higher Fermi level and  $V_{oc}$  in DSCs for the same conduction band electron concentration. Unless stated otherwise,  $\text{TiO}_2$  in the anatase structure is used in the discussed investigations.

In recent years, substantial progress has been made in the development of methods to synthesize new anatase nanostructures such as nanoparticles, nanorods, nanowires, nanobowls, nanosheets, and nanotubes and mesoporous materials such as aerogels, inverse opals, and photonic materials. These methods include sol-gel, micelle and inverse micelle, hydrothermal, solvothermal, sonochemical, microwave deposition techniques, direct oxidation, chemical vapor deposition, physical vapor deposition, and electrodeposition.

For dye-sensitized solar cells, the most common technique for preparation of  $\text{TiO}_2$  nanoparticles is the hydrolysis of a titanium precursor such as titanium(IV) alkoxide with excess water catalyzed by acid or base, followed by hydrothermal growth and crystallization. Acid or basic hydrolysis gives materials of different shapes and properties, and the rate of hydrolysis, temperature, and water content can be tuned to produce particles of different sizes. Transmission electron microscopy measurements revealed that for  $\text{TiO}_2$  nanoparticles prepared under acidic conditions, crystalline anatase particles are formed exposing mainly the  $\langle 101 \rangle$  surface.<sup>246,247</sup> Preparation in acetic acid compared with nitric acid increased the proportion of the  $\langle 101 \rangle$  face about 3-fold.<sup>247</sup> The differences can be explained by different growth rates: in acetic acid crystal growth was enhanced in the  $\langle 001 \rangle$  direction compared with the growth in the presence of nitric acid.<sup>248</sup> The produced particles are formulated in a paste with polymer additives and deposited onto conducting glass substrates using doctor blading or screen printing techniques. Finally, the film is sintered at about 450 °C in air to remove organic components and to make electrical connection between the nanoparticles. Hore et al. found that base-catalyzed conditions led to mesoporous  $\text{TiO}_2$  that gave slower recombination in DSCs and higher  $V_{oc}$  but a reduced dye adsorption compared with the acid-catalyzed  $\text{TiO}_2$ .<sup>249</sup> The porosity of the resulting mesoporous film can be controlled by changing the amount of polymer in the paste and is ideally

about 50–60%. Higher porosities lead to less interconnects between the particles and a decrease in charge collection efficiency.<sup>250</sup>

Since 1991, improvements to the  $\text{TiO}_2$  electrode in the DSC have been made in terms of light absorption, light scattering, charge transport, suppression of charge recombination, and improvement of the interfacial energetics. For state-of-the-art DSCs, the employed architecture of the mesoporous  $\text{TiO}_2$  electrode is as follows:

- (a) A  $\text{TiO}_2$  blocking layer (thickness ~50 nm), coating the FTO plate to prevent contact between the redox mediator in the electrolyte and the FTO, prepared by chemical bath deposition, spray pyrolysis, or sputtering.<sup>251</sup>
- (b) A light absorption layer consisting of a ~10 μm thick film of mesoporous  $\text{TiO}_2$  with ~20 nm particle size that provides a large surface area for sensitizer adsorption and good electron transport to the substrate.
- (c) A light scattering layer on the top of the mesoporous film, consisting of a ~3 μm porous layer containing ~400 nm sized  $\text{TiO}_2$  particles.<sup>252</sup> Voids of similar size in a mesoporous film can also give effective light scattering.<sup>253</sup>
- (d) An ultrathin overcoating of  $\text{TiO}_2$  on the whole structure, deposited by means of chemical bath deposition (using aqueous  $\text{TiCl}_4$ ), followed by heat treatment.

The  $\text{TiCl}_4$  treatment has been in use since the publication of Nazeeruddin et al. in 1993,<sup>40</sup> where it was used to improve the performance of the relatively impure Degussa P25  $\text{TiO}_2$  nanoparticles. Earlier, Kavan et al. developed a  $\text{TiCl}_3$ -based electrodeposition method that gave essentially the same result but was more complex to perform.<sup>254</sup> The  $\text{TiCl}_4$  treatment leads to the deposition of an ultrapure  $\text{TiO}_2$  shell (~1 nm) on the mesoporous  $\text{TiO}_2$ <sup>255</sup> (which may contain impurities or have carbon residues at the surface). The procedure leads to increased dye adsorption due to increased roughness despite a decrease in BET area (in m<sup>2</sup>/g).<sup>246,251,255</sup> It lowers the acceptor levels in  $\text{TiO}_2$  in energy,<sup>255,256</sup> which can improve the injection efficiency. It also improves electron lifetime significantly, leading to an increase in the electron diffusion length.<sup>256,257</sup>

Several methods have been developed that allow for low-temperature deposition of mesoporous  $\text{TiO}_2$  films, which are of special interest when using flexible polymer substrates. A compression technique using commercial P25 powder was developed by Lindström et al.<sup>258,259</sup> Mechanically stable  $\text{TiO}_2$  films were obtained by compressing a powderous film using a 500–1500 kg cm<sup>-2</sup> pressure, yielding solar cell efficiencies of about 3% without sintering. Arakawa and co-workers further optimized this technique and achieved 7.4% efficiency for flexible DSC using an ITO/PEN substrate.<sup>260</sup> Pichot et al. investigated low-temperature sintered  $\text{TiO}_2$  films ( $T = 100$  °C) prepared by spin coating a  $\text{TiO}_2$  colloid solution and obtained 1.2% efficiency for a 1 μm thick film.<sup>261</sup> Minoura and co-workers developed a paste of  $\text{TiO}_2$  particles with a Ti-precursor, which upon application onto an FTO substrate and hydrothermal crystallization at 100 °C gave stable mesoporous films that yielded efficiencies of up to 4.2%.<sup>262</sup> Park et al. developed a method using a highly viscous  $\text{TiO}_2$  paste without binder and obtained efficiencies of 2.5% for a 4 μm thick electrode dried at 150 °C.<sup>263</sup>

In a comparative study of rutile- and anatase-based DSCs, Park et al. found similar  $V_{oc}$  values, although the conduction band edge,  $E_c$ , is 0.1–0.2 eV higher in anatase, while the

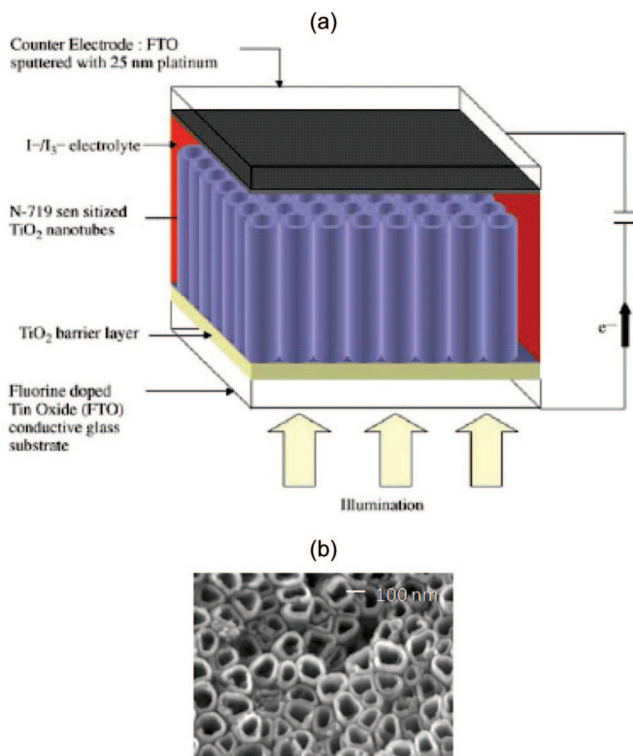


**Figure 14.** (a) Schematic diagram of a nanotube array architecture as a photoelectrode in DSCs.<sup>267</sup> Note that the nanotube array is on top of a compact TiO<sub>2</sub> blocking layer, which is deposited on the FTO contact. This makes it possible to irradiate the photoelectrode through the FTO glass, which is the preferred illumination orientation. (b) Scanning electron microscopy image (top view) of TiO<sub>2</sub> nanotubes. Reprinted from ref 267, copyright 2006, with permission from Elsevier.

observed photocurrent was lower for rutile TiO<sub>2</sub> by ca. 30%.<sup>264</sup> The results were ascribed to the larger particle size and lower internal surface area of the rutile electrode and therefore a decreased amount of dye loading. Mesoporous brookite TiO<sub>2</sub> (containing 25% anatase) electrode gave DSCs that yielded efficiencies of up to 4.1%.<sup>265</sup>

Well-ordered mesoporous TiO<sub>2</sub> structures with a narrow pore size distribution can be obtained using polymer-templated synthesis. Zukalova et al.<sup>266</sup> used an amphiphilic triblock copolymer of ethylene oxide and propylene oxide (Pluronic 123) to prepare ordered TiO<sub>2</sub> structures with a pore size of about 6 nm. With a TiO<sub>2</sub> film thickness of 1  $\mu$ m, a roughness factor of 460 was obtained, and when this film was used in DSCs, power conversion efficiencies of 4.0% were reached, while standard mesoporous films with the same thickness gave 2.7% under the same test conditions.

Ordered arrays of vertically orientated TiO<sub>2</sub> nanotubes can be grown by potentiostatic anodization of Ti metal in fluoride-based electrolytes.<sup>267–274</sup> TiO<sub>2</sub> nanotubes are typically grown using Ti foil, but growth can also be obtained from Ti thin films deposited on FTO-coated conducting glass.<sup>268,269</sup> The length of the nanotubes (<1000  $\mu$ m), wall thickness (5–34 nm), pore diameter (12–240 nm), and tube-to-tube spacing (0–10 nm) can be controlled by the preparation conditions, for example, the anodization potential, time, and temperature, and the electrolyte composition (water content, cation size, conductivity, and viscosity). Initially, TiO<sub>2</sub> nanotubes are usually amorphous, crystallizing upon heat treatment. The concept of a vectorial electron transfer through a nanotube TiO<sub>2</sub> electrode and an SEM image of TiO<sub>2</sub> nanotubes are shown in Figure 14.

For a TiO<sub>2</sub> nanotube-based DSC on a Ti substrate, a 6.9% photoconversion efficiency (N719 dye) was achieved.<sup>271</sup> This device was illuminated through the counter electrode resulting in absorption losses from the counter electrode and the electrolyte. For nanotubes grown on a FTO substrate (thickness 1.1  $\mu$ m), an efficiency of 4.1% was obtained using TiCl<sub>4</sub> after treatment and a strongly absorbing dye.<sup>269</sup>

Zhu et al. investigated the effect of capillary stress occurring during drying on the properties of nanotube-based DSCs. Faster electron transport was observed upon supercritical drying, due to decreased clustering of TiO<sub>2</sub> nanotubes.<sup>274</sup> Jennings et al. investigated the transport, trapping, and transfer of electrons in nanotube-based DSCs in detail.<sup>272</sup> They found that titania nanotube cells exhibit high collection efficiencies for photoinjected electrons and estimated an impressively long electron diffusion length on the order of 100  $\mu$ m. This means that relatively thick nanotube films can be prepared, increasing the light-harvesting efficiency without losing charge carriers to recombination before they are collected at the back contact.

TiO<sub>2</sub> nanotubes can also be prepared using alumina templates. The templates are prepared by anodization of aluminum films on FTO and subsequent immersion in a titanium precursor solution, followed by sintering in a furnace at 400 °C. The alumina template is then removed by immersing the samples in 6 M NaOH solution. Nanotubes and nanorods can be prepared in this way.<sup>273</sup> The roughness factors in these studies were relatively low, ca. 27 for the nanorods and ca. 63 for the nanotubes. Nevertheless, sensitized with the N719 dye, the nanorod DSC gave an overall conversion efficiency of 5.4%, nanotubes 4.5%, and for comparison a nanoparticle DSC 4.7%.

Atomic layer deposition (ALD) is an interesting technique to prepare well-defined and ordered nanostructures. ALD enables controlled layer by layer deposition of metal oxides onto templates such as silica aerogels but also deposition on nanoparticle and nanorod assemblies to form core–shell structures. For example, ALD can be employed to coat aerogel templates conformally with various thicknesses of TiO<sub>2</sub> with subnanometer precision. Hamann et al. used an aerogel template with a porosity of >90%, allowing volume for growth of the TiO<sub>2</sub> layer without clogging the pores.<sup>275</sup> DSCs were prepared reaching efficiencies of 4.3%.

### 5.1.2. ZnO

Historically, ZnO was one of the first semiconductors used in dye-sensitized solar cells. The bandgap and conduction band edge of ZnO is similar to that of TiO<sub>2</sub> (anatase). ZnO has a higher electron mobility than TiO<sub>2</sub>, which should favor electron transport. The chemical stability of ZnO is rather poor compared with that of TiO<sub>2</sub>; it dissolves under both acidic and basic conditions. The use of ZnO in DSCs has increased dramatically in recent years, and in terms of number of publications, ZnO is so far the runner up to TiO<sub>2</sub>. This can be mainly attributed to the relative ease of synthesizing highly crystalline ZnO (in the wurtzite structure) with different morphologies, such as nanoparticles, nanowires, nanorods, nanotubes, tetrapods, nanoflowers, nanosheets, and branched nanostructures. Nanostructured ZnO has been synthesized via a wide range of techniques.

Mesoporous ZnO electrodes can be prepared from a paste containing ZnO nanoparticles, followed by doctor-blading or screen printing onto FTO substrates and sintering. The best result so far was reported by Saito and Fujihara who

used a commercial ZnO powder (20 nm sized particles) and 90 min dye adsorption time at 60 °C (0.3 mM N719 in ethanol).<sup>276</sup> They obtained 6.6% efficiency at AM 1.5 G (100 mW cm<sup>-2</sup>). In earlier work, longer dye-adsorption times were used, and abnormal dye uptake was observed. Keis et al. found that dye precipitation can take place in the ZnO mesoporous structure.<sup>277</sup> Some dissolution of ZnO by the acidic carboxylic anchoring groups of the sensitizer can take place. The resulting Zn<sup>2+</sup> ions form insoluble complexes with the N3/N719 dye, causing precipitation of these complexes in the pores of the film. This gives rise to a filter effect (inactive dye molecules), so that net yield for charge carrier injection is decreased, whereas the light-harvesting efficiency is increased during the sensitization process due to the large number of dye molecules in the film. Thus, careful control of the dye adsorption conditions is necessary for ZnO-based DSCs. Preferably, sensitizers with an anchoring group without protons should be developed. Notably, some organic dyes do not precipitate in the presence of Zn<sup>2+</sup> ions and can therefore be used more easily in combination with ZnO.<sup>278</sup> Nguyen et al. designed a Ru complex with only one carboxylated bipyridyl ligand and found much reduced dye precipitation onto the ZnO electrode compared with N3.<sup>279</sup> They obtained a solar cell efficiency of 4.0%. Park and co-workers improved the chemical stability of ZnO by addition of a SiO<sub>2</sub> shell onto the ZnO colloids.<sup>280</sup> The SiO<sub>2</sub>-coated ZnO films leached less Zn<sup>2+</sup> in acidic solutions, and solar cells with an efficiency up to 5.2% were made with the SiO<sub>2</sub>-modified material, compared with <1% for the initial ZnO under the same experimental conditions.

Electrodeposition is a low-temperature deposition method, where the ZnO is formed directly on the substrate. Yoshida and co-workers developed a successful method based on the cathodic electrodeposition of ZnO from aqueous zinc salt solutions in the presence of oxidants and water-soluble dye molecules.<sup>281–283</sup> This method yields ordered porous ZnO nanostructures that are very suitable for dye-sensitized solar cells. Best results are obtained by desorption of the (templating) dye followed by adsorption of the actual sensitizer. Efficiencies as high as 5.6% have been obtained using electrodeposited ZnO films in combination with the organic dye D149.<sup>281</sup>

Growth of single-crystalline ZnO nanorods directly onto a substrate can be obtained using gas-phase deposition techniques and chemical bath deposition. When they were applied in dye-sensitized solar cells, measured electron transport time in these systems was found to be much faster than in comparable mesoporous ZnO films.<sup>284–286</sup> The measured time constants are probably  $RC$ -times, arising from the capacity ( $C$ ) of the nanorods and the resistance ( $R$ ) of the rods and the substrate. ZnO nanorods appear to be inherently n-doped, and the presence of a space-charge layer cannot be excluded. Fast electron transport was also measured by impedance spectroscopy on DSCs based on polycrystalline ZnO nanotubes, with diffusion coefficients of up to 0.4 cm<sup>2</sup> s<sup>-1</sup>.<sup>287</sup> Law et al. grew ZnO nanowires of about 20 μm length using chemical bath deposition and obtained efficiencies of up to 1.5% in DSCs.<sup>288</sup> Later they improved the result by addition of a shell of Al<sub>2</sub>O<sub>3</sub> or TiO<sub>2</sub> deposited by atomic layer deposition, where TiO<sub>2</sub> gave the best result of 2.3%.<sup>289</sup> ZnO nanorod, nanotube, and nanowire DSCs are so far characterized by relatively low fill factors (typically <0.6).

### 5.1.3. Other Metal Oxides

SnO<sub>2</sub> is a chemically stable oxide that has a conduction band edge  $E_c$  about 0.5 eV lower than that of TiO<sub>2</sub> (anatase). It can therefore be used in combination with dyes with low-lying LUMOs that inject poorly into TiO<sub>2</sub>, such as some perylene sensitizers.<sup>290</sup> Best reported efficiency for a dye-sensitized SnO<sub>2</sub> DSC is 2.8% for a cell sensitized with the organic dye D149 (N719 gave 1.2% in the same study).<sup>291</sup> In combination with the iodide/triiodide redox couple, the open circuit potential will be low in a SnO<sub>2</sub>-based DSC, at best ca. 400 mV. A significant improvement in  $V_{oc}$  and efficiency can be obtained by covering the mesoporous SnO<sub>2</sub> with a very thin shell of another metal oxide, such as ZnO, MgO, and Al<sub>2</sub>O<sub>3</sub>.<sup>292–295</sup> Best efficiencies so far have been obtained using ZnO-coated SnO<sub>2</sub> with efficiencies up to 6.3%.<sup>294</sup> It is not certain that a ZnO shell is formed in this case, the formation of a Zn<sub>2</sub>SnO<sub>4</sub> shell is also possible. Zinc stannate (Zn<sub>2</sub>SnO<sub>4</sub>) is a chemically stable wide bandgap material. In DSC tests, efficiencies up to 3.8% were obtained for this material.<sup>296</sup> Photoelectrochemical characterization suggests that it has a higher conduction band edge energy than TiO<sub>2</sub>.<sup>297</sup>

DSCs based on SrTiO<sub>3</sub>, which has a 0.2 eV higher conduction band edge than TiO<sub>2</sub> (anatase), gave good  $V_{oc}$  but were less efficient than comparable TiO<sub>2</sub>-based DSCs, efficiencies of 1.8% and 6.0%, respectively. Also Nb<sub>2</sub>O<sub>5</sub> exhibits a higher  $E_c$ . Efficiencies in DSCs of up to 5% (at 0.1 sun) are reported.<sup>298</sup>

## 5.2. Dyes

As one of the crucial parts in dye-sensitized solar cells (DSCs), the photosensitizer should fulfill some essential characteristics:

- (1) The absorption spectrum of the photosensitizer should cover the whole visible region and even the part of the near-infrared (NIR).
- (2) The photosensitizer should have anchoring groups (−COOH, −H<sub>2</sub>PO<sub>3</sub>, −SO<sub>3</sub>H, etc.) to strongly bind the dye onto the semiconductor surface.
- (3) The excited state level of the photosensitizer should be higher in energy than the conduction band edge of n-type semiconductor (n-type DSCs), so that an efficient electron transfer process between the excited dye and conduction band (CB) of the semiconductor can take place. In contrast, for p-type DSCs, the HOMO level of the photosensitizer should be at more positive potential than the valence band (VB) level of p-type semiconductor.
- (4) For dye regeneration, the oxidized state level of the photosensitizer must be more positive than the redox potential of electrolyte.
- (5) Unfavorable dye aggregation on the semiconductor surface should be avoided through optimization of the molecular structure of the dye or by addition of coadsorbers that prevent aggregation. Dye aggregates can, however, be controlled (H- and J-aggregates) leading to an improved performance compared with a monomer dye layer as, for example, described in ref 299.
- (6) The photosensitizer should be photostable, and electrochemical and thermal stability are also required.

Based on these requirements, many different photosensitizers including metal complexes, porphyrins, phthalocya-

nines and metal-free organic dyes have been designed and applied to DSCs in the past decades.

### 5.2.1. Metal Complexes

Metal complexes and ruthenium (Ru(II)) complexes, in particular, have been investigated intensively for DSC application because of their broad absorption spectra and favorable photovoltaic properties. Generally, metal complex photosensitizers consist of a central metal ion with ancillary ligands having at least one anchoring group. Light absorption in the visible part of the solar spectrum is due to a metal to ligand charge transfer (MLCT) process. The central metal ion is therefore a crucial part of the overall properties of the complexes. Ancillary ligands, typically bipyridines or terpyridines, can be tuned by different substituents (alkyl, aryl, heterocycle, etc.) to change the photophysical and electrochemical properties and thus improve the photovoltaic performance. Anchoring groups are employed to link the dye with the semiconductor and facilitate the injection of the excited electron into the CB of the semiconductor. One can modify any part of the complex to tune the energy levels of the MLCT states and to optimize electron injection and dye regeneration kinetics. An excellent review on the photophysical properties of Ru complexes and their influences on DSC has recently been published by Ardo and Meyer.<sup>7</sup>

**5.2.1.1. Ruthenium (Ru) Complexes.** Among the metal complexes, Ru complexes<sup>47,77,116,300–347</sup> have shown the best photovoltaic properties: a broad absorption spectrum, suitable excited and ground state energy levels, relatively long excited-state lifetime, and good (electro)chemical stability. Several Ru complexes used in DSCs have reached more than 10% solar cell efficiency under standard measurement conditions. Some representative Ru complex photosensitizers are collected in Table 1.

Ru complexes with carboxylated bipyridine ligands were first used for sensitization of TiO<sub>2</sub> single crystals in 1979.<sup>348</sup> Desilvestro et al. used in 1985 a similar dye, with three carboxylated bipyridine ligands, to obtain the first reported efficient dye-sensitized solar cell with an IPCE of 44%.<sup>37</sup> By improving the light absorption, using a trinuclear Ru complex<sup>38,39</sup> (dye **1**), a novel mesoporous TiO<sub>2</sub> electrode, and an organic solvent based electrolyte, O'Regan and Grätzel achieved in 1991 7.1–7.9% solar cell efficiency in their breakthrough report.<sup>1</sup> In 1993, Grätzel and co-workers<sup>40</sup> published a series of mononuclear Ru complexes, *cis*-(X)<sub>2</sub>bis(2,2'-bipyridyl-4,4'-dicarboxylate)ruthenium(II), where X are Cl, Br, I, CN, and SCN. The thiocyanato derivative, *cis*-(SCN)<sub>2</sub>bis(2,2'-bipyridyl-4,4'-dicarboxylate)ruthenium(II), coded as N3 (dye **2**), was found to exhibit outstanding properties, such as broad visible light absorption spectrum and a photon-to-current conversion efficiency (IPCE) spectrum extending to 800 nm, sufficiently long excited state lifetime ( $\sim$ 20 ns), and strong adsorption on the semiconductor surface due to binding with up to four carboxyl groups. As a result, a solar-to-electric energy conversion efficiency of 10% was first attained with the N3 dye.

Many efforts have been made to change the ligands of Ru complexes and optimize the photosensitizers. To further improve the efficiency of DSCs, extending the spectral response region of the sensitizer to the near-IR region is desirable. Therefore, Grätzel and co-workers<sup>349</sup> designed the N749 dye (dye **3**), also called the "black dye", in which the Ru center has three thiocyanato ligands and one terpyridine

ligand substituted with three carboxyl groups. They found that the red shift in the MLCT band is due to the decrease in the  $\pi^*$  level of the terpyridine ligand and an increase in the energy of the t<sub>2g</sub> metal orbital. Based on this dye, an IPCE spectrum was obtained over the whole visible range extending into the near-IR region up to 920 nm and a 10.4% conversion efficiency ( $J_{sc} = 20 \text{ mA cm}^{-2}$ ,  $V_{oc} = 720 \text{ mV}$ , FF = 0.7) was achieved under AM 1.5 G, 100 mW cm<sup>-2</sup> irradiation.<sup>350</sup>

Nazeeruddin et al.<sup>351</sup> investigated the effect exerted by the proton content of the N3 dye on the performance of DSCs. The doubly protonated form, (Bu<sub>4</sub>N)<sub>2</sub>[Ru(dcbpyH)<sub>2</sub>(NCS)<sub>2</sub>]<sub>2</sub>, named N719 (dye **4**), exhibited an improved power conversion efficiency. The study showed furthermore that deprotonation of the carboxylic acid groups of the N3 dye shifted the oxidation and reduction potentials to more negative potentials for dyes in solution. The N3 and N719 dyes are considered as reference dyes for DSC and are used as a base for designing other Ru photosensitizers by changing ancillary ligands.

Arakawa and co-workers developed a series of Ru complexes employing phenanthroline ligands and studied systematically the effect of the position and the number of carboxyl groups attached to the phenanthroline ligand as an anchor on the photosensitizer performance.<sup>352–355</sup> Among these dyes, Ru(dcphen)<sub>2</sub>(NCS)<sub>2</sub>·(TBA)<sub>2</sub> (dye **5**), showed 6.6% power conversion efficiency ( $J_{sc} = 12.5 \text{ mA cm}^{-2}$ ,  $V_{oc} = 740 \text{ mV}$ , FF = 0.71) under standard AM 1.5 G irradiation. The maximum IPCE value was 78% at 526 nm. This result suggested that two carboxyl groups attached to phenanthroline ligands are necessary for effective electron injection.<sup>355</sup> This concept was developed further resulting in a number of efficient Ru complexes by other researchers.<sup>336,339</sup>

On the other hand, Grätzel and co-workers focused on adjusting the ancillary 2,2'-bipyridyl ligand with different substituents (alkyl, alkoxy, phenylene, etc.) to increase the molar extinction coefficient, suppress dye aggregation on the semiconductor, and optimize the redox potential of the photosensitizer. The amphiphilic heteroleptic ruthenium sensitizer, Z907 (dye **6**), demonstrated prominent thermal stability due to the introduction of two hydrophobic alkyl chains on the bipyridyl ligand.<sup>356–358</sup> In combination with hexadecyl phosphonic acid as a coadsorber, the dye maintained 7% power conversion efficiency under a long-term thermal stress measurement.<sup>357</sup> One strategy for increasing the light-harvesting efficiency is to increase the conjugation length of the ligand. To further extend the  $\pi$ -conjugated system of the bipyridine and enhance the harvesting of solar light, 3-methoxystyryl was introduced into the ancillary ligand to obtain a novel Ru dye, Z910 (dye **7**), which exhibited prominent efficiency (10.2%) and impressive stability. The study demonstrated that enhancing the molar extinction coefficient is a good strategy to improve the photovoltaic performance of Ru dyes.<sup>359</sup> Based on this conclusion, dyes **8–11** have been designed, synthesized, and tested and demonstrated good performance in DSC long-term stability.<sup>77,305,312,335,360–362</sup> Through introduction of the tri(ethylene oxide) methyl ether (TEOME) into the 2,2'-bipyridine ligand, a novel ion coordinating sensitizer, NaRu(4-carboxylic acid-4'-carboxylate)(4,4'-bis[(tri(ethylene glycol) methyl ether] methyl ether]-2,2'-bipyridine)-(NCS)<sub>2</sub> (dye **12**, coded as K51), was obtained.<sup>310</sup> This study revealed that the ion coordinating sensitizer, when incorporated in a DSC using a nonvolatile electrolyte or hole-transporting

material, exhibited a simulated full-sun power conversion efficiency of 7.8% or 3.8%, respectively, where the good performance in the solid state device was attributed to the ability of this sensitizer to coordinate lithium ions. To extend this concept of incorporating ion-coordinating side chains or crown ethers on molecules with larger  $\pi$ -conjugated systems, they developed another ion-coordinating sensitizer, dye **13** (coded as K60), which extended the  $\pi$ -conjugation system of the ligand to enhance the extinction coefficient of the dye and also decreased its solubility, impairing dye desorption.<sup>347</sup> With dye **13**, a power conversion efficiency value of 8.4% was obtained using a nonvolatile organic-solvent electrolyte under AM 1.5 G.

Barolo et al. developed a ruthenium complex with a tetradeятate ligand, *trans*-[Ru(L)(NCS)<sub>2</sub>], L = 4,4''-di-*tert*-butyl-4',4''-bis(carboxylic acid)-2,2':6',2''-quarterpyridine (dye **14**, coded N886).<sup>306</sup> This dye gave a panchromatic absorption spectrum (up to 900 nm) but gave a somewhat disappointing photocurrent of 11.8 mA cm<sup>-2</sup>, with correspondingly low IPCE with a maximum of 40%. The solar cell efficiency was 5.9%.

Nazeeruddin and co-workers reported a ruthenium(II) dye, **15**, [Ru(II)L<sub>2</sub>(NCS)<sub>2</sub>] (where L is 4,4'-bis(carboxyvinyl)-2,2'-bipyridine).<sup>301</sup> By tuning of the HOMO and the LUMO levels, the ruthenium sensitizer showed an enhanced spectral response and an increased molar extinction coefficient yielding close to 8.7% efficiency. Based on this complex, they further developed the system and prepared two new photosensitizers, K9 (dye **16**) and K23 (dye **17**),<sup>341</sup> which showed high short-circuit photocurrents in thin film DSCs in comparison with the Z907 due to increased molar extinction coefficients and enhanced spectral response in the visible and near-IR regions. The result suggested that there would be promising application in solid-state DSCs based on the two dyes.

Thelakkat, Durrant, and co-workers developed Ru dyes with triarylamine-based electron donor groups at the bipyridyl ligands and studied charge recombination kinetics and solar cell performance.<sup>300,317,320</sup> When the triarylamine moiety is connected with a conjugated link, a substantial increase of the extinction coefficient is found (about 2-fold).<sup>320</sup> Upon excitation of the dye and electron injection, rapid intramolecular hole transfer from the Ru center to the donor is found and a long-lived charge separation between photojected electrons and the oxidized donor group was observed. This appears to be a good approach for improving the efficiency in solid-state DSCs. Dyes **18** and **19** were applied in solid-state DSCs and achieved efficiencies of 1.8% and 2.6%<sup>317</sup> or 1.5% and 3.4%, respectively,<sup>320</sup> in separate studies. Under the same conditions, the N719 dye showed a much lower value, 0.7%. These results demonstrate that the introduction of triarylamine donor groups can slow the charge recombination by spatially separating the holes from the electrons in the semiconductor and thus improve the efficiency of solid-state DSCs. Applied in a liquid electrolyte DSC, a very similar Ru complex (dye **20**) achieved an overall efficiency of 10.3%.<sup>344</sup>

Wu and co-workers developed a series of Ru complexes (dyes **21**–**27**), where one of the bipyridyl ligands is substituted with alkyl thiophene, ethylene-dioxythienyl (EDOT), or carbazole.<sup>307,313,314,330</sup> The energy levels of the metal center and the LUMO of the ligands can be raised with incorporation of thiophene ligands, and as a consequence, the MLCT band will be red-shifted. Under identical

cell fabrication and measuring procedures, dye **21** gave an efficiency of 8.5%, dye **22** 9.0%, and dye **23** 7.4% (N3, 7.7%). The significant improvement in efficiency for the dye **22**-based DSC compared with the dye **23** demonstrates the important role of the EDOT moiety in the ancillary ligand of the ruthenium complex.<sup>314</sup> They also functionalized the thiophene-derived Ru complexes with a hole-transport moiety, alkyl-substituted carbazole, and obtained efficient sensitizers (dye **26** and **27**).<sup>330</sup> The efficiency of a liquid state DSC based on sensitizer **26** was 9.7% (N3, 8.5%).

A family of high molar extinction coefficient heteroleptic polypyridyl ruthenium sensitizers (dyes **28**–**33**) were reported by Wang and co-workers,<sup>332,333,337,338,340</sup> featuring conjugated electron-rich units in their ancillary ligands, such as alkyl thiophene, alkyl furan, alkyl selenophene, or alkyl thieno[3,2-*b*]thiophene. Dye **28** (coded as C101) achieved several new DSC benchmark levels under AM 1.5 G illumination: it gave 11.0% efficiency with an acetonitrile-based electrolyte, a long-term stable ( $\eta > 9\%$ ) device using a low volatility electrolyte, and a long-term stable ( $\eta \approx 7.4\%$ ) device employing an ionic liquid electrolyte. They found that because of the high extinction coefficients of the sensitizer, the TiO<sub>2</sub> film thickness may be reduced, which favors the charge collection efficiency.<sup>332</sup> Dye **33** (coded as C103) achieved an efficiency record of stable DSCs with low volatility and ionic liquid electrolyte. The DSC based on this dye showed 9.6–10.0% and 8.5–9.1% efficiencies under AM 1.5 G irradiation with low-volatility and solvent-free electrolytes, respectively. Furthermore, DSCs based on these dyes retained over 90% of the initial performance after 1000 h full sunlight soaking at 60 °C.<sup>337</sup>

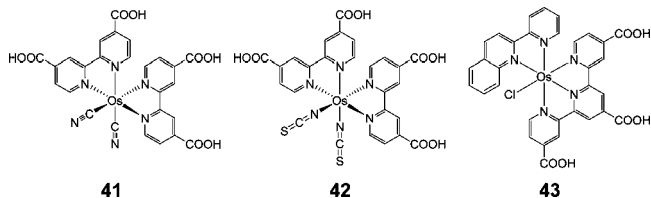
Ko and co-workers introduced organic antenna groups into Ru complexes, which significantly increased the extinction coefficient.<sup>319,331</sup> Among these dyes, dye **34** (coded as JK56) yielded 83% IPCE and 9.2% power conversion efficiency under AM 1.5 G (N719, 8.9%).

Masuda and co-workers designed and synthesized Ru complexes by introduction of a triarylamine functionality into the bipyridyl ligand.<sup>334,342,343</sup> Their study suggested that the new ligand acts as an electron donor in a manner similar to the thiocyanato ligands. With dye **35**, a DSC efficiency of 7.8% was obtained (N719, 7.9%).<sup>342</sup>

Yanagida and co-workers introduced the 2-thiophene-2-yl-vinyl into the ancillary ligand of Ru complexes and obtained dye **36** (HRS-q), which showed a 30% increase in extinction coefficient and a 10 nm red shift of its absorption spectrum compared with N719. An efficiency of 9.5% was achieved for dye **36** (N719, 8.9%).<sup>346</sup>

In order to facilitate dye/redox couple interaction and dye regeneration, Falaras and co-workers modified the ancillary ligand of a ruthenium tris-bipyridyl core with a cyclodextrin (CD) unit, obtaining dye **37**.<sup>316</sup> The dye exhibited an enhanced short-circuit photocurrent density, open-circuit photovoltage, and efficiency in comparison to the dye without the CD unit. Their results indicated that the CD moiety binds the iodide/triiodide redox couple into the CD cavity, which may facilitate dye regeneration.

Chi and co-workers reported a type of ruthenium complexes with tridentate bipyridine-pyrazolate ancillary ligands and attempted to elongate the  $\pi$ -conjugated system as well as to increase the molar extinction coefficient.<sup>315</sup> One of these dyes, dye **39**, showed a similar efficiency (5.7%) as N3 (6.0%) for comparable DSCs. In combination with its superior thermal and light-soaking stability, they concluded

**Figure 15.** Structures of Os complexes.

that “the concomitant tridentate binding properties offered by the bipyridine-pyrazolate ligand may render a more stable complexation, such that extending the lifespan of DSCs is expected”.<sup>315</sup>

Thiocyanate (SCN) ligands as the electron-donating groups have since 1993 been employed in the most efficient Ru dyes. However, the SCN seems to be the weakest part of Ru complex from a chemical stability point of view. Many efforts to replace the SCN donor ligands have been made. Cyclometalated ruthenium complexes,  $[\text{Ru}(\text{C}^{\wedge}\text{N}^{\wedge}\text{N})(\text{N}^{\wedge}\text{N}^{\wedge}\text{N})]$  type, were used for the first time as sensitizers in DSCs by Koten and co-workers.<sup>327</sup> The DSCs sensitized by dye **38** can give short-circuit currents comparable to that of the standard N719 dye with a  $\gamma$ -butyrolactone-based electrolyte. Although dye **38** does not have thiocyanate ligands, its absorption spectrum matches that of N719. Recently, a thiocyanate-free cyclometalated ruthenium sensitizer for DSCs was reported by Grätzel and co-workers, which exhibited an IPCE value of 83% and prominent conversion efficiency, 10.1% at AM 1.5 G.<sup>345</sup> This opens up possibilities to design the next generation of ruthenium sensitizers.

**5.2.1.2. Other Metal Complexes.** Many attempts have also been made to construct sensitizers with other metal ions, such as Os,<sup>127,363–365</sup> Re,<sup>366,367</sup> Fe,<sup>368–370</sup> Pt,<sup>371–374</sup> and Cu.<sup>375–377</sup>

Osmium (Os(II)) complexes were found to be promising photosensitizers for DSCs due to the prominent MLCT absorption band in comparison with the Ru complex. Some Os complexes are shown in Figure 15. Lewis and co-workers focused on developing this kind of sensitizer and reported a class of Os polypyridines.<sup>127,363,364</sup> Dyes **41** and **42**, obtained by replacing the Ru metal ion with Os, extended the light response region without sacrificing the good photovoltaic performance in DSCs. Bignozzi and co-workers also optimized Os complexes and obtained broad photoaction spectra. Dye **43** showed an extended IPCE spectrum up to 1100 nm.<sup>365</sup> Bignozzi and co-workers demonstrated that the lower photocurrent efficiency of Os complexes was due to slower electron transfer from the iodide electrolyte to the osmium dye cation.<sup>378</sup>

Re(I) complexes were employed to study the interfacial charge recombination and its driving force dependence by Hasselmann and Meyer.<sup>367,379</sup> Ferrere and co-workers engineered Fe(II) complexes for DSC application,<sup>368–370</sup> which showed a lower efficiency with IPCE values only around 10–11% in DSCs.

Square-planar platinum (Pt(II)) diimine dithiolate complexes (see Table 2) showed highly solvatochromic charge transfer (CT) absorption. Substituents on the diimine and the dithiolate could tune the electronic and photophysical properties of the LUMO and HOMO, respectively. Sugihara and co-workers introduced dyes **44–50** into DSCs and investigated the redox and optical properties of these Pt-based sensitizers in solution and the photovoltaic behavior on  $\text{TiO}_2$ .<sup>371</sup> The most efficient sensitizer in this series was dye **46**, which showed a high IPCE value of 47% at 500 nm.

**Table 2. Collection of Pt Photosensitizers**

Dye	Structure	Dye	Structure
<b>44</b>		<b>45</b>	
<b>46</b>		<b>47</b>	
<b>48</b>		<b>49</b>	
<b>50</b>		<b>51</b>	
<b>52</b>		<b>53</b>	
<b>54</b>		<b>55</b>	

However, its light-harvesting capacity at longer wavelengths ( $>650$  nm) was very poor. Dye **46** exhibited a photocurrent of  $7.0 \text{ mA cm}^{-2}$  and a photovoltage of 600 mV with a FF of 0.77 under AM 1.5 G, corresponding to an overall efficiency of 3.0%. Although the red-shifted absorption spectra of **49** and **50** cover the entire visible spectrum of solar light, the observed overall cell efficiency as well as the photocurrent and photovoltage values were very low compared with that of **46**, which was probably due to the sluggish halide oxidation rate and the fast recombination of the injected electron with the oxidized state of **49** and **50**. Subsequently, Robertson and co-workers modified this class of photosensitizers and reported the dyes **51–55**.<sup>372–374</sup> Dye **52** is the tetrabutylammonium salt of **51**. The charge recombination dynamics for **51** and **52** were very different, with the **51** and **52** sensitized films exhibiting recombination half times of  $1.7 \times 10^{-5}$  and 0.33 s, respectively. The slower recombination dynamics for **52** are indicative of weaker electronic coupling between the dye and the  $\text{TiO}_2$  surface, consistent with the lower dye coverage obtained with this dye.<sup>374</sup> However, dye **52** showed the better photovoltaic performance. They also studied the effect of changing the position of the bipyridyl substituents from 3,3' to 4,4' and 5,5' positions (**53**, **54**, and **55**, respectively) on the structural and electronic properties. The spectroelectrochemical study showed that the electron for the reduced dyes in all three complexes must be localized on the derivatized bipyridine moiety of the molecule.<sup>372</sup> When all three complexes were fabricated into DSCs, dye **53** with an intermediate dye loading value achieved the best efficiency, 0.64%.

Cu(I) complexes (see Figure 16) were introduced into DSCs by Sauvage and co-workers because of their similar photophysical properties to Ru complexes.<sup>375</sup> Sakaki and co-workers changed the position of anchoring groups ( $-\text{COOH}$ ) and synthesized several derivatives for DSCs. Dye **56** gave

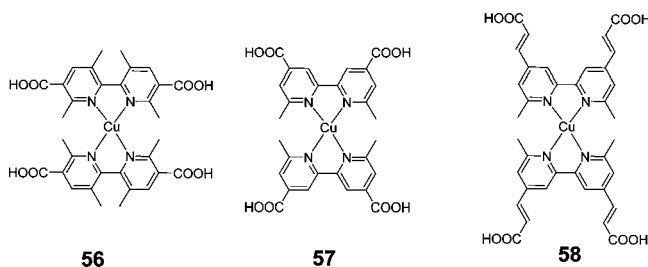


**Figure 16.** Structures of Cu complexes.

a photocurrent of  $4 \text{ mA cm}^{-2}$  and photovoltage of  $630 \text{ mV}$  under AM 1.5 G and an IPCE value of  $30\%$ .<sup>376</sup> Recently, Constable and co-workers reported the dyes **57** and **58**.<sup>377</sup> They found that the IPCE spectra and current–voltage characteristics for devices fabricated with dyes **57** and **58** were significantly different due to the different molar extinction coefficients of the two complexes. Dye **58** with a large  $\pi$ -conjugated system of ligands and high molar extinction coefficient obtained  $2.3\%$  efficiency with liquid electrolyte DSCs.<sup>377</sup>

### 5.2.2. Porphyrins and Phthalocyanines

One of the drawbacks of ruthenium complexes is the limited absorption in the near-infrared region of the solar spectrum. Porphyrin and phthalocyanine systems exhibit intense spectral response bands in the near-IR region and possess good chemical, photo-, and thermal stability, providing good potential candidates for photovoltaic applications.

**5.2.2.1. Porphyrins.** The introduction of porphyrins and chlorophylls as photosensitizers on DSCs is particularly interesting given their primary role in photosynthesis. Owing to appropriate LUMO and HOMO energy levels and very strong absorption of the Soret band in the  $400\text{--}450 \text{ nm}$  region, as well as the Q-band in the  $500\text{--}700 \text{ nm}$  region,<sup>380</sup> porphyrin derivatives can be suited as panchromatic photosensitizers for DSCs. Several studies have demonstrated that porphyrin dyes can show efficient photoinduced electron injection into the conduction band of  $\text{TiO}_2$ .<sup>381\text{--}384</sup> Some representative porphyrin photosensitizers are collected in Table 3.

Kay and Grätzel in pioneering work on mesoporphyrin IX dye (dye **59**) reported high IPCE values of over  $80\%$  and an efficiency value of  $2.6\%$ .<sup>385</sup> They pointed to the importance of using coadsorbers to prevent unfavorable aggregation of this dye. Dye **60** (TCPP),<sup>381,386,387</sup> without any metal ions, is the most common porphyrin photosensitizer for DSCs. Wamser and Cherian obtained IPCE values of  $55\%$  at the Soret peak and  $25\text{--}45\%$  at the Q-band, achieving an overall energy conversion efficiency of about  $3\%$ .<sup>381</sup>

Durrant and co-workers studied the different electron injection and charge recombination properties of **2** (N3), **60**, and **61** (Zn-TCPP) on  $\text{TiO}_2$ .<sup>384</sup> They found that the cation state of the porphyrin dyes was delocalized over the conjugated macrocycle. However, the indistinguishable electron recombination kinetics between these dyes indicated that the location of the cation within the sensitizer has only a minor influence. It is possible that the lower efficiency of porphyrin-sensitized DSCs was due to an increased probability of excited-state decay caused by dye aggregation on the  $\text{TiO}_2$  surface.

Koehorst and co-workers fabricated DSCs with Zn/free-base diporphyrin heterodimers (dyes **62** and **63**) and studied the antenna effect on DSC performance. The two dyes

showed similar IPCE values ascribed to a favorable light-collecting antenna effect.<sup>388</sup>

Bignozzi and co-workers constructed a series of free base porphyrins with different anchoring groups for DSCs.<sup>389</sup> They studied the effect of different anchoring groups and substitution positions on DSC performance. Dyes **60** and **64** with carboxylic and phosphonic functions, respectively, did not exhibit significant differences in DSC performance, which was probably because both dyes were electronically decoupled from  $\text{TiO}_2$  since the meso-aryl groups orientate perpendicularly to the porphyrin macrocycle. However, dyes **65** and **66** showed different IPCE values depending on the substitution position of the phosphonate anchoring groups. They pointed out that this could be due to the differences in the orientation and distance of the chromophore on the  $\text{TiO}_2$  surface imposed by the directionality of the anchoring groups. Dye **66** may lie closer to the surface of  $\text{TiO}_2$  than dye **65** with para-substituted porphyrin.

Waclawik and co-workers compared different porphyrin-containing DSCs.<sup>390</sup> They found that the N3 and porphyrin dye **60** generated very high IPCE values compared with dyes **67** and **68**, which could be ascribed to poor electronic coupling of the latter two sensitizers to the titania conduction band.

Recently, Nazeeruddin and co-workers developed a family of porphyrin dyes with different central metal ions ( $\text{Cu}(\text{II})$  or  $\text{Zn}(\text{II})$ ) and different anchoring groups ( $-\text{COOH}$  or  $-\text{PO}_3\text{H}_2$ ).<sup>391</sup> They concluded that for porphyrins with carboxylic binding groups, the diamagnetic metalloporphyrins containing Zn showed very high IPCE values in comparison to that of the paramagnetic metalloporphyrins containing Cu. Moreover, porphyrins with a phosphonate anchoring group showed lower efficiencies than those with a carboxylate anchoring group. Among these dyes, dye **69**-based DSCs fabricated in a THF dye bath achieved a higher IPCE value of  $75\%$  and overall efficiency of  $4.8\%$ .

Otero and co-workers studied the effect of free porphyrins and various metalloporphyrins in photoelectrochemical cells through adsorbing those dyes on  $\text{SnO}_2$ .<sup>392</sup> The IPCE values were highly dependent on the identity of the central metal ion. Kim and co-workers estimated the relative positions of the HOMO and LUMO levels in the donor and acceptor moieties of porphyrin analogues by using AM1 calculations.<sup>393</sup> The result suggests that the charge-separated state is one of the main factors affecting solar cell efficiency, which will provide structural guidelines for selecting the donor and acceptor moieties of porphyrin analogues.

Giribabu and co-workers employed the rhodanine acetic acid group as anchoring groups at different positions of free-base or zinc porphyrins for DSC applications. In related DSCs, the zinc porphyrins gave a better performance in comparison with the corresponding free-base dyads.<sup>394</sup>

Through modifying the *meso*-tetraphenylporphyrins by substitution at the  $\beta$ -position with functional groups, which could extend the  $\pi$  systems to enhance the red-absorbing Q bands due to the splitting of the four frontier molecular orbitals, Officer and co-workers synthesized a series of porphyrin photosensitizer.<sup>395,396</sup> Density functional theory (DFT) and time-dependent DFT (TDDFT) calculations reveals that the electrons in the LUMO orbitals of dyes **70** and **71** are stabilized and concentrated onto the substituent through  $\pi$ -conjugation, causing enhancement and red shifts of absorption spectra and increasing the possibility of electron transfer from the substituent. The cells based on **70** yielded

**Table 3.** Collection of Representative Porphyrin Photosensitizers

Dye	Structure	Dye	Structure	Dye	Structure	Dye	Structure
59		60		67		68	
61		62		69		70	
63		64		71		72	
65		66		73		74	
				75		76	
				77		78	

close to 85% IPCE with a corresponding overall efficiency of 5.6% under AM 1.5 G irradiation.<sup>397</sup> As a consequence, they further extended the  $\pi$  system in the  $\beta$ -position and obtained more efficient porphyrin sensitizers.<sup>396,398</sup> Dye 72 exhibited an IPCE value of up to 75% and an impressive efficiency of 7.1% in DSCs with a liquid electrolyte and achieved a conversion efficiency of 2.4% in solid-state DSCs. It proved that modification of the  $\beta$ -position of porphyrin is an effective strategy to optimize the energy levels and improve the efficiency of DSCs. Mozer and co-workers studied the reason why the porphyrin dyes showed lower photovoltage compared with Ru sensitizers.<sup>399</sup> Their results revealed that a significantly reduced electron lifetime in porphyrin-based DSCs is the main reason for their generally lower open circuit voltage.

Following the same strategy, Imahori and co-workers also optimized the porphyrin dyes by substituting the  $\beta$ -position of porphyrin with different  $\pi$  systems, such as thiienyl and furyl. The different  $\pi$ -bridges showed different effect on DSC performance due to variation of adsorption behavior and

saturated coverage on the TiO<sub>2</sub> surface. Dye 73 showed the highest IPCE value of ca. 65% and an efficiency of 3.1%.<sup>400</sup> Following this study, they further developed a series of naphthyl-fused zinc porphyrin<sup>401,402</sup> and quinoxaline moiety functionalized porphyrin photosensitizer,<sup>403</sup> which obtained good efficiencies in DSCs.

The role of para-alkyl substituents on *meso*-phenylporphyrin sensitized DSCs was studied by Ballester and co-workers, who discovered that the presence of hydrophobic alkyl chains on the molecular structures of porphyrins could decrease the recombination between the injected electrons and the electrolyte without influencing the electron recombination between the injected electrons and the oxidized dye regeneration.<sup>404</sup>

Also, Kim and co-workers investigated electronic and photovoltaic properties of functionalized porphyrins at *meso*- and  $\beta$ -positions with different carboxylic acid groups in DSCs and claimed that the effective electronic coupling through the bridge played an important role in the charge injection process.<sup>405</sup> The longer distance between the dyes

and the  $\text{TiO}_2$  surface exhibited better performance due to a slow charge recombination rate. Furthermore, the doubly diene substituted porphyrin at two  $\beta$ -positions achieved better photovoltaic performance than that of the mono- $\beta$ -dienylporphyrin. Among those porphyrin derivatives, dye **74** gave an overall conversion efficiency of 3.0% and a maximum IPCE value of 60% in the Soret band region.

Yeh and co-workers also designed and synthesized many meso- or  $\beta$ -derivatized porphyrins with a carboxyl group for DSCs.<sup>406</sup> Through adjustment of photophysical and electrochemical properties with different substitutes, dye **75** as one of these dyes, showed the best photovoltaic properties with 6.0% efficiency under AM 1.5 G illumination (N3, 6.1%).

To investigate the interfacial electron transfer, a family of zinc porphyrins with one to four  $\pi$ -conjugated phenylethynyl (PE) units as a linker of controlled length were synthesized and studied for DSCs by Lin and co-workers.<sup>407</sup> When these porphyrin photosensitizers were fabricated into DSC devices, the efficiency of these devices decreased systematically with increasing length of the linker, although the rates of electron injection between these dyes and  $\text{TiO}_2$  were equal. The best efficiency, 2.7%, was obtained by dye **76**.

Recently, Tan and co-workers reported several new porphyrin dyes with a D- $\pi$ -A structure: the porphyrin acted as a donor and cyanoacrylic acid acted as an acceptor/anchoring group; different thiophene derivatives acted as a  $\pi$  bridge to broaden the absorption of the dyes.<sup>408</sup> They found that the thiophene  $\pi$ -conjugation unit can extend the spectral response region of porphyrin dyes, and the alkyl chain on this unit can improve the photovoltaic performance of DSCs. Dye **77** without a hexyl group showed an efficiency of 4.3%. However, dye **78** containing the hexyl chain achieved higher efficiency of 5.2% and a maximum IPCE value of 72%.

**5.2.2.2. Phthalocyanines.** Phthalocyanines possess intense absorption in the Q-band (around 700 nm), as well as promising electrochemical, photochemical, and thermal properties, and are thus of interest to use as NIR photosensitizers for DSCs. The solubility of these dyes is normally very poor and needs to be improved by structural optimization in order to facilitate the dye-sensitization process. Another major problem with phthalocyanines is their strong tendency to aggregate on the semiconductor surface, which requires a coadsorber to suppress dye aggregation. To date, a large number of phthalocyanine dyes have been synthesized for applications in DSCs.<sup>233,409–424</sup> Zinc (Zn(II)) phthalocyanines have been studied widely by many groups.<sup>410,412,413,416–419</sup> Some phthalocyanine dyes used in DSC are listed in Table 4.

As the pioneering work, Grätzel and co-workers employed a Ru phthalocyanine photosensitizer (dye **79**) to fabricate the DSCs and obtained a high IPCE value exceeding 60%.<sup>409</sup> The most important result was that they established a new pathway for attaching phthalocyanines to semiconductor surfaces through axially attached pyridine ligands opening up a new way to improve the near-IR response of DSCs. They also developed an efficient Zn phthalocyanine dye (dye **80**), which showed a high IPCE of 45% in the NIR and a corresponding efficiency of 1%.<sup>410</sup>

Grennberg and co-workers<sup>411</sup> reported a series of Zn-free phthalocyanines with ester groups, which have better solubility than those with carboxyl groups in organic solvents. However, among these dyes, only dye **81** and **82** can adsorb on the semiconductor surface due to the limited interaction

**Table 4. A Collection of Representative Phthalocyanine Photosensitizers**

Dye	Structure	Dye	Structure
<b>79</b>		<b>80</b>	
<b>81</b>		<b>82</b>	
<b>83</b>		<b>84</b>	
<b>85</b>		<b>86</b>	
<b>87</b>		<b>88</b>	
<b>89</b>		<b>90</b>	

between the metal-free macrocyclic ring plane and semiconductor surface. A method for anchoring phthalocyanines substituted with ester groups was developed.<sup>412</sup> The  $\text{TiO}_2$  film is pretreated with  $(\text{CH}_3)_3\text{COLi}$  to change the surface hydroxyl groups into deprotonated oxygen anions, thus making the surface more reactive toward the ester-functionalized phthalocyanines. According to this method, dye **83** was used in DSCs and gave a 4.3% IPCE value at 690 nm.

Sun and co-workers synthesized a phthalocyanine dye with tyrosine groups, dye **84**.<sup>413</sup> The tyrosine group plays an important role in the photosynthetic oxygen-evolving photosystem II (PSII) reaction center, because it can donate an electron to the oxidized chlorophylls ( $\text{P}680^+$ ). The introduction of tyrosine units into phthalocyanine should result in an electron-transfer process from tyrosine to the oxidized ZnPc, thereby suppressing the back-electron transfer. Also the bigger substituting tyrosine groups can reduce the dye aggregation on the semiconductor surface. With dye **84**-based DSCs, an IPCE value of ~24% at 690 nm and an overall conversion efficiency of 0.54% were achieved. Sun and Sundström have also investigated the kinetics of this tyrosine-

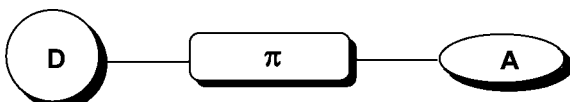


**Figure 17.** Schematic drawing of D- $\pi$ -A organic dyes.

substituted phthalocyanine dye on  $\text{TiO}_2$  by femtosecond spectroscopy. They found that the electron injection from the excited state of the phthalocyanine dye to the conduction band of  $\text{TiO}_2$  is very fast. However, the charge recombination is also fast. This might explain the reason the DSCs based on this type of dye have low efficiency.

In following work, Durrant and co-workers investigated several metal phthalocyanines containing axial ligands with a carboxyl group,<sup>233,420,422</sup> such as dyes **85** and **86**. Their study revealed that this kind of structure can suppress the dye aggregation, and they point out that a key factor in achieving further improvements in phthalocyanine-based DSCs is optimization of the triplet electron injection yield.

Nazeeruddin and co-workers developed the unsymmetrical zinc phthalocyanines (dyes **87** and **88**).<sup>417,421</sup> The **87**-based DSCs yielded a maximum IPCE value of 75% and a conversion efficiency of 3.0% under AM 1.5 G in a liquid-electrolyte cell. When the dye was used in solid-state DSCs, an IPCE value of 43% was achieved.

Recently, Imahori and co-workers reported two novel phthalocyanine dyes with high peripheral substitutions, dyes **89** and **90**, for DSCs.<sup>419</sup> The Zn-phthalocyanine dye **90** gave a functioning DSC with 0.57% power conversion efficiency and a 4.9% maximal IPCE in the near-infrared region. However, the metal-free phthalocyanine dye **89** did not work in DSCs due to the lower LUMO level than that the conduction band of  $\text{TiO}_2$ . The aggregation of these two dyes on  $\text{TiO}_2$  was effectively suppressed by the high degree of substitutions.

### 5.2.3. Organic Dyes

Organic dyes as an alternative to the noble Ru complexes sensitizers exhibit many advantages: (1) The molecular structures of organic dyes are in diverse form and can be easily designed and synthesized. (2) Concerning the cost and environment issues, organic dyes are superior to noble metal complexes. (3) The molar extinction coefficients of organic dyes are usually higher than those of Ru complexes, making them attractive for thin film and solid-state DSCs. (4) To date, organic dyes exhibit higher efficiencies compared with that of Ru complexes in p-type DSCs. Generally, donor- $\pi$ -bridge–acceptor (D- $\pi$ -A) structure is the common character of these organic dyes (see Figure 17). With this construction it is easy to design new dye structures, extend the absorption spectra, adjust the HOMO and LUMO levels and complete the intramolecular charge separation. When a dye absorbs light, intramolecular charge transfer occurs from subunit A to D through the  $\pi$ -bridge. For n-type DSCs, the excited dye injects the electron into the conduction band of the semiconductor via the electron acceptor group, A. However, in p-type DSCs, the excited dye captures the electron from the valence band of the semiconductor to complete the interfacial charge transfer. Many efforts have been made to change the different parts of organic dyes to optimize DSC performance. To date, hundreds of n-type organic dyes,<sup>63,425</sup> including coumarin dyes,<sup>130,132,426–435</sup> indoline dyes,<sup>57,436–447</sup> tetrahydroquinoline dyes,<sup>448–451</sup> triarylamine dyes,<sup>58,133,452–497</sup> heteroanthracene dyes,<sup>299,489,498–502</sup> carbazole

dyes,<sup>503–509</sup> *N,N*-dialkylaniline dyes,<sup>452,510–512</sup> hemicyanine dyes,<sup>513–521</sup> merocyanine dyes,<sup>522–525</sup> squaraine dyes,<sup>526–535</sup> perylene dyes,<sup>290,536–543</sup> anthraquinone dyes,<sup>544</sup> boradiazaindacene (BODIPY) dyes,<sup>545,546</sup> oligothiophene dyes,<sup>547,548</sup> polymeric dyes,<sup>549–555</sup> and natural dyes<sup>556–564</sup> have been adopted to act as sensitizers for DSCs and have obtained impressive efficiencies. Sensitizers for p-type semiconductors<sup>565–572</sup> aimed for use in tandem DSCs have also been developed in recent years. Some representative organic dyes are collected in Table 5.

**5.2.3.1. Coumarin Dyes.** Arakawa, Hara, Wang, and co-workers developed a class of organic dyes consisting of a coumarin unit and a cyanoacrylic acid unit linked by vinylene, isophorone, or thiényl.<sup>130,132,426–435</sup> The coumarin unit acts as electron donor. The cyanoacrylic acid group is considered as the electron acceptor due to the strong electron-withdrawing ability of cyano and carboxyl groups. Dye **91**, recognized as the original coumarin sensitizer, exhibited an effective electron injection process.<sup>573</sup> However, when this dye was used in DSCs, it showed a lower efficiency than Ru complex-based DSCs due to the narrow light response range in the visible region. The introduction of vinylene –CH=CH– red-shifts the absorption spectra. Based on this design, dyes **92–94** exhibit wide absorption spectra and improved efficiencies. The red shifts in the absorption spectra of the three dyes are attributed to a shift of the HOMO levels to higher energies rather than to a decrease in energy of the LUMO levels. In addition, the lengthening of the dye with the vinylene units also enhances dye aggregation on the  $\text{TiO}_2$  surface resulting in a decrease of electron injection yield owing to the intermolecular charge transfer. Coumarin dyes should thus be suppressed in terms of aggregation by the use of coadsorbants.<sup>132,430</sup> Under optimized conditions, **93**-based DSCs gave 6.0% efficiency under AM 1.5 G.<sup>132</sup> In subsequent experiments, they found that there were two problems associated with the introduction of vinylene units: the complicated synthesis procedure and possible isomerization. In view of this, thiényl and isophorone units have been employed to expand the conjugated system, giving the dyes **95–102**. The number of thiophene units did not affect the absorption spectra of dyes **97–99**; however, it affects the photovoltaic properties of dyes **97–99** due to different aggregation issues on the  $\text{TiO}_2$  surface. Dye **98** exhibited ultrafast electron injection within 100 fs.<sup>130</sup> As a result, the **98**-based DSCs gave 6.1–8.1% overall efficiency under AM 1.5 G.<sup>130,427–429</sup>

Linking one more CN group to the  $\pi$ -bridge of dyes **101** and **102** further extends the absorption region of organic dyes. However, the absorption spectrum of the **101** dye with one thiényl group was red-shifted compared with the **102** dye.<sup>435</sup> The added –CN group enhances the electron-withdrawing ability of the electron acceptor part, but the enhancement appears to be slightly less when the added –CN group is further separated from the cyanoacrylic acid group. Dye **101** showed a high photovoltaic performance, yielding 7.6% efficiency based on a volatile electrolyte and prominent photostability under visible light soaking with 6% efficiency for 1000 h using a nonvolatile electrolyte.<sup>434,435</sup> Recently, Katoh and co-workers compared some coumarin dyes through irradiation of the dyes adsorbed onto  $\text{TiO}_2$  films under ambient conditions and pointed out that the dyes containing oligothiophene moieties showed high stability.<sup>574</sup>

**5.2.3.2. Indoline Dyes.** Horiuchi, Uchida and co-workers first reported this type of organic dye with simple synthesis

**Table 5.** Some Representative Organic Dyes

Coumarin dyes				Indoline dyes			
Dye	Structure	Dye	Structure	Dye	Structure	Dye	Structure
91		92		113		114	
93		94		Tetrahydroquinoline dyes			
95		96		115		116	
97		98		117		118	
99		100		119		120	
101		102		Tri-arylamine dyes			
Indoline dyes				Dye	Structure	Dye	Structure
103		104		121		122	
105		106		123		124	
107		108		125		126	
109		110		127		128	
111		112		129		130	
				131		132	
				133		134	

Table 5. Continued

Tri-arylamine dyes				Tri-arylamine dyes			
Dye	Structure	Dye	Structure	Dye	Structure	Dye	Structure
135		136		155		156	
137		138		157		158	
139		140		159		160	
141		142		161		162	
143		144		163		164	
145		146		165		166	
147		148		167		168	
149		150		169		170	
151		152		171		172	
153		154		173		174	

Table 5. Continued

N,N-dialkylaniline dyes				Perylene dyes			
Dye	Structure	Dye	Structure	Dye	Structure	Dye	Structure
175		176		197		198	
177		178		199		200	
179		180		201		202	
Hemicyanines							
181		182		203		204	
183		184		Other dyes			
185		186		205		206	
Merocyanines							
187		188		207		208	
Squaraines							
189		190		209		210	
191		192		p-type dyes			
193		194		211		212	
195		196		213		214	

procedures, low costs, and good efficiencies obtaining 6.1% power conversion efficiency of dye **103** in 2003.<sup>436</sup> To further improve the DSC performance, an additional rhodanine framework was introduced to the molecular structure of **103** to extend the absorption spectrum, giving a series of novel indoline dyes.<sup>437</sup> Among these dyes, dye **104** showed most prominent efficiency, 8.0%, under AM 1.5 G irradiation. Since then, many aspects of indoline dyes have been studied.<sup>57,438–447</sup> Through optimizing the TiO<sub>2</sub> electrode thickness, Grätzel and co-workers achieved 9.0% efficiency based on **104**.<sup>440</sup> Schmidt-Mende et al. employed **103** to fabricate solid-state DSCs and obtained an efficiency over 4.0%, which was superior to that of an N719-based DSC.<sup>439</sup> After structural optimization, Ito and co-workers developed an efficient indoline dye **105** with a rhodanine framework substituted with n-octyl to suppress the dye  $\pi$ -stacked aggregation on the semiconductor surface and obtained a 9.5% efficiency.<sup>57</sup> This is one of the best efficiencies for organic dye-sensitized solar cells. Moreover, endowing the sensitizer with an octyl chain can effectively suppress electron recombination between electrons in the conduction band of TiO<sub>2</sub> and electrolyte, resulting in higher open-circuit voltage and short-circuit current.<sup>443</sup> Matsui and co-workers modified the indoline dyes by introducing the thiophene-conjugated system as a  $\pi$  bridge.<sup>444</sup> They found that introduction of the thiophene unit into dye **106** could improve the photovoltaic properties. For example, DSCs based on dye **107** gave 3.8% efficiency, and dye **106** showed 2.6% efficiency under the same measurement conditions. However, the introduction of thiophene into dye **104** giving dye **108** did not improve the efficiency of DSC. This result suggests that the HOMO level of **106** is too high in energy resulting in a decrease in regeneration yield. Recently, Tian and co-workers reported a simple indoline dye **109**, which achieved 7.4% efficiency in DSC. Under the same conditions, the referenced N719-based DSCs showed a lower efficiency of 7.0%.<sup>446</sup> Ko and co-workers developed a new series of indolene dyes substituted by bis-dimethylfluorenyl, dyes **110**–**114**.<sup>442,445</sup> A maximum overall efficiency of 8.4% under AM 1.5 G with a DSC based on **113** was obtained.

**5.2.3.3. Tetrahydroquinoline Dyes.** Dyes **115**–**120** are some representative tetrahydroquinolines. This kind of organic dye was developed by Sun, Yang, and co-workers.<sup>448,449,451</sup> On the basis of these dyes, they systematically investigated the relationship between the dye structures and performance of DSCs. They found the elimination of the C=C bond and adoption of suitable electron spacers to be useful for getting higher efficiencies of DSCs. They considered the low performance of C=C bond containing dyes to be due to the existence of a twisting process, which leads to possible cis–trans photoisomerization.<sup>450</sup> The results suggested that the organic dyes with rigid molecular structures are helpful for getting higher overall efficiencies in DSCs. However, the dye with more thiophene units could easily increase the recombination reaction of electrons in the TiO<sub>2</sub> and I<sub>3</sub><sup>–</sup> in the electrolyte leading to a lower photovoltage.<sup>449</sup> As a result, **117**-based DSC showed the higher efficiency of 4.5% under AM1.5 G (N3, 6.2%). The dithieno[3,2-*b*;2',3'-*d*]thienyl (DTT) unit was introduced into the organic dye **119**. Moreover, a new type of organic dye for DSCs, in which the anchoring group was separated from the acceptor groups of the dye, was successfully obtained giving a new class of D– $\pi$ –A organic dyes for sensitization in the NIR region.<sup>451</sup> Among these dyes, dye **120**-based DSCs gave a maximum

IPCE value of 86% at 660 nm and an overall 3.7% efficiency, which was one of the highest IPCE values reported so far for the D– $\pi$ –A organic dyes in the NIR region.

**5.2.3.4. Triarylamine Dyes.** This class of organic sensitizers has been investigated widely due to prominent electron-donating ability and hole-transport properties of the triarylamine unit. To date, a very large number of triarylamine dyes have been developed and most of them have shown good power conversion efficiencies in DSCs.<sup>58,133,452–497</sup> Yanagida and co-workers first introduced the triphenylamine unit as electron donor in organic dyes and obtained overall DSC efficiencies of 3.3% and 5.3% for dye **121** and **122**, respectively (N719, 7.7%).<sup>452</sup>

Later, Sun and co-workers further optimized triphenylamine dyes and reported a series of efficient organic dyes.<sup>458–463</sup> Dye **123** with simple structure and short synthesis route showed over 5.1% efficiency (N719, 6.0%).<sup>458</sup> When this dye was applied in thinner film DSCs (ca. 3  $\mu$ m), it exhibited better efficiency than N719.<sup>459</sup> This result suggests that these dyes are suitable for solid-state DSCs. Adjusting the structures of organic dyes by introducing one more triphenylamine unit as electron donor or additional methoxy groups in the electron donor, or both, they also obtained dyes **124**–**126**.<sup>460</sup> The introduction of methoxy groups in the electron donor can extend the absorption region of organic dyes in the visible light. Among these dyes, the **126**-based DSC achieved the highest efficiency, 7.2%, under AM1.5 G irradiation. When these dyes were fabricated to solid-state DSCs, dye **125** gave a prominent efficiency of 3.3%. With one more thiophenyl  $\pi$ -bridge and longer alkyl chains in the electron donor, dye **127** achieved 7.3% efficiency in liquid DSCs and a 4.4% efficiency in solid-state DSCs. Based on an ionic liquid electrolyte, **127**-based DSCs exhibited prominent photochemical stability.<sup>463</sup> Sun, Yang, and co-workers also developed a series of triphenylamine dyes consisting of different substituted phenylene  $\pi$ -bridges and different electron acceptors and studied in detail the effect of different dye baths and dye structures on DSC performances. They found that the different dye baths for semiconductor sensitization had a crucial effect on the performance of the DSCs due to different dye loading, absorption spectra, and binding modes of the anchored dyes on the TiO<sub>2</sub> surface in various solvents.<sup>461</sup> On the basis of optimized dye bath, dye **128** showed a power conversion efficiency of 5.3% under AM 1.5 G. The electron-withdrawing units, substituted phenylene or rhodanine acetic acid, resulted in a negative effect on the DSC performances, although the electron-withdrawing units of the rhodanine acetic acid give a red shift of the absorption spectrum. Dye **129** with two cyano groups in phenylene only showed 0.44% efficiency due to the strong electron-withdrawing ability of the cyano units, which could hinder electron injection. Dye **130** containing rhodanine acetic acid as electron acceptor also showed lower efficiency than that of dye **128** with a cyanoacrylic acid unit as electron acceptor. The LUMO electron density of the dye with rhodanine acetic acid unit did not overlap with the semiconductor and promoted a higher probability for electron injection to short-lived surface trap states compared with the situation for the dye with the cyanoacrylic acid unit.<sup>491</sup> With linkage of one more triphenylamine unit and dye **131** with a C=C bond, dye **132** exhibited an additional strong absorption peak in the UV region and effective intramolecular energy transfer and charge transfer, which showed positive effects on DSC performance.<sup>462</sup>

Lin and co-workers also developed a series of triarylamine dyes.<sup>453–457</sup> Among these dyes, based on benzothiadiazole and benzoselenadiazole chromophores,<sup>454</sup> an efficiency value of 3.8% was realized for dye **133** containing the benzothiadiazole bridge in which the nonplanar charge-separated structure probably hinders charge recombination. They also reported advanced fluorene-based organic dyes with a narrow absorption region, of which dye **134** achieved 5.2% efficiency (N3, 5.5%).<sup>453</sup> Replacing the thiophene unit of dye **123** with furan, Lin and co-workers achieved an efficient organic dye **135**, which gave 7.4% overall efficiency.<sup>457</sup> Under the same conditions, reference dye **123** showed a lower value, 6.1%.

Great efforts in developing dimethylfluorenylamino-based organic dyes have been made by Ko and co-workers.<sup>464–472</sup> The tailored dimethylfluorenylamino moiety can ensure greater resistance to degradation when exposed to light or high temperature, because it possesses a bipolar character that allows the formation of both stable cation and anion radicals.<sup>469</sup> For dyes **136** and **137**,<sup>464</sup> the IPCE spectrum of **137** is red-shifted by about 30 nm compared with that of **136** as a result of extended  $\pi$ -conjugation, which is consistent with the absorption spectra. Under AM 1.5 G illumination, dyes **136** and **137** gave efficiencies of 7.2% and 8.0%, respectively. More structural modifications of fluorine-based organic dyes have been performed through changing the  $\pi$  bridge or electron acceptor and introducing the alkyl chains into fluorene or  $\pi$ -bridge. Dyes **138** and **139** are two successful examples of the molecular optimization with alkyl chains.<sup>469</sup> The introduction of long alkyl chains into thiophene  $\pi$ -bridge of dyes **138** and **139** can enhance the tolerance toward water in the electrolytes. A **139**-based DSC with volatile electrolyte yielded an overall conversion efficiency of 8.6%, whereas the conversion efficiency of the same sensitizer-based DSC with a solvent-free ionic-liquid electrolyte was 7% under AM 1.5 G. Remarkably, the **139**-based solar cells fabricated using a solvent-free ionic-liquid electrolyte exhibited an excellent stability under light soaking at 60 °C for 1000 h. Also, the introduction of long alkyl chains into dimethylfluorenylamino units can improve the photovoltaic performance and stability of the organic dyes.<sup>471</sup> Dyes **140**–**142** are the representative organic dyes with *p*-phenylene vinylene units.<sup>470</sup> Different numbers of *p*-phenylene vinylene units show significant effects on photovoltaic properties of dyes **140**–**142**. The maximum power conversion efficiency of the DSCs based on **142** containing three *p*-phenylene vinylene units reached 7.0% under AM 1.5 G. Ko and co-workers introduced the trialkylsilyl electron acceptors, recognized as efficient binding groups for TiO<sub>2</sub>, into organic dyes (**143** and **144**).<sup>472</sup> Although the efficiencies of **143**- and **144**-based DSCs were not high enough compared with that of the DSCs based on the dye containing a cyanoacrylic unit, the stronger binding property of the trialkoxysilyl anchoring group could improve the long-term stability of the DSCs.

Chen and co-workers reported a family of triphenylamine dyes with an increased electron density of donor moiety as an effective way to improve the dye performance.<sup>474–478</sup> Dye **145** with a CH<sub>2</sub>=CH-substituted triphenylamine electron-donating group gave 5.8% efficiency under AM 1.5 G irradiation due to the increase of the electron density in the donor subunit. The corresponding dye (**131**) without the CH<sub>2</sub>=CH- substitution exhibited a lower efficiency of 4.3%.<sup>474</sup> Changing the electron acceptor or extending the  $\pi$ -conjugate system, they obtained various efficient organic

dyes.<sup>475–477</sup> Recently, they employed the diphenylvinyl-substituted triphenylamine as the electron donor in dye **146**, which achieved a power conversion efficiency of 6.3% (AM 1.5 G) and exhibited good stability under one sun irradiation for 20 days.<sup>478</sup>

Wang and co-workers have made a great progress in developing efficient triarylamine organic dyes.<sup>58,479–485</sup> Dye **147** consists of dimethylfluorenylamino electron donor, DTT,  $\pi$ -bridge, and cyanoacrylic acid acceptor exhibiting a broad absorption band and high molar extinction coefficient,  $44.8 \times 10^3 \text{ M}^{-1} \text{ cm}^{-1}$  at 525 nm in chloroform.<sup>480</sup> When this dye was fabricated into DSCs, it achieved 8.0% efficiency in liquid electrolyte based DSCs with a maximum IPCE of 93% at 530 nm and yielded 7.0% efficiency in solvent-free ionic electrolyte based DSCs with excellent light soaking stability at 60 °C for 1000 h. Using the thienothiophene (TT) to replace the DTT unit, they obtained another efficient organic dye, **148**, which exhibited an impressive 4.8% efficiency in solid-state DSCs.<sup>482</sup> Later, they further optimized the dye structure with a 3,4-ethylenedioxythiophene (EDOT)  $\pi$ -bridge, which could red-shift the photocurrent action spectra of dyes compared with thiophene and bithiophene.<sup>484</sup> Dye **149** with a biEDOT unit gave higher efficiency, 8.3%, compared with that of the bithiophene counterpart **137**. They attributed the improved efficiency with the **149** dye to its better spectral match with the solar irradiation spectrum by introducing the biEDOT unit. Through using the alkoxy-substituted triphenylamine as electron donors and changing different  $\pi$ -bridges, they further obtained a series of triphenylamine dyes, such as dyes **150**–**154**.<sup>58,479,481,483,485</sup> Among these dyes, dye **154** containing both EDOT and TT  $\pi$ -bridges showed an absorption band with a peak at 552 nm, exceeding 90% IPCE values from 440 to 590 nm.<sup>58</sup> Efficiencies of 9.8% and 8.1% with liquid electrolyte and solvent-free ionic electrolyte under AM 1.5 G were obtained, respectively. The two efficiency values are the records of DSCs based on organic dyes so far. Furthermore, the high performance cell based on **154** with ionic electrolyte still retained >96% of its initial efficiency after 1000 h accelerated tests under full sunlight soaking at 60 °C.

Yang and co-workers reported some modified triarylamine dyes,<sup>486–488</sup> dyes **155** and **156** employing the *N,N,N',N'*-tetraphenylbenzidine (TPD) unit as donor yielding efficiencies of 5.6% and 4.3% under AM 1.5 G, respectively.<sup>488</sup> Dye **155** achieved higher IPCE values and broader IPCE spectrum compared with that of **156** due to the enhanced absorption of the introduction of the thiophene unit. Under the same test conditions, the referenced N3-based DSCs gave an efficiency of 6.4%.

Tian and co-workers developed starburst triarylamine dyes for DSCs.<sup>490</sup> They consider that high rates of charge separation and collection compared with interfacial charge-recombination processes in DSCs will be further reinforced by incorporating starburst dendronized triarylamine moiety into the molecule due to their excellent hole-transport capability. Based on this finding, they synthesized dye **157** employing a two carbazole unit substituted triphenylamine group as electron donor and an isophorone unit as  $\pi$ -conjugated bridge, which showed an IPCE value of 85% and an overall conversion efficiency of 6.0% under AM 1.5 G irradiation.

Müllen and co-workers obtained a series of organic dyes based on rigid ladder-type pentaphenylene spacers.<sup>489</sup> Among these dyes, dye **158** showed a broader absorption band in

the visible region along with a weak NIR absorption band due to the formation of an amino radical cation. The DSCs based on this dye gave the highest IPCE value of 73% and a power conversion efficiency of 2.3% in liquid DSCs (N719, 4.6%; N3, 6.2%) and 0.8% in solid-state DSCs. Although the power conversion efficiencies of these organic dyes are not so high, their work explores new  $\pi$ -bridge models and the effects of molecular design on photophysical and photoelectrochemical properties.

The structural modifications of triphenylamine dyes were performed unremittingly by other scientists,<sup>493–497</sup> giving many efficient organic dyes, such as dyes **159–162**. The development of triarylamine dyes encourages further structural optimization of low-cost organic dyes, boosting the practical application of DSCs.

**5.2.3.5. Heteroanthracene Dyes.** Heteroanthracene dyes applied in DSCs include xanthene, phenothiazine, and phenoxazine. Low-cost xanthene dyes such as mercurochrome, eosin Y, and fluorescein were adopted as sensitizers in early DSCs.<sup>299,489,498–500</sup> However, this class of organic dyes usually showed relatively low efficiency due to their narrow light-harvesting region and instability.<sup>425</sup> Recently, Sun, Yang, and co-workers developed a series of efficient phenothiazine and phenoxazine organic dyes.<sup>501,502</sup> Phenothiazine and phenoxazine units possess strong electron-donating ability and are suitable to act as photosensitizers. Based on a simple structure, phenothiazine dye **163** achieved an efficiency of 5.5% under AM 1.5 G.<sup>501</sup> The introduction of phenylene vinyl and rhodanine acid in phenothiazine dyes (**164–166**) did not yield improved overall efficiency. Later, they reported a novel phenoxazine dye **167** consisting of a thietyl  $\pi$ -bridge and a corhodanine electron acceptor, in which the alkyl chains were adopted to increase the solubility and suppress aggregation.<sup>502</sup> Although the **167**-based DSCs did not obtain a higher efficiency value than 3.0%, they showed a broad IPCE spectrum over the whole visible range extending into the near-IR region up to 920 nm, which is the broadest IPCE spectrum in the organic dye-based DSCs. This result shows that besides some Ru complexes, organic dyes can achieve a broad spectral response up to the near-IR region. Müllen and co-workers reported a novel phenothiazine dye based on a rigid ladder-type pentaphenylene  $\pi$ -bridge, which obtained an efficiency of 1.8%.<sup>489</sup>

**5.2.3.6. Carbazole Dyes.** Kourumura and co-workers reported efficient carbazole sensitizers for DSC<sup>503</sup> and investigated systematically the effect of a  $\pi$ -conjugated system of *n*-hexyl-substituted oligothiophenes on DSC performance.<sup>504</sup> They found that the photovoltaic performance of these dyes markedly depended on the molecular structures of the dyes in terms of the number and position of *n*-hexyl chains and the number of thiophene moieties. The existence of *n*-hexyl chains linked to the thiophene groups caused the retardation of charge recombination, resulting in an increase in electron lifetime. Photovoltage and hence overall conversion efficiency of DSCs were improved upon addition of *n*-hexyl chains to the thiophene groups. For example, the  $V_{oc}$  (0.69–0.75 V) for DSCs based on **170** and **171** dyes, which have long alkyl chains, were higher than that for **169** (0.63–0.67 V) under the same conditions. A DSC based on **171** consisting of *n*-hexyl-substituted quarter-thiophene produced 8.3% efficiency under simulated AM 1.5 G.<sup>504</sup>

Ko and co-workers developed some organic dyes containing an *N*-aryl carbazole moiety for DSCs.<sup>505</sup> With structural modification, a dye **172**-based DSC achieved a maximum

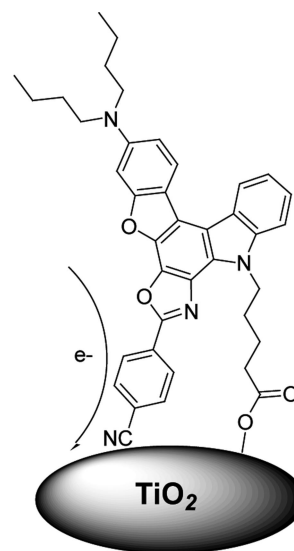


**Figure 18.** Schematic configuration of **173** on  $\text{TiO}_2$  surface.

conversion efficiency of 5.2% under AM 1.5 G and a maximum IPCE value of 77% at 430 nm. Under the same test conditions, a DSC based on N719 showed 7.8% efficiency.

Efforts on structural optimization of benzofuro[2,3-*c*]oxazolo[4,5-*a*]carbazole-type fluorescent dyes (such as **173** and **174**) for DSCs have been made by Harima and co-workers.<sup>506–509</sup> They have studied in detail the effect of the position of the carboxyl group on DSC performance, and found that despite the lengths of alkyl chains, the electron-withdrawing group CN of the dyes was located close to the semiconductor surface due to the flexibility of alkyl chains, and a good electron injection yield is achieved between the CN and  $\text{TiO}_2$  surface (see Figure 18).<sup>508</sup> This provides a new strategy for the molecular design and synthesis of donor–acceptor  $\pi$ -conjugated dyes for DSCs. The result suggests that a carboxyl group of donor–acceptor  $\pi$ -conjugated sensitizer is not essential as the electron acceptor but only as the anchoring group for attachment of the dye on the semiconductor surface. This strategy has been adopted by Sun, Yang, and co-workers, and they have developed new NIR organic dyes such as **120** as mentioned above.<sup>451</sup>

**5.2.3.7. *N,N*-Dialkylaniline Dyes.** This class of dyes has been investigated by many researchers (Table 5).<sup>452,510–512</sup> Arakawa, Hara, and co-workers employed the *N,N*-dialkylaniline unit as electron donor, methine ( $-\text{CH}=\text{CH}-$ ) or thietyl as  $\pi$ -bridge, and cyanoacrylic acid as electron acceptor to develop a new series of organic dyes (dyes **175–178**).<sup>510,511</sup> Both the introduction of additional *N,N*-dialkylaniline units and the expansion of the conjugated system contributed to a red shift in absorption spectra of the dyes (**176–178**). Finally, they obtained an overall power conversion efficiency of 6.8% under AM 1.5 G with a DSC based on the **177** dye.<sup>511</sup> Later, Yang and co-workers developed two new *N,N*-dialkylaniline dyes containing thienothiophene (**179**) or thiophene segments (**180**) as  $\pi$ -conjugation systems and rhodanine acetic acid as electron acceptor.<sup>512</sup> Both dyes showed good performance for DSCs. Especially the DSC based on **180** achieved a good conversion efficiency of 6.2% under AM 1.5 G irradiation. Their result shows that the thienothiophene unit can act as a suitable  $\pi$ -conjugation system for organic dyes.

**5.2.3.8. Hemicyanines.** For DSCs, the workable D– $\pi$ –A-type hemicyanine dyes are cationic dyes and usually consist

of basic *p*-dialkylaniline groups as electron donor and cationic moieties as strong electron acceptor linked by methine ( $-\text{CH}=\text{CH}-$ )  $\pi$ -bridge (Table 5).<sup>513–521</sup>

Many efforts for developing this class of organic sensitizers have been made by Huang and co-workers.<sup>513–518</sup> In 2000, they reported a novel hemicyanine sensitizer (**181**) containing a benzothiazolium propylsulfonate unit as electron acceptor and anchoring group for DSCs.<sup>514</sup> In DSCs, they reported maximum IPCE values close to 100% and a short-circuit photocurrent under  $94.6 \text{ mW cm}^{-2}$  simulated solar light of more than  $15 \text{ mA cm}^{-2}$ . On the basis of this study, they further optimized the structures of hemicyanine dyes and reported some efficient sensitizers, such as **182**–**184**.<sup>515,517,518</sup> Their investigations showed that introduction of a hydroxyl group in the donor unit can greatly improve the electron injection efficiency between the excited dye and semiconductor due to an improved interaction between the dye and semiconductor. Additionally, the DSCs sensitized by **184**, bearing a hydroxyl group, obtained a remarkably high overall efficiency of 6.3% under illumination of  $80 \text{ mW cm}^{-2}$  white light.<sup>518</sup> Through modifying the structure of **184**, Wang and co-workers gained a series of advanced hemicyanine dyes.<sup>520</sup> They found that the dyes with carboxyl units showed superior efficiencies to those of dyes with sulfonate moieties. Moreover, the dyes with the combination of carboxyl and hydroxyl anchoring groups led to high efficiencies in DSCs. As a consequence, a DSC based on the **185** dye showed a wide IPCE spectrum with the maximum of 74% and an efficiency of 5.2% under AM 1.5 G ( $80 \text{ mW cm}^{-2}$ ). Lianos and co-workers developed a new hemicyanine dye (**186**) with two carboxylic groups in the electron donor unit as anchoring group, which achieved a maximum IPCE value of 45% and an overall conversion efficiency of 0.7%.<sup>521</sup>

**5.2.3.9. Merocyanines.** Originally, Kamat and co-workers studied the effect of dye (**187**) aggregations on DSC performance.<sup>522</sup> The result reveals that the IPCE value of the monomeric form (~40%) is nearly five times greater than the corresponding value of the H-aggregate form (~8%). They minimized the aggregation effects on the  $\text{TiO}_2$  surface by using molecular spacers such as aerosol-OT (AOT) molecules. This study provides a strategy to suppress the dye H-aggregation on the semiconductor surface and improve the photovoltaic properties for DSCs.

Arakawa and co-workers have developed a new series of benzothiazole merocyanine dyes containing different alkyl chains and different methylene chain lengths between the carboxy unit and the electron donor.<sup>523–525</sup> They found that these dyes easily formed J-aggregates on  $\text{TiO}_2$  surfaces. Being different from the H-aggregation of **187**, the J-aggregates of the dyes with long alkyl chains obtained high overall conversion efficiency. Furthermore, the increase of alkyl length is more facile to form the J-aggregates and thus improves the photovoltaic properties. However, the increase of methylene length between the carboxy group and the electron donor in dyes revealed that the distance between the dye and the  $\text{TiO}_2$  surface affected the photovoltaic properties. The most optimized dye, **188**, achieved a maximum efficiency of 4.5% under AM 1.5 G.<sup>524</sup>

**5.2.3.10. Squaraines.** Squaraine dyes exhibit sharp and intense absorption bands in the visible and near-infrared (NIR) regions. A number of squaraine dyes<sup>526–535</sup> have been adopted for DSCs.

Zhang and co-workers<sup>526</sup> developed three squaraine sensitizers (**189**–**191**) with different substituents on the hetero-

cyclic nitrogen atoms. They found that the three dyes showed strong absorption bands at around 630 nm in solution, which were bathochromically (i.e., red) shifted according to the different substituents in the order of  $(\text{CH}_2)_3\text{SO}_3^-\text{Py}^+ > \text{CH}_2\text{CH}_2\text{OH} > \text{CH}_3$ . When the three dyes were used in DSCs, dye **191** exhibited the best efficiency of 2.2%. They considered that the interaction of the attaching group of squaraines with active hydroxy groups at the  $\text{TiO}_2$  surface can influence the photovoltaic properties. The sensitization performance is improved with the increase of adsorption in the order of  $\text{CH}_3$  (weak)  $<$   $\text{CH}_2\text{CH}_2\text{OH}$  (medium)  $<$   $(\text{CH}_2)_3\text{SO}_3^-\text{Py}^+$  (strong).

Das and co-workers<sup>527</sup> reported a family of symmetrical and unsymmetrical squaraine dyes and systematically investigated the relationship between the structures and photovoltaic properties of the dyes in DSCs. They concluded that DSCs employing unsymmetrical squaraines as sensitizers produced photocurrents with much higher efficiencies compared with DSCs containing symmetrical squaraines. For example, dye **192** with unsymmetrical structure showed a higher efficiency value of 2.1% than that of the symmetrical dye **193**, which achieved 1.0% efficiency. They consider that dye aggregation on the  $\text{TiO}_2$  is the key effect on the sensitization properties of symmetrical squaraines dyes, whereas efficient unsymmetrical squaraine sensitization exhibits both the monomeric and aggregated forms on the  $\text{TiO}_2$  surface.

Following these studies, Grätzel and co-workers<sup>530</sup> further optimized the structure of squaraine dye and reported a blue organic squaraine dye (**194**), incorporating two carboxylic acid attaching groups, successfully used in both liquid and solid-state DSCs. The dye achieved 3.7% and 1.5% efficiencies under AM 1.5 G in liquid and solid-state DSCs, respectively.

Subsequently, Palomares and co-workers studied the role of the aggregates on the injection kinetics for a mesoporous  $\text{TiO}_2$  film sensitized by squaraine dye **195**. They found that the electron injection only occurred from the monomers and the yield remained high (~95% of electrons are injected into the conduction band of  $\text{TiO}_2$ ) despite the presence of H-aggregates on the film. Furthermore, they found that dye regeneration dynamics were too slow (>100 s) in iodide/iodine based electrolytes, but sufficiently fast (<1 s) in solid state DSCs using spiro-MeOTAD.<sup>531</sup>

Nüesch and co-workers<sup>532,534</sup> made great progress in developing efficient squaraine dyes. They reported an advanced squaraine sensitizer (**196**), which yielded the highest IPCE value of 85% and 4.5% power conversion efficiency under AM 1.5 G. They considered that the high efficiency of this sensitizer was ascribed to its particular molecular structure. The carboxylic acid group as a part of the conjugated  $\pi$ -system of the dye also provided strong electronic coupling to the conduction band of  $\text{TiO}_2$  and the asymmetric structure constructed by the octyl chain prevented dye aggregation and limited self-quenching of the excited state. Their result provided promising design and development routes of squaraine dyes for DSCs.

**5.2.3.11. Perylene Dyes.** Rylene derivatives such as perylene have been used commercially as colorful pigments and dyes for many years due to their excellent chemical stability and lightfastness. Moreover, this kind of dye usually exhibits a high molar extinction coefficient in visible light ( $\sim 10^5 \text{ M}^{-1} \text{ cm}^{-1}$ ).<sup>290</sup> These properties are advantageous for DSC applications. Through adjustment of the different

substituents on heteroatoms N or the perylene framework, various perylene sensitizers<sup>290,536–543</sup> with rainbow colors have been synthesized for DSC fabrication.

Gregg and Ferrere<sup>290,536,537</sup> studied the perylene dyes and reported a series of workable perylene sensitizers for DSCs. Originally, they employed the suitable perylene dyes to sensitize the SnO<sub>2</sub> semiconductor, possessing a lower conduction band edge energy level,  $E_c$ , compared with TiO<sub>2</sub>, and obtained an efficiency value of 0.89% in a DSC based on the **197** dye.<sup>290</sup> Later, they treated the TiO<sub>2</sub> film with UV irradiation and found improved photocurrent and power conversion efficiency.<sup>536</sup> For example, a DSC based on **198** showed 0.05% efficiency without UV treatment, whereas a relative high efficiency value of 1.2% was achieved based on the same DSC after UV irradiation. They claimed that the UV irradiation moved  $E_c$  to a lower energy level, as also observed by Hagfeldt et al.,<sup>575</sup> which promoted electron injection from excited perylene dyes. To design suitable perylene sensitizers for TiO<sub>2</sub>-based DSCs, Gregg and Ferrere further developed a generation of new perylene sensitizers with better solubilities, more negative excited-state energies, and better visible light absorption properties for solar energy conversion.<sup>537</sup> These dyes can sensitize the TiO<sub>2</sub> excellently. Among these dyes, dyes **199** and **200** gave 1.9% and 1.3% efficiencies under AM 1.5 G, respectively. Under the same test condition, a reference N3-based DSC showed an efficiency value of 4.4%.

Edvinsson and co-workers<sup>538</sup> reported some perylene molecules with different intramolecular charge-transfer (ICT) characters and systematically studied the relation between the ICT character for different donating groups and the results of their electrochemical and photochemical properties as well as their performance in DSCs. Based on dye **201** with the highest ICT character, the DSCs achieved almost 4% solar energy conversion efficiency (N719, 6.0%) and a high IPCE value of 70% under AM 1.5 G irradiation.

Imahori and co-workers<sup>539</sup> used the strong electron-donating group pyrrolidine and different substituents to decorate the perylene framework and heteroatom N, respectively, and obtained a series of novel perylene sensitizers. Although all these dyes exhibited an intense ICT absorption band from 500 to 800 nm, the photovoltaic properties of these dyes were significantly different. Dye **202** with a 2,6-diisopropylphenyl unit gave the highest efficiency value of 2.6%, with an IPCE spectrum extending to 800 nm, under AM 1.5 G. However, dye **203** with a cyclohexyl substituent showed a lower efficiency value of 1.5%. The results suggested that the larger substituent (2,6-diisopropylphenyl) could inhibit the dye aggregation on the TiO<sub>2</sub> surface effectively.

Many structural modifications of perylene sensitizers have been made with little progress in terms of solar cell efficiency.<sup>540–542</sup> Recently, however, Li et al.<sup>543</sup> successfully designed and synthesized an efficient perylene dye (**204**) containing two thiophenol groups in the 1 and 6 positions of the perylene framework, which showed two absorption peaks at 620 nm ( $\epsilon = 22\,727\text{ M}^{-1}\text{ cm}^{-1}$ ) and 462 nm ( $\epsilon = 13\,704\text{ M}^{-1}\text{ cm}^{-1}$ ). When the dye was fabricated into DSCs, 6.8% and 1.8% power conversion efficiencies in liquid and solid-state DSCs under AM 1.5 G solar conditions were obtained, respectively. However, this dye showed a narrow IPCE spectrum (ca. 370–670 nm). Extending the spectral response of the sensitizer into the red and near-IR spectral region is required to further improve the power conversion efficiency.

**5.2.3.12. Other Organic Dyes.** Besides the groups of organic dyes mentioned above, other types of organic sensitizers have been used in DSCs. Yang and co-workers<sup>544</sup> synthesized some anthraquinone dyes with different absorption spectra for DSCs. However, these dyes showed low power conversion efficiencies. The best efficiency value obtained by **205**-based DSCs was 0.13% under AM 1.5 G. By calculating the molecular frontier orbitals of anthraquinone by density functional theory (DFT), they considered that the strong electron-withdrawing character of the two carbonyl groups on the anthraquinone framework may suppress the efficient electron injection from the dye to the conduction band of TiO<sub>2</sub> resulting in the low cell performance.

Akkaya and co-workers<sup>545</sup> introduced the boradiazaindacene (BODIPY) dye into DSCs as photosensitizer. Based on dye **206** with a NIR absorption spectrum (600–800 nm), a DSC achieved 1.7% power conversion efficiency with a panchromatic IPCE spectrum. Although the efficiency value was not so high, their work paved a road to develop novel panchromatic photosensitizers for DSCs. Later, Ziessel, Thummel, and co-workers<sup>546</sup> further optimized this class of organic dyes and synthesized three novel BODIPY dyes. To improve the stability of these dyes, ethynyl units with side chains were adopted to replace the traditional fluorine atoms on boron. Among these dyes, dye **207** showed the broadest IPCE spectrum.

In addition, Zhai and co-workers<sup>547</sup> reported oligothiophene dyes for DSCs. Based on the simple dye **208**, an efficiency value of 3.4% was achieved under AM 1.5 G. Subsequently, Otsubo, Harima, and co-workers<sup>548</sup> further developed the oligothiophene sensitizers through adjusting the number of thiophenes and introducing alkyl chains into the corresponding thiophene frameworks. However, the efficiency values of oligothiophene dyes were not improved due to dye aggregation caused by strong intermolecular  $\pi$ -conjugated interactions.

Recently, polymeric dyes (polyaniline, polypyrrole, poly-thiophenes, poly(*p*-phenylene ethynylene), etc.)<sup>549–555</sup> have been employed as photosensitizers in DSCs. An anionic conjugated polymer (**209**) containing benzothiadiazole and polyfluorene reported by Liu, Ramakrishna, and co-workers yielded an efficiency of 1.4% at AM 1.5 G.<sup>554</sup> Ohshita, Harima, and co-workers<sup>555</sup> reported some novel disilanylene–oligothiylene polymeric photosensitizers, which sensitized the TiO<sub>2</sub> electrode by the formation of Ti–O–Si bonds. Dye **210**-based DSCs showed an efficiency value of 0.12% and a maximum IPCE value of 15% at 490 nm. Broadening the absorption spectrum and suppressing the dye aggregation of polymeric photosensitizers will be the key strategy for the improvement of photovoltaic properties.

Natural products as photosensitizers for DSCs can be extracted from flowers, fruits, vegetables, etc.<sup>385,556–564</sup> However, the power conversion efficiencies of these dyes were much lower than those of synthetic dyes. Therefore, there will be a long way to go for commercial application of DSCs based on natural sensitizers.

#### 5.2.4. The Anchoring of the Dye on the Oxide Surface

Generally, the molecular adsorption modes on the host surface can be summarized in six different modes: “(a) covalent attachment brought about by directly linking groups of interest or via linking agents, (b) electrostatic interactions, brought about via ion exchange, ion-pairing or donor–acceptor interactions, (c) hydrogen bonding, (d) hydrophobic interac-

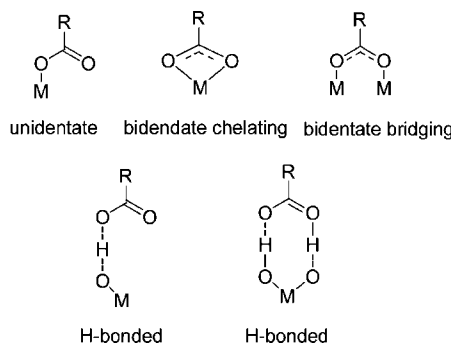


**Figure 19.** Binding modes for carboxylate unit on TiO<sub>2</sub> surface.

tions leading to self-assembly of long chain fatty acid derivatives, (e) van der Waals forces involved in physisorption of molecules on solid surfaces, and (f) physical entrapment inside the pores or cavities of hosts such as cyclodextrins, micelles, etc.”.<sup>576</sup> The adsorption modes of dyes on semiconductor surfaces are very important for the DSC efficiency.<sup>577</sup> To construct workable and efficient DSCs, the dye must be adsorbed on the surface of the semiconductor intimately. Therefore, the first kind provides an approved strategy to accomplish a strong interlinkage between the dye and the semiconductor. It requires that the dye should possess an anchoring group, which should react with surface hydroxyl groups of the semiconductor oxide to form chemical bonds. The standard anchoring group for sensitizers is carboxylic acid ( $-COOH$ ). Its derivatives, such as ester, acid chloride, acetic anhydride, carboxylate salt, or amide, have also been used. Furthermore, sulfonate ( $-SO_3^-$ ) and silane ( $SiX_3$  or  $Si(OX)_3$ ) have also been adopted, see ref 7 and references therein. Efficient sensitizers with phosphonic acid binding groups were first developed by Pechy et al.<sup>578</sup> They found that a ruthenium complex with a single phosphonic acid bound about 80 times stronger to TiO<sub>2</sub> than N3 (which has four carboxylic acid groups) and did not desorb from TiO<sub>2</sub> in the presence of water, in contrast to N3.

Nevertheless, most of the photosensitizers employ the carboxylic acid as anchoring group due to its relative stability and easy synthesis. However, there are different binding modes between the oxide surface and the carboxylic acid (Figure 19).<sup>579</sup> In general, the carboxylic acid group can coordinate to the TiO<sub>2</sub> surface in three ways:<sup>432,580</sup> unidentate mode, chelating mode, and bridging bidentate mode. By measuring the FT-IR to obtain vibrational data of dyes adsorbed on TiO<sub>2</sub> surfaces, we can use the Deacon–Phillips rule to determine the binding modes by calculating the frequency separation,  $\Delta\nu = \nu_{as}(COO-) - \nu_s(COO-)$ , between the asymmetric ( $\nu_{as}$ ) and symmetric stretching ( $\nu_s$ ) modes of the carboxylate unit. The  $\Delta\nu$  values are in the order of unidentate > ionic form  $\approx$  bidentate bridging > bidentate chelating.<sup>432,461,581</sup>

The binding modes can be determined by the molecular structure and adsorption environment.<sup>461</sup> The bidentate structure is superior to unidentate structure in the stability of the anchored dye and interfacial quantum yields of electron injection due to the intimate contact with the semiconductor surface.<sup>580</sup>

### 5.2.5. Combining Sensitizers

Several different approaches have been developed to use more than one type of dye in DSC. In order to increase the spectral response of the DSC, sensitizers with different

absorption spectra can be adsorbed together onto the mesoporous TiO<sub>2</sub> surface, using a mixed dye solution for sensitization. Spitzer and co-workers combined cyanine dyes absorbing light in the blue, yellow, and red regions and found increased photocurrents in DSCs compared with the single dyes.<sup>582</sup> Noda and co-workers achieved an AM 1.5 G efficiency of 11% by combining a Ru complex (the black dye) and an organic sensitizer (D131).<sup>583</sup> They found that the organic sensitizer could replace the chenodeoxycholic acid coadsorber that is normally used in sensitization with the black dye.

Hayase and co-workers developed a method for sequential dye adsorption.<sup>584</sup> They first adsorbed the black dye on the outer part of the porous electrode using a pressurized CO<sub>2</sub> process during a short time, followed by sensitization of the inner part using an organic dye by conventional methods. A method for dye adsorption in a double layer was developed by Clifford et al.<sup>585</sup> After adsorption of the first dye, an ultrathin layer of aluminum oxide is applied, followed by adsorption of the second dye. Using this cosensitization method, Choi et al. achieved 8.7% efficiency by combining two organic dyes.<sup>586</sup>

A fundamentally interesting approach is to include additional energy relay dyes in the DSC. McGehee and co-workers included highly luminescent dyes in the redox electrolyte<sup>587</sup> or the solid hole conductor.<sup>588</sup> They demonstrated that the energy relay dye contributed to the generated photocurrent by means of efficient Förster resonant energy transfer to the sensitizing dye that is adsorbed onto the TiO<sub>2</sub> surface.

### 5.2.6. Summary: Development of Dyes for DSC

In summary, hundreds of dyes have been synthesized and tested in DSCs so far. This raises the questions: What have we learned from the past two decades regarding the design of sensitizers for DSC? What are the rules we should bear in mind when we design a new generation of dyes for even better DSC performance? We would like to briefly discuss these issues in this review to grasp the main points in design of dyes.

1. For Ru complexes, one 4,4'-dicarboxylate-bipyridine ligand provides good anchoring to TiO<sub>2</sub> as well as good electronic coupling of the dye excited states with TiO<sub>2</sub> conduction band states. The LUMO should be located on this ligand. A second bipyridyl ligand can be modified with electron donor moieties to broaden the absorption spectra and to increase the molar extinction coefficient. The remaining ligands are usually isothiocyanate ligands ( $-NCS$ ), which raise the HOMO energy of the complex, leading to a red-shifted absorption. For stability reasons, these monodentate ligands may need replacement. Some promising results have been obtained in this respect with cyclometalated ligands.
2. Organic dyes have enormous versatility, making it difficult to come up with a single strategy for dye design. Generally, however, it seems to be favorable that a spacial separation of HOMO and LUMO orbitals exists, such that excitation leads to increased electron density in the molecules close to the attachment group and the TiO<sub>2</sub> with decreased electron density in the part of the molecule facing the electrolyte. Combining a donor and an acceptor group with a rigid  $\pi$ -conjugated system has led to many useful dyes. It should be noted, however, that such a design will lead to a dye with a

- high reorganization energy, which will influence its performance negatively.
- Bulky chains on the proper positions of an organic dye can be crucial for good DSC performance. Ideally, the dye should form a closely packed monolayer, blocking contact between redox mediator and  $\text{TiO}_2$ . Simultaneously, dye molecules should not form inactive aggregates, but should rather be isolated individual units.
  - Favorable interaction with the redox mediator is vital. Dyes may be equipped with a functional group that promotes rapid charge transfer of the hole to the redox mediator.
  - Strong anchoring of the dyes is essential for long-term stability. Desorbed dyes can lead to an unwanted filter effect, dye degradation and decrease of the counter electrode performance.
  - The dye should have a long lifetime in its oxidized state and should also be stable at elevated temperatures.

### 5.3. Electrolytes and Hole Conductors

In the 1991 *Nature* paper, Grätzel and O'Regan<sup>1,589</sup> used an electrolyte that was based on a mixed solvent, 80:20 by volume, between ethylene carbonate and acetonitrile. The redox components were added as 0.5 M tetrapropylammonium iodide and 0.04 M iodine, whereas no extra additives were used. The composition of the electrolyte was adjusted using lower concentrations of lithium or potassium iodide, however not producing higher conversion efficiencies than the simplest composition. A conversion efficiency of 7.9% was achieved, and it is remarkable that after more than 15 years of intense research, using a multitude of alternative solvents, redox couples, and various additives, we still mostly use the same categories of nanoparticles, dyes, and electrolytes.

#### 5.3.1. Liquid Redox Electrolytes

The demands on the liquid redox electrolyte are that they should be chemically stable, have low viscosity in order to minimize transport problems, and be a good solvent for the redox couple components and various additives but at the same time not cause significant dissolution of adsorbed dye or even the semiconducting material of the electrodes. Because many organometallic sensitizing dyes are sensitive toward hydrolysis, water and reactive protic solvents are normally not optimal choices. Finally, the redox electrolyte should be compatible with a suitable sealing material to avoid losses by evaporation or leakage. The two major types of solvents simultaneously fulfilling most of the criteria are

based on fairly polar organic solvents and, more recently, ionic liquids (discussed in section 5.3.3). First, some general features of the electrolyte solvents are discussed. Properties of some frequently used solvents for DSC electrolytes are listed in Table 6.

Organic carbonates constituted the initial choice of electrolyte solvents, and mixtures of organic carbonates have also been reported,<sup>590</sup> along with many other mixtures together with various types of dyes and cell constructions. Early work on monolithic cells included mixtures of nitriles aiming at higher boiling points in order to minimize evaporation and cell sealing problems,<sup>591</sup> which of course in general is a problem using organic solvents. In combination with plastic substrates, 3-methoxypropionitrile (MPN) has been shown to give good performance,<sup>105</sup> and it is today one of the most common electrolyte solvents used. Arakawa and others investigated the effects of a large number of common organic solvents as electrolytes with dissolved  $\text{LiI}/\text{I}_2$ , including THF, DMSO, DMF, various nitriles, alcohols, etc.<sup>592</sup> In terms of photoconversion efficiency they were all rather similar, although strongly donating solvents tended to give conduction band effects similar to nitrogen-donating additives.<sup>593</sup> The study of pure and mixed electrolytes based on propylene carbonate,  $\gamma$ -butyrolactone, *N*-methylpyrrolidone, and pyridine showed similar results, where stronger donating solvents enhance photovoltage but decrease photocurrent.<sup>594</sup> The need for organic solvents with a potential of long-term stability has triggered a search for less volatile, often called robust, solvents or electrolytes. Ionic liquids (vide infra) is one such class of solvents, but also organic solvents, such as MPN, have been shown to give improved long-term stability.<sup>595</sup>  $\gamma$ -Butyrolactone has also appeared as a chemically stable solvent, also for the formation of quasi-solid cells<sup>596</sup> and in monolithic solar cells.<sup>597</sup> Solubility is an important factor in the choice of electrolyte solvent, for instance, highlighted by the unwanted precipitation of a solid iodide-triiodide compound from electrolytes containing a popular additive, 1-methyl-benzimidazole.<sup>598</sup> The use of pyridine-acetylacetone mixtures has been investigated with the aim to avoid the need for iodide addition, relying only on heterolytic splitting of iodine to form iodide in the solution.<sup>599</sup> Bridging the gap between liquid and gelated electrolytes, low molecular mass oligomers have been used as nonvolatile solvents as well with quite good results.<sup>600</sup> The use of organic dyes also allow protic solvents to be used, for instance, ethanol in combination with a p-type semiconducting material and cyanine dyes.<sup>601</sup>

Many iodide salts have been tested in liquid electrolyte DSCs. In aprotic solvents, the position of the  $\text{TiO}_2$  conduction

**Table 6. Properties of Frequently Used Solvents for Electrolytes in Dye-Sensitized Solar Cells<sup>a</sup>**

solvent	mp/bp (°C) <sup>b</sup>	$\epsilon_r^c$	viscosity (mPa s) <sup>d</sup>	$D_{\text{I}_3^-}$ (cm <sup>2</sup> s <sup>-1</sup> ) <sup>e</sup>	comment
water	0/100	80	0.89	$1.1 \times 10^{-5}$	
ethanol	-114/78	24	1.07		
acetonitrile	-44/82	36.6	0.34	$1.5 \times 10^{-5}$	used in record cells
propionitrile	-92/97	28	0.41		
valeronitrile	-96/140	20	0.71		
glutaronitrile	-29/286	37	5.3		
methoxyacetonitrile	/119			$7.6 \times 10^{-6}$	
3-methoxypropionitrile	-57/165	36	1.1	$4-5 \times 10^{-6}$	most used in stability studies
$\gamma$ -butyrolactone	-44/204	42	1.7	$3.9 \times 10^{-6}$	
propylene carbonate	-49/242	65	2.5	$(2-3) \times 10^{-6}$	
PMImF <sup>f</sup>	-55/ <sup>g</sup>		880 <sup>g</sup>	$1.9 \times 10^{-7}$	

<sup>a</sup> Water is also shown for comparison. <sup>b</sup> Melting point/boiling point at 1 atm. <sup>c</sup> Relative dielectric constant. <sup>d</sup> Viscosity at 25 °C of the pure solvent (mPa s = cP). <sup>e</sup> Apparent diffusion coefficient for triiodide in a DSC electrolyte.  $D_{\text{I}_3^-}$  will depend on electrolyte composition. <sup>f</sup> 1-Methyl-3-propylimidazolium iodide (ionic liquid). <sup>g</sup> With 0.5 M  $\text{I}_2$  added.

band edge depends on the type and concentration of cations in the electrolyte. Redmond and Fitzmaurice found that  $\text{Li}^+$  and  $\text{Mg}^{2+}$  bind specifically onto the mesoporous  $\text{TiO}_2$  electrode, thereby determining the conduction band position.<sup>93</sup> Liu et al. found that the  $V_{oc}$  of DSCs increases as function of cation in the order:  $\text{Li}^+ < \text{Na}^+ < \text{K}^+ < \text{Rb}^+ < \text{Cs}^+$ .<sup>602</sup> Hagfeldt and co-workers studied the charge accumulation and recombination induced by different alkali metal cations, where lithium ions deviated most clearly giving lower photovoltages and shorter electron lifetimes.<sup>603</sup> In a study of the effects of monovalent to trivalent main group iodides on solar cell performance, it was found that the higher the cation charge density, the larger effects on photoelectrochemical properties were observed caused by the expected band shifts and recombination losses.<sup>604</sup>

Adsorption of cations onto the titania surface affects the local iodide concentration, as was demonstrated by Pelet et al.<sup>605</sup> The higher the effective charge of the cation, the stronger the positive effects for dye regeneration. The concentration of lithium cations in the electrolyte was shown to significantly affect the electron transport in the titania film, suggesting ambipolar diffusion.<sup>606</sup> This study was later extended to more cations and higher concentrations, giving a more complex image suggesting adsorption to titania.<sup>607</sup>

The competitive photovoltaic effects of lithium and 1,2-dimethyl-3-hexyl imidazolium ions were investigated by Park et al.<sup>608</sup> A series of alkylammonium iodides and lithium iodide were compared by Arakawa and co-workers, and large differences in photovoltage and photocurrent were observed, although not in an obviously systematic manner.<sup>592</sup> Yanagida and co-workers in a similar study could observe effects from more long-chain, aliphatic ammonium ions.<sup>609</sup> Hara et al. introduced different imidazolium iodides as sources for iodide with increasing efficiencies as a result,<sup>610</sup> later extended by others with respect to interactions with the iodine-based redox couple and the semiconductor surface.<sup>611–613</sup> Recently, new sources of iodide have been investigated with the main aim to improve blocking of the titania surface through better cation interaction.<sup>614</sup>

Interestingly enough, added water has been shown to retard recombination reactions, thus showing a potential to improve cell efficiency.<sup>615</sup>

### 5.3.2. Gel and Polymer Electrolytes

Electrolytes based on both organic solvents and ionic liquids can be gelated, polymerized, or dispersed with polymeric materials. Both types of liquids have been used as starting materials, and the inclusion of gelating or polymeric agents transforms the electrolyte into a quasi-solid electrolyte.<sup>616</sup> This type of electrolyte is discerned from hole conductors by the fact that a redox mediator is included (almost exclusively the iodide/triiodide couple) and that charge transport occurs mainly by diffusion of molecules, rather than by hopping of charge. When a large concentration of iodine is added, however, a Grotthus mechanism of charge conduction can occur in gelated media, as suggested from spectroscopic data supporting the formation of polyiodides.<sup>617</sup> Typically, these quasi-solid electrolytes show conversion efficiencies that are slightly lower than that of the host liquid redox electrolyte. This effect can most likely be attributed to limitations in the mobility of the redox couple components within the quasi-solid electrolyte. Gelating a mixture of organic carbonates using polymethylhydrosiloxane forming network structures gave efficiencies almost up to 3%.<sup>618</sup> Quite

high efficiencies of about 6% were obtained by gelating a 3-methoxypropionitrile (MPN) based electrolyte using 5 wt % poly(vinylidenefluoride-*co*-hexafluoropropylene) (PVDF-HFP), yielding thermally stable DSCs exhibiting comparably low losses in charge transport efficiency.<sup>619,620</sup> Similar performance was also achieved for another gelator based on 2,4-di-*O*-dimethylbenzylidene-D-sorbitol (DMDBS).<sup>621</sup> Also amide-coupled polymeric gels have given good results.<sup>622–625</sup> Ionic polymers integrating the  $\text{I}^-/\text{I}_3^-$  redox couple have also been tested.<sup>626,627</sup> In order to improve pore filling, *in situ* photopolymerization of poly[di(ethylene glycol)-2-ethyl hexyl ether acrylate] (PDEA) have been executed.<sup>628</sup> Low molecular weight has also been acclaimed to affect pore filling, and thus performance.<sup>629</sup> The use of ethanol as solvent medium for gelation has been denoted environmentally friendly.<sup>630</sup> A recent review on developments in both gelated and hole-conducting solid-state cells was made by Wang et al., highlighting both problems and possibilities of polymeric electrolytes.<sup>631</sup> Interface properties and fundamental understanding of essential processes were identified as future challenges. The effects of varying iodine and iodide concentrations in poly(vinylpyridine-*co*-acrylonitrile) [P(VP-*co*-AN)] have been studied.<sup>632</sup> Different alkali metal iodides (cations) cause photovoltage to increase with increasing ionic radius in poly(ethylene oxide)-based (PEO) gel electrolytes attributed to a decrease in recombination reaction,<sup>633</sup> a more clear trend than that observed in liquid electrolytes. Commercial superglue offers surprisingly good performance as gel matrix.<sup>634</sup> Hayase and co-workers investigated the gelation of ionic-liquid based electrolytes by polyvinylpyridine that was crosslinked using reaction with different alkyl dihalides, and found that longer alkyl chains led to better solar cell performance.<sup>635</sup> Hydroxystearic acid has recently been used as low molecular mass gelator.<sup>636</sup> A series of polymers with different glass transition temperatures as gelating agents indicate a correlation between transition temperature and ultimate conversion efficiency.<sup>637</sup> In a detailed study on gelation by imidazole polymers, interface charge transfer at the electrodes was identified as an important factor for photovoltaic performance.<sup>638</sup> There is also a clear trend of increasing use of ionic liquids as media, rather than organic solvents, for solidification.<sup>639</sup> For instance, thixotropic gels were made using bis(imidazole) ionic liquids,<sup>640</sup> and silica particles were shown to increase performance in gels originating from binary ionic liquid mixtures.<sup>641</sup> Binary imidazolium ionic liquids have also been used together with PEO-type polymers.<sup>642</sup> Silane-functionalized benzimidazolium iodide ionic liquids gave gelation at a temperature of 60 °C. Interestingly, the DSC performance improved after gelation.<sup>643</sup>

A large number of the gelated electrolytes are more or less complex composites. Poly(ethylene oxide) (PEO) polymers have over the last 5 years or so grown to be extremely popular as matrix materials and exist in several forms as electrolyte supports in solid state cells. Various pure (of different molecular weight), mixed (often with PVDF), and composite electrolytes have been used involving nanocomposites with silica, titania, and many other inorganic additives.<sup>644–674</sup> The oligomer size or molecular weight was shown to influence conductivity and photoelectrochemical properties and suggest the existence of an optimal chain length.<sup>675,676</sup> Just as for liquid electrolytes, the effects of sequestering agents aimed at, in particular, lithium cations have been shown to increase photocurrents.<sup>677</sup> At higher

iodine/iodide concentrations, polyiodide species were shown to form.<sup>678,679</sup> Also, composites based on poly(ethylene oxide dimethyl ether) (PEODME) have shown very high performances caused by enhanced ionic conductivity.<sup>680</sup> Inorganic/organic nanocomposites of various compositions have been formulated and investigated,<sup>681–694</sup> containing metal oxides, carbon materials, ionic and hole conducting materials, etc. One of the more interesting aspects is to include hybrid crystalline materials with channels for iodine/iodide conduction,<sup>695</sup> which in contrast to liquid electrolytes do not seem to benefit from Grotthus type of conductivity at higher iodine concentrations.<sup>696</sup> The conductivity of PEO electrolytes can be improved by the introduction of oligomers.<sup>697</sup> The terminal groups of the oligomers have significant effects on DSC performance, due to, for instance, interaction with the iodine-based redox couple.<sup>698</sup> Recent developments appear to mimic those in liquid electrolytes, moving toward more complex and multicomponent electrolyte systems. Examples of such development involve ternary quasi-solid systems composed of polymer, oligomer, and nanofiller, giving a slight boost in overall efficiency.<sup>699,700</sup> Although conductivities appear to be high in comparison with liquid electrolytes, mass transport under irradiation and electrode interface effects are limiting factors. It is also relevant to note that high conductivity as such is no guarantee for good conversion efficiency; it is the mobility or conductivity of redox-active species and the kinetics of the reactions at the oxide/dye/electrolyte interface that are of pivotal importance. Also quaternary ammonium functionalized poly(ethylene oxide) and other polymers and functional groups have been employed as conducting electrolytes.<sup>701–704</sup> Polysaccharides have been shown to work as electrolyte solidifiers.<sup>705,706</sup> In PEO-based polymeric systems the cation size of added iodides was shown to strongly influence performance and was discussed in terms of intercalation and surface adsorption.<sup>707</sup> Both gelated and hole-conducting electrolytes were reviewed by De Paoli et al. in 2004.<sup>708</sup> Two critical reviews of the status of the field were very recently published by De Paoli and co-workers and Wang highlighting the possibility to up-scale flexible solar cells based on quasi-polymeric electrolytes.<sup>709,710</sup> Considering the amount of work invested in these systems, it is remarkable that the maximum conversion efficiencies remain fairly constant around 5%. Most likely, fundamental insights into interface processes will be required for significant improvements in performance.

A solid polymer electrolyte based on poly(epichlorohydrin-co-ethylene oxide), containing sodium iodide and iodine but only trace amounts of solvent, exhibited rather low efficiencies.<sup>711,712</sup> The poor performance was later attributed to high internal resistance.<sup>713</sup> More recently, promising results for solvent-free polymer electrolytes were obtained using poly(vinyl pyridine) iodides (efficiency up to 5.6%).<sup>714</sup>

Plastic molecular crystals have been applied as battery and fuel cell electrolytes and were also successfully used in DSCs. An electrolyte based on succinonitrile doped with *N*-methyl-*N*-butylpyrrolidinium iodide and iodine, with an appearance of a waxy solid, gave an effective diffusion coefficient for triiodide of  $2 \times 10^{-6} \text{ cm}^2 \text{ s}^{-1}$  and yielded solar cell efficiencies of up to 6.7% (0.5 sun; 5% at 1 sun).<sup>715</sup>

### 5.3.3. Ionic Liquid Electrolytes

Ionic liquids were first tested in the Grätzel lab with respect to dye-sensitized solar cells with the main aim to qualify new nonvolatile electrolyte solvents.<sup>716</sup> The first ionic liquids

tested belong to the imidazolium family, and these are the most commonly used in electrochemical applications, also in solar cells. Both good photoelectrochemical performance and stability were observed. In addition, the concept of Grotthus conductivity was verified at the higher iodine concentrations used to compensate for mass transport limitations of the rather viscous ionic liquids. Both organic cations and anions affect fundamental properties of ionic liquids, as well as photoelectrochemical properties.<sup>717</sup> A thorough review of the utilization of ionic liquids in dye-sensitized solar cells was recently reported.<sup>639</sup> The ionic liquid electrolytes were divided into two sections, pure ionic liquids and quasi-solid electrolytes based on ionic liquids. The area is vastly dominated by imidazolium-based electrolytes, and some of the main conclusions were that the combination of photochemical stability and low viscosity, and thus ion mobility, remains a challenge. As noted above, ionic liquids have become a frequently used medium for gelation to provide quasi-solid-state devices, also including nanoparticle additives.

A special class of ionic liquid electrolytes are made by the inclusion of long-chain hydrocarbon substitutes on the organic cation forming ionic liquid crystalline systems.<sup>718</sup> Yanagida et al. have studied dodecyl-substituted imidazolium iodides and compared their performance with non-liquid-crystal systems of similar composition<sup>241,719</sup> in DSCs. The high photocurrents and conversion efficiencies observed were attributed to the self-assembled, low-dimensional structures enhancing a Grotthus mechanism of conductivity of the iodine/iodide components of the system despite the high viscosity of the electrolyte medium. Grätzel and co-workers have shown the importance of tuning the components, where hydrocarbon substituents to the sensitizing organometallic dye strongly influence performance.<sup>321</sup> We note that a recent study raises the question whether in more concentrated systems, for example ionic liquids, the role of the Grotthuss mechanism may have been overestimated by neglecting the possible impact of ion association.<sup>322</sup>

Recent developments involve the use of eutectic mixtures in order to reduce melting points and effectively in this way reduce mass transport limitations. The approach has proven to be highly successful with cell performances over 8% as a result.<sup>720,721</sup> Interesting results have been reported for tetrahydrothiophene-based liquids as well.<sup>722</sup> Also, new types of iodide salts have been investigated with less pronounced effects.<sup>723</sup> The inclusion of a silica layer between the electrodes in bifacial ionic liquid based dye-sensitized solar cells improved their performance by preventing shunt losses when the counter electrode is placed close to the photoanode.<sup>724</sup> One of the main conclusions of the Gorlov review was that the different components in the DSC need to be specifically adapted to new electrolyte classes, and some steps toward the design and investigation of new sensitizing dyes for ionic liquid systems have been initiated.<sup>443,482</sup> Building on the idea of efficient charge transport in one-dimensional morphology, also nanotubes of titania have been investigated together with ionic liquids with good performance despite the considerably lower surface area.<sup>725</sup> Recent developments have been highlighted by Zakeeruddin and Grätzel.<sup>726</sup> In a series of substituted imidazolium iodides as electrolytes, Kim et al. found that small cation substituents gave higher diffusion coefficients of triiodide and thus higher photocurrents, whereas larger substituents displayed an increase in photovoltage.<sup>727</sup> In rather low-viscosity imida-

zolium dicyanamide ionic liquids, triiodide diffusion was shown to be a limiting factor at low temperature, whereas recombination reactions limited the performance at high temperatures.<sup>728</sup> In a series of imidazolium ionic liquids with a vinyl group on the organic cation, viscosity and thus conductivity were shown to be of major importance for performance.<sup>729</sup> Low-melting but solid imidazolium-based iodide salts applied by melting onto or into the photoelectrode have been used as solid electrolytes as well with quite good results.<sup>730</sup> The diffusion constant of triiodide was shown to be higher in binary imidazolium ionic liquids than in pure iodide liquids.<sup>731</sup> New ionic liquids based on *N*-methyl-*N*-allylpyrrolidinium, cyclic guanidinium, or dicationic bis-imidazolium have recently been reported.<sup>732–734</sup> Layered titanates have been introduced into ionic liquids in order to enhance conductivity.<sup>735</sup> One can thus discern two main current strategies to overcome the mass transport problems in ionic liquid electrolytes; either to use eutectic multicomponent melts in order to lower melting points and consequently minimize internal melt structures affecting viscosity and ion mobility or to include solid components to boost conductivity.

### 5.3.4. Additives

Additives play a central role in the enhancement of photoelectrochemical performance of DSCs. Most additives are understood at a fairly phenomenological level, and their effects are often attributed to modification of redox couple potential, band shifts of the semiconducting electrode material, effects of surface blocking, or surface dye organization. Most additives that have been reported contain an electron-donating nitrogen heterocycle, such as 4-*tert*-butylpyridine.

4-*tert*-Butylpyridine (TBP) was first applied in DSCs by Grätzel and co-workers in 1993, demonstrating a remarkable increase in  $V_{oc}$  of these cells in combination with LiI-based electrolytes.<sup>40</sup> On the basis of intensity-modulated photovoltage spectroscopy (IMVS) measurements, it was shown that TBP shifts the titania band edge toward higher energies.<sup>736</sup> Haque et al. studied the effects of TBP and lithium cations on shifts of TiO<sub>2</sub> conduction band and trap levels, as well as on recombination kinetics between electrons in TiO<sub>2</sub> and oxidized dye molecules.<sup>737</sup> The change in the kinetics was attributed to the change in TiO<sub>2</sub> energy levels. The effects of TBP were studied in more detail in DSCs showing that both band edge shift and increased electron lifetime play a role.<sup>94</sup> An in situ Raman spectroscopic study showed that TBP binds to the titania surface and most likely also to iodine or the dye molecules.<sup>738</sup> Further surface analysis studies support a defect covering hypothesis.<sup>739,740</sup> The best working organometallic dyes tend to contain thiocyanate ligands, and the dissociation of these ligands into the electrolyte solvent has been proposed as one possible reason for cell performance degradation. In a vibrational spectroscopic study TBP was proposed to suppress the loss of SCN<sup>−</sup> from the ruthenium-based dyes.<sup>741</sup>

Although TBP and Li<sup>+</sup> ions have opposite effects on the conduction band and trap states, and thus on the kinetics of electron injection and recombination, it is a very common combination of additives in solar cell electrolytes. The reason for the good overall performance of this combination is not fully understood. Adding to the complexity results from ionic liquids with varying amounts of water, the interplay between lithium cations, TBP, and water appeared to be essential and complicated.<sup>742</sup>

A large number of pyridines and other N-heterocycles have been investigated as additives in DSC, generally giving similar results as TBP. A series of pyridine derivatives and ammonia improved mainly photovoltage through reduction of recombination reaction rates.<sup>743</sup> Essentially the same effects were observed for 4-ethoxy-2-methylpyridine as additive.<sup>744</sup> 1-Methyl-benzimidazole was shown to interact with lithium cations and triiodide anions to reduce titania surface coordination and consequently suppress recombination reactions.<sup>745,746</sup> Kusama, Arakawa, and co-workers have studied the effects of large series of different types of nitrogen-donating additives, including pyrimidines, amino-triazoles, quinolines, benzimidazoles, alkylaminopyridines, and alkylpyridines, etc.,<sup>745,747–752</sup> and also later sulfur-containing groups as donors, such as aminothiazoles.<sup>753</sup> The interaction between iodine and different nitrogen-donating additives were investigated at density-functional and perturbation-theory levels and found to be of the expected donor–acceptor type.<sup>754–757</sup> The deduced additive effects concern both the titania surface and interactions with the iodine-based redox couple components,<sup>758</sup> where correlations were made between charge-transfer interaction and photovoltage.<sup>757,759</sup> Periodic density-functional calculations have shown nitrogen-containing additives to shift the TiO<sub>2</sub> conduction band to higher energies in accordance with experiment.<sup>760,761</sup>

In contrast to TBP and similar additives, guanidium thiocyanate shifts the conduction band edge of TiO<sub>2</sub> toward lower energies, suggesting adsorption of the cation onto the TiO<sub>2</sub> surface. In addition, it increases the electron lifetime in DSCs.<sup>762</sup> Coadsorbants, adsorbed onto the TiO<sub>2</sub> during the dye adsorption procedure, can have similar effects as additives in the electrolytes. They are discussed in section 5.4.

### 5.3.5. Alternative Redox Couples

The ubiquitous combination of I<sup>−</sup> and I<sub>3</sub><sup>−</sup> appears very hard to replace; it simply performs better than all alternatives tested so far. Its success relies mainly on the slow recombination reaction.<sup>763,764</sup> The corrosive and photochemical properties of iodine are strong driving forces in the search for alternative redox couples. Two main directions can be identified, one toward molecular species of similar types as the iodine-based one and another aiming at transition-metal-based systems. Gregg and Pichot tested iodine-, ferrocene-, and hydroquinone-based redox couples and found the electrochemical potential to be highly correlated to observed photovoltage.<sup>765</sup> Arakawa and co-workers used a LiBr/Br<sub>2</sub> mixture as redox couple in a series of electrolytes with rather low efficiencies as a result.<sup>592</sup> However, the Br<sup>−</sup>/Br<sub>3</sub><sup>−</sup> redox system was shown to give better results using eosin as sensitizer.<sup>766</sup> Interhalogen redox couples were studied by Gorlov and co-workers in organic solvents and ionic liquids displaying a rather complex equilibrium system not meeting the parent iodide/triiodide system in performance.<sup>767</sup> The step away from halogens to pseudohalogens is not so large, and the use of the corresponding SCN<sup>−</sup>/(SCN)<sub>3</sub><sup>−</sup> and SeCN<sup>−</sup>/(SeCN)<sub>3</sub><sup>−</sup> redox couples have shown to be very promising from an electrochemical and noncorrosion aspect, for instance, generating similar photovoltages as the standard I<sup>−</sup>/I<sub>3</sub><sup>−</sup> couple, although chemical instability is a disqualifying property for practical use.<sup>64,66,768</sup> Stable organic radicals originating from 2,2,6,6-tetramethyl-1-piperidinyloxy (TEMPO) have shown promising performance as a replacement to the

standard iodine-based redox system with efficiencies above 5%, despite suffering from drawbacks caused by higher recombination rates (common for all one-electron systems).<sup>769</sup> The compound *N,N'*-di-*m*-tolyl-*N,N'*-diphenylbenzidine (TPD) has also been tested as redox mediator.<sup>68</sup> New redox couples based on sulfur-containing species have very recently been reported reaching an efficiency of 6.4% at AM 1.5 G. In contrast to the iodine-based redox couple, these are non-corrosive but are obviously two-electron systems involving the formation/breakage of an S–S bond.<sup>770</sup>

As for transition metal systems, the Co<sup>2+/3+</sup> system appears promising involving, for instance, cobalt(II)/(III)-bis[2,6-bis(1'-butylbenzimidazol-2'-yl)pyridine] (Co(dbbib)<sub>2</sub><sup>2+β3+</sup>).<sup>771</sup> The kinetics of electron transfer appears to be very good but that also includes back-donation in recombination reactions. In a study of a selection of cobalt(II)/(III)-polypyridine complexes, lithium ions were found to improve performance, in contrast to the iodide/triiodide system.<sup>51</sup> The diffusion constant of the cobalt-based redox couple cobalt(II/III)-tris(4,4'-di-*tert*-butyl-2,2'-bipyridine) (Co(DTB)<sub>3</sub><sup>2+β3+</sup>) was found to be least an order of magnitude lower than that for the triiodide ion inside the pores of dye-sensitized TiO<sub>2</sub>,<sup>772</sup> which leads to mass transport problems at higher irradiation. In a study of a few cobalt(III/II)-tris(bipyridine) compounds, mass transport limitations were identified as a limiting factor.<sup>773</sup> Yanagida and co-workers studied a series of copper(I)/(II) complexes as redox systems because of expected low reorganizational energies upon reduction/oxidation.<sup>774</sup> High photovoltages were obtained and efficiencies of up to 1.4%. With similar thoughts in mind, also mediator mixtures containing ferrocene have been used.<sup>775</sup> Rapid back reaction has previously shown ferrocene to be less suitable as redox mediator on its own.<sup>68,776</sup> High recombination rates seems to be a general problem using one-electron redox systems requiring extra measures to block recombination from the TCO and semiconductor surfaces. In an optimization study using different cobalt complexes, different sensitizing dyes, different film thicknesses, etc., the importance of a blocking underlayer was highlighted.<sup>777,778</sup> Quite recently, Mirkin and co-workers report the use of Ni(III)/Ni(IV) bis(dicarbollide) as a reasonably efficient alternative redox couple. Detailed analyses of electron kinetics are needed in order to verify its good and bad properties with respect to wanted and unwanted electron transfer.<sup>779,780</sup> Finding good ways to block recombination reactions or alternatively to identify new one-electron redox systems with inherent slow recombination appears to be the current challenge.

### 5.3.6. Solid Organic Hole Conductors

There is a general drive away from volatile electrolytes or electrolyte components. One route is to use ionic liquid systems. Another route involves organic hole conductors of various types and techniques of application. In organic hole conductors, positive charge moves by a hopping mechanism between neighboring molecules or moieties, as opposed to redox electrolytes where charge transport is due to movement of redox molecules. The hole conductors typically also contain additives of salts allowing for some ionic conductivity, which is important for local charge compensation.

Organic hole conductors can be divided into two classes, conducting polymers and molecular hole conductors. The first report using conducting polymers in DSCs was from Yanagida and co-workers, who reported efficiencies of about 0.1% for polypyrrole systems doped with LiClO<sub>4</sub>.<sup>781</sup> The use

of a carbon counter electrode was shown to increase efficiencies considerably. The polypyrrole was electropolymerized *in situ* in the pores of the TiO<sub>2</sub> film. Chemically polymerized poly(3,4-ethylenedioxothiophene) (PEDOT) was shown to give reasonable results in the presence of ionic constituents.<sup>782</sup> This system has later been improved using electropolymerization, hydrophobic sensitizers,<sup>783–785</sup> and various doping agents.<sup>786,787</sup> Effects of lithium salts on PEDOT with different anions identified the bis-trifluoromethanesulfonylimide anion to give the best results.<sup>787</sup> Recently, this work has been extended to anions containing perfluoroalkyl chains mainly affecting conductivity.<sup>788</sup> The performance of different organometallic dyes in solid-state DSCs was reviewed by Yanagida et al.<sup>789</sup> A selection of polycarbazoles has also been studied, and their energy levels were modified in comparison with dye and semiconductor levels.<sup>790</sup> As for other systems, pore filling has been identified as a major fundamental factor influencing efficiencies.<sup>791</sup> Similar effects were shown for polyanilines (PANI),<sup>792</sup> as well as an improvement of performance using polymer-based counter electrodes.<sup>793</sup> In situ electrochemically polymerized poly(*o*-phenylene diamine) containing multiwall carbon nanotubes have also been tested as hole-conducting material in DSCs.<sup>794</sup> Spin-coating is a common technique for polymer application, such as for poly(3-octylthiophene) (P3OT), which represents an obvious alternative for hole conduction as well as light absorption based on thiophenes.<sup>795</sup> Reasonable results have also been obtained with spin-coated poly(4-undecyl-2,2'-bithiophene) as hole conductor.<sup>796</sup> ZnO is a material that easily forms nanorods highly suitable for maximizing semiconductor–polymer contact. Such structures were investigated together with a poly-3-hexylthiophene (P3HT) polymer with promising results.<sup>797</sup> Solid-state DSCs based on dyes with thienyl groups and P3HT doped with ionic liquids and TBP as hole conductor showed good performance (efficiency 2.7%), attributed to the good interaction between dye and polymer and good electrostatic shielding effect due the ions.<sup>798</sup>

Triarylamine-based compounds, such as 2,2',7,7'-tetrakis(*N,N*-di-*p*-methoxyphenylamine)-9,9'-spirobifluorene (spiro-MeOTAD), are the most popular molecular hole conductors in solid-state DSCs. They were first introduced by Bach et al. in 1998.<sup>799,800</sup> Compounds such as 2,2',7,7'-tetrakis(*N,N*-diphenylamine)-9,9'-spirobifluorene (spiro-TAD) and 2,2',7,7'-tetrakis(*N,N*-di-*m*-methylphenylamine)-9,9'-spirobifluorene (spiro-*m*-TTB) were applied through vapor deposition.<sup>801</sup> The spiro center is acclaimed to increase thermal stability. Studies of nondoped spiro-MeOTAD displayed very low hole conductivity combined with efficient recombination as two practical problems.<sup>802</sup> Rau et al. made a comparison between liquid and solid electrolytes and concluded that recombination is a larger problem in the solid cells than in the liquid ones.<sup>803</sup> It is notable that the organic hole conductors also are subjected to modifications using similar additives as in liquid electrolytes, such as lithium salts and TBP, in order to increase conversion efficiencies.<sup>804</sup> The observed effects are in part analogous to the ones in liquid electrolytes, although the complexity of the system cannot rule out that also effects from ion conduction play a role. The addition of non-redox-active lithium salts increased the hole conductivity considerably, an effect not fully characterized.<sup>805</sup> The importance of the interplay between sensitizing dye, hole conductor, and cation additives was highlighted by the effects caused by cation coordinating dyes,<sup>310,806</sup> in part attributed

to longer electron lifetimes.<sup>807</sup> In a mechanistic study of triarylamine-based hole conductors, it was concluded that the photocurrent was directly proportional to the hole-transfer yield, emphasizing the importance of efficient pore-filling and interface energetics rather than hole conductivity.<sup>808–810</sup> In an impedance spectroscopy study, a higher recombination rate compared to that observed in DSCs with ionic liquid electrolytes was identified as a major limiting factor with respect to liquid cells.<sup>811</sup> Mechanistic studies also highlighted the fact that it is conduction in the titania film rather than in the hole conductor that is a limiting factor in solid-state cells.<sup>812</sup> Such anticipations have also been supported by results using different hole-conducting materials.<sup>813</sup> A liquid hole conductor was studied based on tris-[4-(2-methoxy-ethoxy)-phenyl]-amine (TMEPA) and was shown to have similar properties as the solid-state analogues.<sup>814</sup> The record solar cell efficiency for DSCs with solid molecular hole conductors currently lies at 5.1%.<sup>815</sup>

A general problem with solid hole conductors in DSCs is the pore filling. It does not need to be 100%, but for efficient cells, it is necessary that all dye molecules are in contact with both the TiO<sub>2</sub> and the hole conductor and that there are no (or very few) interruptions in the hole-conducting path. These limitations have led to the fact that most efficient DSCs with organic hole conductors have a TiO<sub>2</sub> film thickness of about 2 μm only. The pore filling of mesoporous TiO<sub>2</sub> with spiro-MeOTAD was estimated by Snaith et al. from the thickness of the overstanding layer after the spin-coating procedure.<sup>816</sup> McGehee and co-workers determined it using UV-vis spectroscopy redissolving the hole conductor after deposition.<sup>817</sup> Both studies suggest that more than 60% pore filling can be achieved for films less than 3 μm thick. An XPS profiling study showed that spiro-MeOTAD was infiltrated homogeneously in a 5 μm film.<sup>817</sup> Using photo-induced absorption spectroscopy Cappel et al.<sup>818</sup> showed that in principle all dye molecules appeared to be in contact with the hole conductor in a 6 μm thick TiO<sub>2</sub> film. An interesting approach to overcome pore-filling problems is to melt the hole conductor to fill the pores.<sup>819</sup>

### 5.3.7. Inorganic Solid Hole Conductors

Already in 1995, Tennakone et al. used CuI precipitated from solution as inorganic hole conductor in dye-sensitized solar cells.<sup>70</sup> CuI has also been used with other semiconductor materials.<sup>820</sup> CuI precipitated from acetonitrile solution has shown to work as p-type inorganic conductor together with an organometallic dye showing rather high conversion efficiencies of about 3%.<sup>821</sup> However, photodegradation appears to be a larger problem than it is in liquid cells.<sup>822</sup> A similar synthetic approach was employed for CuSCN.<sup>823,824</sup> The use of CuSCN as hole conductor resulted in similar charge transport properties as in liquid cells, but recombination reactions were orders of magnitude faster giving considerable losses.<sup>825</sup> Also, a CuBr-based sulfide compounds and NiO have been used as hole conductors.<sup>826,827</sup> The feasibility of both CuSCN and Au metal as hole conductors were illustrated in flat device structures by Lenzmann et al.<sup>828</sup> By layering gold nanoclusters onto a flat titania surface, Lai et al. could obtain measurable conversion efficiencies.<sup>829</sup> Transport properties of CuSCN have been shown to be superior to liquid electrolytes.<sup>830</sup> Just as for organic hole conductors, losses caused by recombination reactions constitute a major problem. Therefore, O'Regan et al. have investigated the effects of a tunnel barrier based on alu-

mina.<sup>831</sup> The intended reduction in recombination was achieved, but experimental difficulties and lack of fundamental understanding of the recombination processes were highlighted. A general problem appears to be the formation of too large crystallites in the mesoporous films used, not fully counteracted by crystal growth inhibitors.<sup>832,833</sup>

## 5.4. Surface Passivation of Dye-Sensitized TiO<sub>2</sub>

The recombination reaction between electrons in the TiO<sub>2</sub> and electron acceptors in the electrolyte (or solid-state hole conductors) can be suppressed in various ways: by the use of coadsorbers, by additives in the electrolyte, or by thin blocking layers covering the TiO<sub>2</sub> surface. It should be noted that the dye itself can have a significant blocking effect.<sup>834</sup> Coadsorbers are added to the dye bath upon dye adsorption. They can occupy spaces between dye molecules and can assist favorable packing of dye molecules by avoiding aggregation.<sup>429,835</sup> This is helpful for many organic dyes. Usually they are added in a large concentration and bind weakly on the TiO<sub>2</sub> so that the dye replaces them upon adsorption. Cholic acid derivates were found to decrease the dark current in combination with coumarin dyes,<sup>429</sup> while they increased recombination of electrons with triiodide in case of Ru(dcbpy)<sub>2</sub>(NCS)<sub>2</sub> as a sensitizer.<sup>836</sup> Hexadecylmalonic acid and 1-decyldiphosphonic acid were used successfully in combination with the amphiphilic Ru complex Z907: they reduced dye coverage and dark current but increased solar cell efficiency and stability.<sup>837,838</sup> The use of  $\omega$ -guanidinoalkyl acids led to reduced recombination and shifted the TiO<sub>2</sub> conduction band edge toward higher energies.<sup>839</sup>

Several types of additives that are added to the iodide/triiodide electrolyte, such as 4-*tert*-butylpyridine and guanidium thiocyanate, suppress the reaction of electrons in TiO<sub>2</sub> with triiodide, presumably mostly by binding to the TiO<sub>2</sub> surface. These additives are discussed in section 5.3.4.

Ultrathin metal oxide layers have been applied on the surface of the mesoporous electrode to improve their performance in the dye-sensitized solar cell. Kumara et al. applied Al<sub>2</sub>O<sub>3</sub> on mesoporous SnO<sub>2</sub> and found a much increased  $V_{oc}$  and an improved DSC performance for small amounts of Al<sub>2</sub>O<sub>3</sub>, while large amounts decreased the photocurrent.<sup>840</sup> Kay and Grätzel tested a large series of insulating oxides on SnO<sub>2</sub> and found that basic oxides improved the dye adsorption and the DSC performance.<sup>841</sup> The optimum thickness was only a few Ångströms. A decrease in UV response of the photocurrent was found for Al<sub>2</sub>O<sub>3</sub>-coated TiO<sub>2</sub>. Chen et al. found improved DSC performance with Nb<sub>2</sub>O<sub>5</sub>-coated TiO<sub>2</sub> electrodes.<sup>842</sup> Palomares et al. applied Al<sub>2</sub>O<sub>3</sub>, SiO<sub>2</sub>, and ZrO<sub>2</sub> on the surface of TiO<sub>2</sub> electrodes by a dip-coating technique using metal alkoxy precursors.<sup>843</sup> They found that recombination between electrons and oxidized dye molecules were slowed in all cases. Thicker Al<sub>2</sub>O<sub>3</sub> layers were found to decrease the quantum efficiency for electron injection, which led to a reduced photocurrent. Alarcon et al. showed that increased thickness of Al<sub>2</sub>O<sub>3</sub> onto TiO<sub>2</sub> led to the same effects and found that the optimum Al<sub>2</sub>O<sub>3</sub> coverage for standard DSCs corresponded to submonolayer coverage.<sup>844</sup> O'Regan et al. demonstrated that in solid-state DSCs with CuSCN as hole conductor the recombination rate between electrons in TiO<sub>2</sub> and holes in CuSCN was strongly reduced by addition of a thin Al<sub>2</sub>O<sub>3</sub> blocking layer, leading to improved  $V_{oc}$  and fill factor.<sup>223</sup> Hamann et al. used atomic layer deposition (ALD) to prepare ultrathin Al<sub>2</sub>O<sub>3</sub> blocking layers on mesoporous

$\text{TiO}_2$  in a very controlled way.<sup>845</sup> This allowed them to use fast ferrocene-based redox mediators. The electron lifetime increased exponentially with the number of ALD cycles, but the photocurrent decreased strongly at the same time.  $\text{SiO}_2$  blocking layers on mesoporous  $\text{ZnO}$  electrodes were found to increase their chemical stability.<sup>846</sup>

Efficient surface passivation can also be obtained using carbonates. Sugihara and co-workers obtained good results with  $\text{CaCO}_3$  (1% Ca molar ratio with respect to Ti as measured by XPS), giving longer electron lifetimes and increased  $V_{\text{oc}}$  and  $J_{\text{sc}}$ .<sup>847</sup> Zhang and Zaban used an in situ passivation technique by adding  $\text{CO}_2$ ,  $\text{Li}_2\text{CO}_3$ , or  $\text{K}_2\text{CO}_3$  to the electrolyte, leading to deposition of isolating carbonates on the dyed mesoporous electrode and improved solar cell performance.<sup>848</sup>

Gregg et al. developed a silanization treatment to form a blocking layer on the mesoporous electrode after dye adsorption.<sup>221</sup> Their aim was to block parts of the electrode not covered by dye from the electrolyte so that they could use fast one-electron redox couples. They demonstrated for the first time a working mesoporous  $\text{TiO}_2$  solar cell using ferrocene as the redox mediator.

## 5.5. Counter Electrodes

### 5.5.1. Platinized Conducting Glass

Counter electrodes for DSCs with iodide/triiodide electrolytes can be rather easily prepared by deposition of a thin catalytic layer of platinum onto a conducting glass substrate. Without platinum, conducting tin oxide ( $\text{SnO}_2:\text{F}$ ) glass is a very poor counter electrode and has a very high charge transfer resistance, more than  $10^6 \Omega \text{ cm}^2$ , in a standard iodide/triiodide electrolyte.<sup>237</sup> Pt can be deposited using a range of methods such as electrodeposition, spray pyrolysis, sputtering, and vapor deposition. Best performance and long-term stability has been achieved with nanoscale Pt clusters prepared by thermal decomposition of platinum chloride compounds.<sup>81</sup> In this case, very low Pt-loadings ( $5 \mu\text{g cm}^{-2}$ ) are needed, so that the counter electrode remains transparent. Charge transfer resistances of less than  $1 \Omega \text{ cm}^2$  can be achieved. Pt films prepared by other methods such as electrodeposition<sup>81</sup> and vapor-deposition<sup>849</sup> on TCO substrates were found to dissolve in iodide/triiodide electrolytes and are therefore not suitable as counter electrodes in DSCs.

### 5.5.2. Carbon Materials

Carbon materials are suited as catalysts for the reduction of triiodide. Kay and Grätzel developed a counter electrode from a mixture of graphite and carbon black for use in DSCs with the monolithic cell geometry.<sup>850</sup> The function of the graphite was electronic conduction as well as catalytic activity, while the high-surface area carbon black was added for increased catalytic effect. Pettersson et al. optimized the performance of the counter electrode by using two carbon layers: one for enhanced adhesion to the substrate and one for enhanced catalytic effect (doped with Pt) as well as good electronic conductivity.<sup>597</sup>

Films prepared on TCO substrates from carbon powders with particle sizes on the order 30 nm (carbon black) showed low charge transfer resistance, down to  $1 \Omega \text{ cm}^2$  when the film thickness was up to  $20 \mu\text{m}$ .<sup>851,852</sup> Activated carbons with BET areas of more than  $1000 \text{ m}^2 \text{ g}^{-1}$ , mixed with carbon black were also found to be suitable as a component in

counter electrodes.<sup>853</sup> Single wall carbon nanotubes showed good catalytic properties for triiodide reduction as well as good conductivity.<sup>854</sup>

### 5.5.3. Conducting Polymers

Poly(3,4-ethylenedioxythiophene) (PEDOT) doped with toluenesulfonate anions shows good catalytic properties for the reduction of triiodide and was successfully applied in DSCs.<sup>855–857</sup> Films were prepared onto TCO substrates and a charge transfer resistance of less than  $1 \Omega \text{ cm}^2$  could be obtained for films that were more than  $1 \mu\text{m}$  thick. Other conducting polymers (polyaniline, polypyrrole) were much less suited.<sup>855</sup>

### 5.5.4. Cobalt Sulfide

Very recently, electrodeposited CoS has been identified as a suitable catalyst for the iodide/triiodide redox couple.<sup>858</sup> Deposited on a flexible substrate (ITO/PEN) it outperforms Pt on the same substrate, with a charge transfer resistance down to  $1.8 \Omega \text{ cm}^2$ , while thermal Pt on FTO gave  $1.3 \Omega \text{ cm}^2$  using the same ionic liquid electrolyte.

## 5.6. Tandem Cells and p-Type DSCs

The DSC technology discussed so far relies on a single absorber and has therefore a limitation to the maximum efficiency that can be reached, the Shockley–Queisser limit of about 31%, in the same way as a single bandgap semiconductor photovoltaic device. To make DSCs a third-generation technology, efficiencies beyond this limit must be reached. One possible way of achieving this is to fabricate tandem solar cells with DSC. This can be achieved by placing DSCs with different absorption spectra after one another, using either series or parallel electrical connection,<sup>859,860</sup> or more interestingly, by making both electrodes of one photoelectrochemical solar cell photoactive. For a tandem DSC device with both electrodes photoactive, the theoretical limit is 43%.<sup>30</sup> A schematic idealized energy level diagram of a tandem DSC indicating the desired electron transfer processes is shown in Figure 20.

In this figure, irradiation takes place from the photoanode side. This part of the tandem cell operates as the conventional n-type DSC. The sensitizer adsorbed on the n-type semiconductor is designed to absorb high-energy photons in the blue part of the solar spectrum. Low-energy photons, red part of the solar spectrum, are transmitted to the p-type DSC. Here the photoexcited sensitizer reduces the redox couple

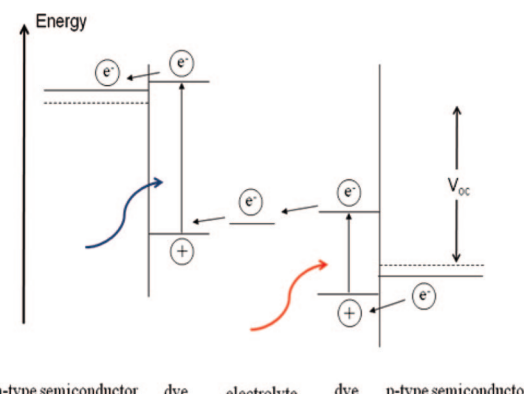


**Figure 20.** A schematic idealized energy level diagram of a tandem DSC indicating the desired electron transfer processes.

and an electron in the valence band of the semiconductor is transferred to the HOMO level of the dye (or, in other words, a hole from the dye is injected into the VB of the semiconductor). In this type of tandem cell, the redox system in the electrolyte is analogous to the so-called recombination layer referred to in conventional multijunction devices. The  $V_{oc}$  is then the difference between the quasi-Fermi levels above the valence band of the photocathode and below the conduction band of the photoanode and is therefore the sum of the  $V_{oc}$ 's of the individual n- and p-type devices. In the tandem DSC, we note that the redox potential of the electrolyte does not determine the  $V_{oc}$  of the tandem device but must be matched for efficient electron transfer reactions at the respective photoelectrodes. The total current is limited by the lower performing electrode, and the currents from both sides must be matched.

An intrinsic property of DSCs is that the device can be designed by appropriate choice of the sensitizer to absorb and quantitatively convert incident photons to electric current in selective spectral regions of the solar emission, while maintaining high transparency in the remaining wavelength range. Another interesting property of sensitized nanostructured electrodes is that their short-circuit photocurrent output can readily be varied by changing the film thickness and effective pore size. This, along with the ease of formation of multilayer structures by simple techniques, such as screen printing, constitutes a great advantage with regard to conventional solar cells, to fabricate and optimize tandem cells. Research and development of tandem DSCs is very much in its infancy. First, efficient photocathodes must be developed. Unlike the n-type devices, there have been few reports of p-type DSCs.

Early studies on dye-sensitization of p-type semiconductors were carried out by Tennakone et al.<sup>861,862</sup> CuSCN was used as the p-type semiconductor sensitized with SCN<sup>-</sup> salts of cationic dyes such as methyl violet and the standard I<sup>-</sup>/I<sub>3</sub><sup>-</sup> redox couple was used. Low photocurrents on the order of 100  $\mu$ A cm<sup>-2</sup> were obtained when the films were illuminated by a 60 W tungsten filament lamp, due to a low porosity of the CuSCN film.

In 1999, He et al. reported dye-sensitized nanostructured NiO photocathodes.<sup>565</sup> NiO is a transparent (band gap energy is  $\sim$ 3.6 eV) p-type semiconductor with a cubic (bunsenite) structure. The valence band lies around 0.54 V vs NHE at pH 7.<sup>88</sup> Erythrosin B and tetrakis(4-carboxyphenyl)porphyrin (TPPC) were used as photosensitizers, and under illumination a cathodic current was generated at wavelengths corresponding to the absorption spectrum of the dyes when irradiated with monochromatic light. For erythrosine B, a short-circuit photocurrent of 0.23 mA cm<sup>-2</sup> and a  $V_{oc}$  = 98.5 mV at simulated sunlight (68 mW cm<sup>-2</sup>) were obtained. The overall efficiency was low (<0.01%) and the  $V_{oc}$  was limited by the small energy difference between the NiO valence band and the redox system. Thus, NiO is not the preferred choice as a p-type semiconductor in a tandem DSC with the conventional n-type DSC based on TiO<sub>2</sub> and I<sup>-</sup>/I<sub>3</sub><sup>-</sup> as the photoanode. It has, however, become a model system for research and development of p-type DSCs.

He et al. further reported on a tandem DSC assembled from an erythrosine B-sensitized NiO cathode and an N3-sensitized TiO<sub>2</sub> anode.<sup>863</sup> The electrolyte was 0.5 M LiI/0.05 M I<sub>2</sub> in 1:1 ethylene carbonate/propylene carbonate. The  $V_{oc}$  of the tandem cell was 732 mV, approximately the sum of the  $V_{oc}$ 's from the n-type device (650 mV) and the p-type

device (83 mV). The overall efficiency,  $\eta$  = 0.39%, was low because of the low current on the p-side and the J-V curve was s-shaped because of the mismatch in generated photocurrent between the anode and cathode.

Most of the NiO cathodes in the studies of p-type DSCs have been prepared using the procedure reported by Boschloo and Hagfeldt<sup>88</sup> where a Ni(OH)<sub>2</sub> colloidal solution is prepared from a NiCl<sub>2</sub> precursor. An improvement of the NiO material for the performance was reported by Nakasa et al. who used a sol-gel method with a triblock copolymer template to prepare NiO.<sup>864</sup> N3 or 3-carboxymethyl-5-[2-(3-octadecyl-2-benzothiazolinylidene)ethylidene]-2-thioxo-4-thiazolidine were used as the sensitizers and I<sup>-</sup>/I<sub>3</sub><sup>-</sup> as redox couple. A tandem DSC was prepared by assembling the photocathode with an N3-sensitized TiO<sub>2</sub> anode, and an efficiency of 0.78% was obtained when illuminated through the cathode. The shape of the J-V curve was still s-shaped, however, since the currents from each side were still not matched. Sumikura et al. have prepared a number of NiO electrodes using different poly(ethylene oxide)-poly(propylene oxide)-poly(ethylene oxide) triblock copolymers<sup>865</sup> in a similar way to that described by Nakasa et al.<sup>864</sup>

Morandeira et al. reported the charge transfer dynamics of coumarin 343-sensitized NiO and showed that hole injection from the dye to the VB is ultrafast and occurred in around 200 fs. The low IPCE values (<10%) obtained with the coumarin/NiO system thus cannot be ascribed to injection problems but were attributed to a fast charge recombination in around 20 ps.<sup>567</sup> For regeneration of the dye to compete with this fast process, the redox mediator (probably I<sub>3</sub><sup>-</sup>) must thus be preassociated with the dye.

Sensitizers tested on p-type NiO include porphyrins (**60**, **211**),<sup>565,566</sup> coumarin (**91**),<sup>567-569</sup> and perylene dyes (**212**).<sup>570</sup> No higher maximum IPCE value than 10% was, however, obtained with these dyes. Recently, Sun, Hagfeldt, and co-workers<sup>571,572</sup> developed organic D- $\pi$ -A dyes (**213** and **214**) with the attaching group (carboxyl unit) on the electron donor part (triphenylamine) and two electron acceptor groups (malononitrile groups). Upon light excitation, electron density moves from the donor to the acceptor part of the dye, which provides an efficient electron transfer pathway from the dye to the electrolyte. In NiO-based p-type DSCs **213** and **214** yielded high IPCE, reaching a maximum of 44% for **214** on a transparent NiO film (1–1.4  $\mu$ m thick) and a liquid I<sup>-</sup>/I<sub>3</sub><sup>-</sup> electrolyte.<sup>572</sup> This has increased to 64%<sup>866</sup> by improving the NiO electrode with the application of a double layer oxide film based on the templated method described by Sumikura et al.<sup>865</sup>

Nattestad et al.<sup>867</sup> developed efficient sensitizers for p-type semiconductors using a similar concept. A triphenylamine donor was coupled to a perylenemonoimide acceptor using oligothiophene-conjugated linkers. They achieved 0.41% efficiency and 62% IPCE in a p-type DSC with a dye-sensitized NiO electrode in combination with an iodide/triiodide redox couple, and obtained 1.08 V open circuit potential in a tandem DSC with 1.91% overall efficiency.

In order to significantly improve the efficiencies of p-type DSCs, either the NiO semiconductor or the I<sup>-</sup>/I<sub>3</sub><sup>-</sup> electrolyte must be replaced. A recent work for the latter was reported by Gibson et al. employing a cobalt polypyridyl redox complex to a NiO-based DSC in conjunction with perylene-based dyes.<sup>868</sup> A “dyad” perylene dye contained a coupled naphthalene diimide acceptor unit, which had a more positive reduction potential than the perylene chromophores. On

illumination, an electron transfer cascade from the NiO across the chromophores to the acceptor unit occurred, extending the distance between the  $\text{NiO}(\text{h}^+)$  and the unpaired electron in the reduced dye, increasing the lifetime of the charge-separated state by 5 orders of magnitude. A 3-fold increase in photovoltage was observed compared with the  $\text{I}^-/\text{I}_3^-$  redox system, and a  $V_{\text{oc}} = 0.35$  V was obtained. A tandem cell was assembled with an N719-sensitized  $\text{TiO}_2$  photoanode where the current was matched to the cathode by tuning the  $\text{TiO}_2$  film thickness. The fill factor (0.62) was improved compared with the previously reported tandem DSCs, and the  $V_{\text{oc}}$  was approximately the sum of the p-type and n-type devices (0.91 V). The current was still low because of the substantial overlap of the absorption spectra of the dyes used and the relatively low ionic strength of the electrolyte because of the low solubility of the bulky cobalt complex. The overall efficiency was 0.55%.

There are only a few charge transport studies of dye-sensitized mesoporous NiO electrodes. Zhu et al. studied the effects of cations in the electrolyte on hole transport times ( $\tau_{\text{tr}}$ ) and lifetimes ( $\tau_h$ ) in C343-sensitized NiO.<sup>869</sup> The transport times were found not to vary significantly with light intensity in contrast with what is observed for transport of electrons in  $\text{TiO}_2$ .  $\tau_{\text{tr}}$  was shown to vary significantly with the type of cation in the electrolyte solution, decreasing in the order  $\text{Li}^+ > \text{Na}^+ > \text{TBA}^+$ . The authors attributed this to adsorption of the cations affecting the hopping of charge at the NiO/electrolyte interface, suggesting that the holes can be chemically ascribed to  $\text{Ni}^{3+}$  at the surface. These observations could partly explain the extremely fast recombination between the dye radical anions and the holes in the NiO observed spectroscopically. Mori et al. studied the transport properties of templated NiO sensitized with different dyes, including C343.<sup>870</sup> Calculated diffusion coefficients were 3 orders of magnitude lower than the typical values for electrons in dye-sensitized  $\text{TiO}_2$  solar cells but the hole lifetimes were comparable.

For a high-efficiency tandem cell based on a dye-sensitized  $\text{TiO}_2$  photoanode, the valence band of the photocathode must be substantially lower in energy than NiO. So far there have, however, not been any reports of other p-type semiconductors that perform better than NiO. For example, CuSCN mentioned above and CuO, studied by Sumikura et al.,<sup>871</sup> do not have a significantly lower valence band potential than NiO. Nakabayashi et al. photosensitized a p-type diamond electrode with  $\text{Ru}(\text{bpy})_3^{2+}$ . The sensitizer injected holes into the diamond valence band.<sup>872</sup> However, only a small photocurrent was measured.

## 6. Characterization Techniques

In order to fully understand the DSC and the complex interaction of its components, it will be essential to study the complete solar cell, besides the investigations of the separate components. Thus, a number of nondestructive analysis methods that together form the so-called toolbox techniques for dye-sensitized solar cells have been developed. The main goals with the toolbox concept are (i) to measure internal processes on complete DSC devices under normal solar light conditions, (ii) to test and assist in the development of theoretical models describing the different electron transfer and transport processes, (iii) to analyze problems associated with stability and reproducibility, and (iv) to optimize new material components. Several of these tool-box techniques are reviewed in the following sections.

## 6.1. Efficiency Measurements, $I$ – $V$ , IPCE, and APCE

The current–voltage ( $I$ – $V$ ) characteristics of a solar cell under illumination are used to determine the power conversion efficiency,  $\eta$ . Because dye-sensitized solar cells have a relatively slow electrical response due to their high interfacial capacity, the voltage scan should be sufficiently slow to avoid errors in the current measurement due to capacitive (dis)-charging. Alternatively, the currents from a rapid forward and reverse voltage scan can be averaged.<sup>873</sup> From the  $I$ – $V$  curve, the short-circuit current,  $I_{\text{sc}}$  (or short circuit current density,  $J_{\text{sc}}$ ), is determined at the  $V = 0$  V intercept, while the open-circuit potential,  $V_{\text{oc}}$ , is found at the  $I = 0$  intercept. The maximum output power of the solar cell is found where the product  $|I| \times |V|$  reaches a maximum (the maximum power point). The power conversion efficiency is given by

$$\eta = \frac{|JV|_{\text{max}}}{P_{\text{in}}} = \frac{J_{\text{sc}} V_{\text{oc}} \text{FF}}{P_{\text{in}}} \quad (22)$$

where  $P_{\text{in}}$  is the power density of the incident light and FF is the fill factor. The fill factor is a value between 0 and less than 1 that describes the shape of the  $I$ – $V$  curve, where a high value indicates a more preferable rectangular shape.

In a solar cell, power is dissipated through the resistance of the contacts and during charge transport, and through leakage currents within the device or around the sides of the device. These effects are electrically equivalent to resistances in series and in parallel (shunt) and reduce the fill factor. Series resistance is particularly problematic at high current densities, whereas the shunt resistance is a problem in poorly rectifying devices.

It is common practice to use white light from a solar simulator as the light source for efficiency measurements. The standard irradiance spectrum for the solar cell measurements is AM 1.5 G, as discussed before, see section 2 and Figure 2. Because most solar simulators do not provide an ideal AM 1.5 G spectrum, a careful correction needs to be made to account for the spectral mismatch, as is described in detail elsewhere.<sup>874,875</sup>

The spectral response of dye-sensitized solar cells is determined by measuring the monochromatic incident photon-to-current conversion efficiency (IPCE). It is customary that the IPCE is measured under short-circuit conditions. There are two principle IPCE methods: the DC and the AC method. In the DC method, monochromatic light is obtained by passing white light through a monochromator or a bandpass filter, and the photocurrent is measured. In the AC method, the monochromatic light is usually mechanically chopped, and the AC-photocurrent response is measured using a lock-in amplifier. The latter method has the advantage that white bias light can be added, so that the solar cell is working under true operational conditions. It should be noted that DSCs have slow response times compared with solid-state photovoltaics, so that a low chopping frequency must be chosen. In the DC method, the generated photocurrent may be 2–3 orders of magnitude lower than that in full sunlight. This method will therefore only give useful results if the photocurrent increases linearly with light intensity, which is usually the case for DSCs. A very useful test is to calculate  $J_{\text{sc}}$  in full sunlight from the obtained IPCE spectrum:

$$J_{\text{sc}} = \int \text{IPCE}(\lambda) e\phi_{\text{ph}, \text{AM1.5G}}(\lambda) \, d\lambda \quad (23)$$

where  $e$  is the elementary charge and  $\phi_{\text{ph,AM1.5G}}$  is the photon flux in AM 1.5 G,  $100 \text{ mW cm}^{-2}$ .

The IPCE can be expressed as follows:

$$\text{IPCE}(\lambda) = \text{LHE}(\lambda)\varphi_{\text{inj}}(\lambda)\varphi_{\text{reg}}\eta_{\text{CC}}(\lambda) \quad (24)$$

where LHE is the light-harvesting efficiency,  $\varphi_{\text{inj}}$  and  $\varphi_{\text{reg}}$  are the quantum yields for electron injection and dye regeneration, respectively, and  $\eta_{\text{cc}}$  is the charge collection efficiency ( $\text{LHE} = (1 - 10^{-A})$ , with  $A$  being the absorbance of the film).

From a fundamental viewpoint, the so-called APCE values provide further insight into the properties of the device. APCE is the absorbed photon to current conversion efficiency and shows how efficient the numbers of *absorbed* photons are converted into current. APCE is obtained by dividing the IPCE number by the light-harvesting efficiency (LHE, 0–100%). The IUPAC name for LHE is absorptance.

## 6.2. Electrochemical Methods

Electrochemical methods are used to characterize all components of the DSC separately. It gives important information on the energy levels of the component, on the reversibility of electrochemical reactions and on the kinetics of electrochemical processes. The standard equipment in electrochemistry is a potentiostat connected to a three electrode cell, with a working electrode, reference electrode, and counter electrode. The modern potentiostat comes with a range of useful techniques.

### 6.2.1. Cyclic Voltammetry, Differential Pulse Voltammetry, and Square Wave Voltammetry

Cyclic voltammetry is the most widespread electrochemical technique. The potential is swept at a constant rate and reversed at a certain point, while the current is monitored continuously. The measured current arises from Faradaic processes, for example, electron transfer reactions at the electrode, and non-Faradaic processes, for example, capacitive charging of the electrode/electrolyte interface. From cyclic voltammograms, the formal potentials of redox processes can be determined and information on the reversibility of the electron transfer process is obtained. Current peaks will depend on the scan rate used, and from the dependence, conclusions can be drawn whether the redox active species is free in solution or adsorbed to the electrode surface. Better resolution is obtained with techniques such as differential pulse voltammetry and square wave voltammetry, but these methods do not give information on reversibility.

Electrochemical methods are the standard techniques to assess the energy levels of dyes used in DSCs. Usually, characterization is done on dye molecules dissolved in an inert electrolyte, but binding the dye onto a metal oxide surface can affect its oxidation and reduction potential. Zaban et al. showed that the redox potentials of a selection of dyes adsorbed onto  $\text{TiO}_2$  showed a pH-dependent oxidation potential in contact with aqueous electrolyte,<sup>104,876</sup> whereas it could be pH-independent for dye in solution.<sup>876</sup> Yan and Hupp, showed, however, that not all dyes demonstrate pH-dependent oxidation potential upon adsorption onto  $\text{TiO}_2$ .<sup>877</sup>

### 6.2.2. Electrochemical Impedance Spectroscopy

In electrochemical impedance spectroscopy (EIS), the potential applied to a system is perturbed by a small sine wave modulation and the resulting sinusoidal current response (amplitude and phase shift) is measured as a function of modulation frequency. The impedance is defined as the frequency domain ratio of the voltage to the current and is a complex number. For a resistor (R), the impedance is a real value, independent of modulation frequency, while capacitors (C) and inductors (L) yield an imaginary impedance, whose value varies with frequency. The impedance spectrum of an actual system, that is, the impedance measured in a wide range of frequencies, can be described in terms of an equivalent circuit consisting of series and parallel connected elements R, C, L, and W, which is the Warburg element that describes diffusion processes.

EIS is a useful tool to study complete dye-sensitized solar cells<sup>219,226,238,878</sup> and the DSC counter electrode/redox electrolyte.<sup>81,237</sup> Using EIS, the following parameters can be obtained: series resistance, charge transfer resistance of the counter electrode, diffusion resistance of the electrolyte, the resistance of electron transport and recombination in the  $\text{TiO}_2$ , and the chemical capacitance of the porous  $\text{TiO}_2$  electrode.

### 6.2.3. Spectroelectrochemistry

Electrochemistry can relatively easily be combined with different kinds of spectroscopy. UV-vis spectroelectrochemistry has been used to study the accumulation of electrons in mesoporous  $\text{TiO}_2$  electrodes.<sup>93,192,879</sup> The onset of electron accumulation can be correlated to the conduction band edge of mesoporous  $\text{TiO}_2$ . Redmond and Fitzmaurice studied this onset in a range of organic electrolytes and found that cations such as  $\text{Li}^+$  and  $\text{Mg}^{2+}$  determine the position of the  $\text{TiO}_2$  conduction band,  $E_c$ , due to their specific adsorption onto the mesoporous electrode.<sup>93</sup> Spectroelectrochemistry is also used to determine the spectra of the oxidized and reduced sensitizer, which is important for laser spectroscopy studies.

## 6.3. Photoelectrochemical Methods

Photoelectrochemical techniques offer the possibility to study dye-sensitized cells under actual operating conditions. This is of great importance, because it is a complex system with many interactions. Many of the techniques described below are easily and quickly performed and do not require as much data fitting as impedance spectroscopy.

### 6.3.1. Electron Transport Measurements

Because of the nonlinear response of electron transport and recombination as a function of light intensity, these processes are best studied using methods where a small perturbation of light intensity is applied on top of a larger constant light intensity. Rapid modulation of light intensity is easily obtained using light-emitting diodes (LEDs) with appropriate drivers or diode lasers with an intensity modulation option. In intensity-modulated photocurrent spectroscopy (IMPS), a sinusoidal modulation of light intensity is applied, and the resulting photocurrent response is measured as function of modulation frequency using phase-sensitive detection,<sup>182,183</sup> similar to impedance spectroscopy. Because this technique is rather time-consuming, time-resolved small modulation techniques using pulsed light<sup>223,880,881</sup> or square

wave modulation<sup>882,883</sup> have been developed. In all these techniques, the simplest analysis involves the determination of a time constant for photocurrent response,  $\tau_{pc}$ , which depends on both electron transport and electron recombination, according to<sup>884</sup>  $(\tau_{pc})^{-1} = (\tau_{tr})^{-1} + (\tau_n)^{-1}$ , where  $\tau_{tr}$  is the electron transport time and  $\tau_n$  is the electron lifetime. In DSC with iodide/triiodide electrolyte under short-circuit conditions, the electron lifetime is usually much larger than the transport time, so the measured photocurrent response time is nearly equal to the transport time. The chemical diffusion coefficient,  $D_n$ , can be calculated from the electron transport time using eq 25.

$$D_n = \frac{d^2}{C\tau_{tr}} \quad (25)$$

where  $d$  is the thickness of the mesoporous  $TiO_2$  film and  $C$  is a constant with a value of about 2.5, which depends slightly on absorption coefficient of the film and direction of illumination.<sup>881,882</sup>

An alternative technique devised to measure electron transport time in DSCs is a photovoltage rise method.<sup>220</sup> Here the cell is kept under open-circuit conditions, and the characteristic time constant for photovoltage rise is measured after application of a short light pulse superimposed on a constant bias illumination. The electron transport time is calculated from the rise time using the capacity values of the  $TiO_2$  and the substrate/electrolyte interface, which have to be measured independently. The electron lifetime is determined in the same experiment from the voltage decay. The advantage of this method is that it can be performed under conditions where the  $RC$  time constant of the DSC, arising from the series resistance of  $TiO_2$  and conducting substrate and the large capacity of the mesoporous  $TiO_2$ , does not limit the transport measurement. Effects of the  $RC$  constant can occur, for instance, when a potential is applied to the DSC under potentiostatic conditions, rendering the whole of the mesoporous  $TiO_2$  conductive.<sup>885</sup> A reasonable agreement has been found between the two types of transport measurement.<sup>220,886</sup>

The chemical diffusion coefficient obtained from the electron transport measurements describes the movement of photoinduced excess charge in a concentration gradient. The obtained value differs from that of the tracer diffusion coefficient ( $D_{tracer}$ ), which describes the movement of individual electrons under (quasi-) equilibrium conditions, that is, in absence of a concentration gradient. Theoretical,<sup>188</sup> computational,<sup>887</sup> and experimental work<sup>887</sup> demonstrated that the two diffusion coefficients are related as follows:

$$D_n = T_n D_{tracer} \quad (26)$$

where  $T_n$  is the thermodynamic factor, which is equal to one if the electrons follow Boltzmann statistics.<sup>188</sup> In dye-sensitized solar cells, however,  $T_n$  has a value of 2–4, independent of light-intensity.<sup>887</sup> This is attributed to the electron transport mechanism, which involves multiple trappings in an exponential distribution of localized states.  $T_n$  can be calculated from the ratio of extracted charge under short-circuit conditions and the calculated “expected charge”,  $J_{SC}\tau_{tr}$ .<sup>887</sup>

### 6.3.2. Electron Lifetime Measurements

Electron lifetime measurements are usually performed in a similar way as the transport measurement, with the

difference that the open-circuit potential is monitored rather than the short-circuit photocurrent.<sup>216</sup> Photogenerated electrons are not extracted at the back contact but will recombine with acceptors in the electrolyte. For small-modulation techniques, the characteristic response time of the photovoltage corresponds to the electron lifetime,  $\tau_n$ . This type of measurement can in principle be done under any galvanostatic (constant current) condition,<sup>223,885</sup> although it is troublesome to determine electron lifetime in the mesoporous film under short circuit conditions.

An alternative method to determine electron lifetime is the  $V_{oc}$  decay method.<sup>217</sup> Here the open-circuit potential of a DSC is monitored as function of time when the light is switched off. The electron lifetime is calculated from the slope of the  $V_{oc}$  transient:

$$\tau_n = -\frac{kT}{e} \left( \frac{dV_{oc}}{dt} \right)^{-1} \quad (27)$$

The advantage of this method is that the lifetime can be determined in a wide potential range with one single measurement. It can also be performed without using light, by application of a negative potential before open circuit decay.<sup>888</sup>

Finally, time-dependent charge extraction (see section below) can be used to calculate the electron lifetime.<sup>180,883</sup> Assuming first-order recombination kinetics, the lifetime is given by

$$\tau_n = Q(t) \left( \frac{dQ(t)}{dt} \right)^{-1} \quad (28)$$

where  $Q(t)$  is the charge extracted after decay in the dark for time  $t$ . Comparison of the different methods shows that the small-modulation method and the  $V_{oc}$  decay give essentially the same result,<sup>180,218</sup> while the final method leads to lifetime values larger by a constant factor of about 4.<sup>180</sup> This difference can be ascribed to the fact that the small amplitude methods derive a lifetime based on the recombination of photoinduced excess charge, whereas the time-dependent charge extraction method determines an average lifetime for all electrons present in the mesoporous  $TiO_2$  film. The constant factor can be ascribed to the thermodynamic factor, see section 6.3.1.

### 6.3.3. Electron Concentration Measurements

The total concentration of electrons in the mesoporous  $TiO_2$  film under solar cell operating conditions can be determined using different methods. In charge extraction methods, the light is switched off and all remaining charge in the film is extracted as a current during a certain period and integrated to obtain the charge. Under short-circuit conditions, this simply corresponds to the integration of the photocurrent transient recorded after the light is switched off.<sup>883,887</sup> Starting from open-circuit conditions, the cell connection has to switch from open to short circuit simultaneously with off-switching of the light. When the  $V_{oc}$  is allowed to decay in the dark for different periods before charge extraction, a complete charge–potential curve can be obtained by repeated experiments.<sup>889</sup> When charge extraction measurements are used, it should be realized that not all electrons will be extracted due to recombination losses and limitations in extraction time (electron transport becomes very slow at low electron concentrations).

In an alternative method, the capacity of the mesoporous film is measured rather than the charge.<sup>890</sup> At a certain open-circuit potential, obtained by bias illumination, a light pulse is added and the resulting voltage rise is measured. The photocurrent transient resulting from the light pulse is measured separately under short-circuit conditions and used to calculate the injected charge induced by the light pulse. The capacity is calculated from the ratio of injected charge and voltage change. Integration of capacity with respect to the range of open-circuit potentials gives the charge–potential relation.

Finally, near-infrared transmission measurements can be done to determine the total electron concentration in mesoporous dye-sensitized solar cells.<sup>891</sup> An optical cross section of  $5.4 \times 10^{-18} \text{ cm}^2$  was determined at 940 nm for electrons in mesoporous TiO<sub>2</sub>, corresponding to a decadic extinction coefficient of  $1400 \text{ M}^{-1} \text{ cm}^{-1}$ , in good agreement with spectroelectrochemical studies on mesoporous TiO<sub>2</sub> ( $1200 \text{ M}^{-1} \text{ cm}^{-1}$  at 700 nm).<sup>192</sup>

Approximate electron concentration in the mesoporous TiO<sub>2</sub> film of a DSC under operating conditions (one sun) is on the order of  $10^{18}\text{--}10^{19} \text{ cm}^{-3}$ ,<sup>180,891</sup> corresponding to about 4–40 electrons per TiO<sub>2</sub> particle, assuming spherical 20 nm-sized particles.

#### 6.3.4. Measurements of the Electron Quasi-Fermi Level

Two methods have been developed to determine the quasi-Fermi level in mesoporous TiO<sub>2</sub>. The first method is a switching method and can be performed on standard dye-sensitized solar cells.<sup>180,883</sup> The DSC is illuminated under short-circuit conditions (or kept at a certain applied potential), when simultaneously, the light is switched off and the cell is switched to open circuit, while the potential is measured. The potential will rise to reach a value that is similar to the quasi-Fermi level of the electrons in TiO<sub>2</sub>, as it was present in the illuminated film. Considering that there was a gradient in the Fermi level, the resulting value will be an average value. Model calculations suggest that even under short-circuit conditions, the Fermi level under illumination conditions is relatively flat in the whole mesoporous film, except for about 1 μm directly adjacent to the conducting substrate, so that the measured value gives a good indication of the Fermi level in most of the film. Additionally, the rise of the potential gives information on the electron transport in the mesoporous film, and the following decay of the potential information on the electron lifetime.

The second method requires the deposition of an additional titanium electrode on top of the mesoporous TiO<sub>2</sub> film.<sup>892,893</sup> The surface of the metal is passivated by thermal oxidation and does not lead to an additional recombination pathway for electrons in the TiO<sub>2</sub>. The potential of the additional electrode can be measured under operating conditions and directly gives the quasi-Fermi level at the outside of the mesoporous TiO<sub>2</sub> film. Both methods give similar results and show that in standard DSCs, illuminated at 1 sun, the quasi-Fermi level under short circuit in the mesoporous TiO<sub>2</sub> is located about 0.5–0.6 V negative of the redox potential of the electrolyte.

#### 6.3.5. Charge Collection Efficiency and Diffusion Length

The charge collection efficiency can be estimated from electron transport and lifetime measurements as follows:<sup>219</sup> For a correct calculation of the charge collection efficiency,

$$\eta_{\text{CC}} = 1 - \frac{\tau_{\text{pc}}}{\tau_{\text{e}}} = \frac{1}{1 + \tau_{\text{tr}}/\tau_{\text{n}}} \quad (29)$$

it is required that the transport time and lifetime are measured at the same quasi-Fermi level in the mesoporous TiO<sub>2</sub>. If  $\tau_{\text{pc}}$  (measured at short-circuit) and  $\tau_{\text{n}}$  (measured at open-circuit) are used to calculate  $\eta_{\text{CC}}$ , the resulting value will underestimate the true  $\eta_{\text{CC}}$  value under short-circuit conditions. To determine the latter,  $\tau_{\text{n}}$  must be determined under conditions where the quasi-Fermi level in the mesoporous TiO<sub>2</sub> is equal to that under short-circuit conditions. This can be achieved by (1) measuring the quasi-Fermi level under short-circuit conditions (see section 6.3.4) and determining  $\tau_{\text{n}}$  from the relation between  $\tau_{\text{n}}$  and  $V_{\text{oc}}$  or (2) measuring the extracted charge under short-circuit conditions and determining  $\tau_{\text{n}}$  from the relation between  $\tau_{\text{n}}$  and extracted charge (see section 6.3.2). Impedance spectroscopy<sup>878</sup> and photovoltage rise/decay measurements<sup>220</sup> can be used to determine  $\tau_{\text{tr}}$  and  $\tau_{\text{n}}$  simultaneously at the same quasi-Fermi level. The charge collection efficiency can also be determined from IPCE using eq 24.

The electron diffusion length,  $L$ , in the DSC is closely related to the charge collection efficiency.  $L$  is a wavelength-independent parameter, whereas  $\eta_{\text{CC}}$  depends on wavelength. Södergren et al. derived expressions for the IPCE of mesoporous DSCs as a function of the diffusion length, absorption coefficient, and film thickness, assuming quantitative electron injection.<sup>172</sup> In recent works by Halme et al.<sup>894</sup> and Barnes et al.,<sup>895</sup> these relations were used to determine the electron diffusion length in DSCs under various conditions. Dynamic, small amplitude methods (impedance spectroscopy, electron transport, and lifetime measurements) can also be used to determine the electron diffusion length:<sup>186,187</sup>

$$L = \sqrt{D_{\text{n}}\tau_{\text{n}}} \quad (30)$$

Interestingly, the values of  $L$  determined in this way were at least a factor 2 larger than those obtained from IPCE measurements.<sup>895</sup> Bisquert and Mora-Sero<sup>896</sup> demonstrated in a simulation study that this can be attributed to the fact that recombination kinetics in DSCs are nonlinearly dependent on the electron concentration in the conduction band, whereas linearity is assumed in the IPCE method.

#### 6.3.6. Photoinduced Absorption Spectroscopy

Photoinduced absorption (PIA) spectroscopy, where excitation is provided by a on/off modulated LED or laser giving intensities comparable to one sun, is listed here under photoelectrochemical techniques, because it too allows for investigation of dye-sensitized cells under actual operating conditions, and it can easily be combined with simultaneous electrochemical measurements.<sup>897,898</sup> Small changes in optical transmission are detected using a detector system with a lock-in amplifier tuned at the frequency of the modulation. It is very useful in qualitative studies, for instance, to check whether a dye is injecting electrons into TiO<sub>2</sub> after photoexcitation and whether a dye is regenerated when in contact with a redox electrolyte.<sup>159</sup> The kinetics of slower processes in the DSC ( $t > 10^{-5} \text{ s}$ ) can be followed using PIA. Because the PIA signal is proportional to the lifetime of the observed species, it can be sensitive to a small fraction of dye molecules that is not in contact with the redox couple or hole conductor and therefore has a long lifetime of the oxidized state.<sup>899</sup>

## 7. Module Development/DSC Modules

The manufacturing, reliability, performance, and stability of a DSC module are more complex compared with the test cell situation due to the larger size. Moreover, interconnected cells in a DSC module may interact through, for example, mismatched performance of the cells or unwanted mass transport of electrolyte between adjacent cells. Several different designs for up scaling the DSC cell to a module level can be found in the literature. In this section, we review these designs and module performances (section 7.1), accelerated and outdoor testing of DSC modules (section 7.2), and the manufacturing processes (section 7.3). Thereafter, we discuss the status of DSC module development (section 7.4). The number of publications dealing with DSC module development is low in comparison to the ones dealing with material development of DSCs. Additionally, module work is often presented as conference contributions. The rather scarce published information on DSC modules is related to the direct relevance of the module design and the production process methods to the development of commercial products. Very few publications deal with modules manufactured on flexible substrates.

We define a DSC module as a device that, in relation to a test cell, is significantly increased in size in both the *x*- and the *y*-direction and carries specific solutions to decrease the energy (resistive) losses caused by the electron transport in the device. The term sandwich is used to define a device structure carrying the working and counter electrodes on two substrates. The term monolithic is used to define a device structure carrying the working and counter electrode on one and the same substrate.

The DSC modules are made on different types of substrates. For the monolithic structure where only one substrate is required, a TCO glass is conventionally used. For the sandwich construction, different substrate combinations are used, such as two pieces of TCO glass, one TCO glass and one metal foil, two TCO-coated polymer sheets, and one TCO-polymer sheet and one metal foil.

A complexity involved in reviewing the performance of DSC modules is that different definitions of the device efficiency are used. In some cases, the active area efficiency is used whereas in other cases the total area module efficiency is used. Moreover, various module sizes are used, and the measurements are taken at different light intensities. Lower efficiency values are in general obtained in publications dealing with module stability. Caution should thus be taken when comparing DSC module results from different publications.

In the present table of record solar cell efficiencies,<sup>900</sup> a DSC module efficiency of 9.2% is listed, achieved by Sony, Japan.<sup>901</sup>

### 7.1. Module Designs and Performance

Using the above-mentioned definitions, the dominating DSC module designs can be divided into five categories, further presented below and schematically shown in Figure 21. Our ambition has been to find relevant examples of the different module categories. Unless stated otherwise, the N3/N719 dye was used as the sensitizer.

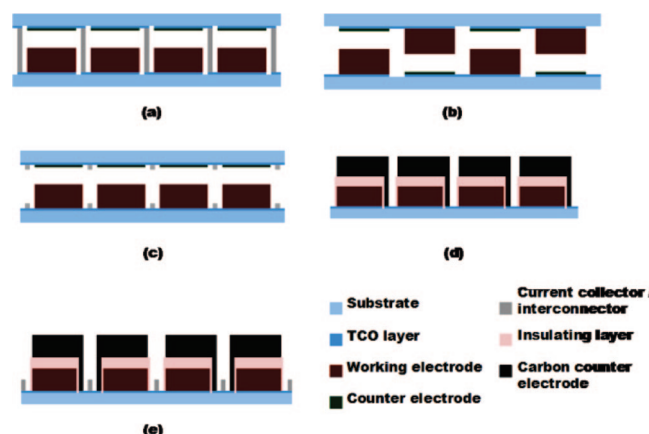


**Figure 21.** Schematic cross sections of examples of constructions of the five categories of DSC modules: (a) sandwich Z-interconnection; (b) sandwich W-interconnection; (c) sandwich current collection; (d) monolithic serial connection; (e) monolithic current collection. Each module consists of four working and counter electrodes. The proportions of the module layers and substrates are not drawn to scale but have been adjusted to illustrate the device constructions.

#### 7.1.1. Sandwich Z-Interconnected Modules

This DSC module design is based upon a sandwich construction with the working electrodes deposited on a first substrate and the counter electrodes on a second substrate. A conducting material is used to make electrical connections between the substrates to serial-connect adjacent cells, Figure 21a. Unless an inert combination of conductor and electrolyte is used, these conductors must be efficiently insulated from the electrolyte to avoid corrosion. Moreover, the electrolytes of adjacent cells must be separated from each other to avoid unwanted mass transport.

Yun et al.<sup>902</sup> have developed glass-based Z-interconnected modules of size  $10 \times 10 \text{ cm}^2$ . Silver was used as the cell interconnecting material and a polymer was used for insulation between silver and the electrolyte and for the external encapsulation. An active area efficiency up to 6.6% at  $1000 \text{ W/m}^2$  is reported. Even if the module efficiencies are not explicitly stated, they can be roughly calculated from the active area surface of  $47.5 \text{ cm}^2$ . Using a device area of  $9 \times 9 \text{ cm}^2$ , module efficiencies around 3.9% are obtained. Sastrawan et al. have realized  $30 \times 30 \text{ cm}^2$  Z-interconnected modules on glass.<sup>903</sup> Silver was used as the interconnecting material and so-called glass frits were used for insulation between silver and the electrolyte and for the external encapsulation: An active area efficiency of 3.5% was obtained at  $1000 \text{ W/m}^2$ .

The sandwich Z-interconnection device has also been applied on flexible substrates. Miyasaka et al.<sup>904</sup> and Ikegami et al.<sup>905</sup> have developed such devices on plastic substrates. Devices of size  $30 \times 30 \text{ cm}^2$  consisting of 10 serial-connected cells have been designed toward consumer electronics, Figure 22. A double-sided conducting tape was used to make the Z-interconnections on the long side of the cells. Efficiencies of about 2% at  $300 \text{ W/m}^2$  were obtained.

#### 7.1.2. Sandwich W-Interconnected Modules

This sandwich module design carries cells with alternating working and counter electrodes on each substrate, Figure 21b. Consequently, every second cell is illuminated through the counter electrode. Interconnects are thus avoided but the cells must be separated by an effective seal to avoid mass transport



**Figure 22.** The  $900\text{ cm}^2$  sandwich Z-interconnected flexible DSC module. Reprinted with the permission from Peccell Technologies, Inc., Japan.

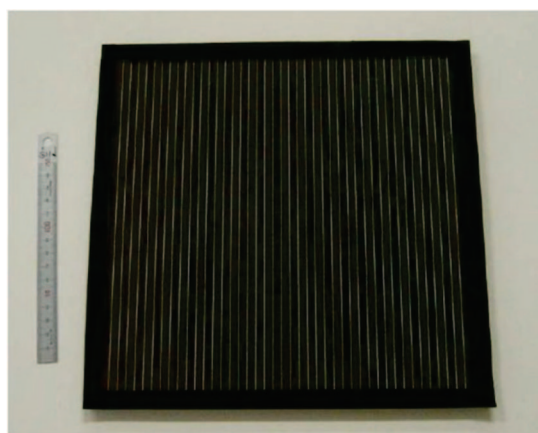


**Figure 23.** The  $625\text{ cm}^2$  sandwich W-interconnected glass-based DSC module. Reprinted with the permission from Sharp Corporation, Japan.

between adjacent cells. The design allows a high ratio of active area in a device but requires a good cell matching; that is, the cells illuminated through the working electrode should generate as much current and voltage as the ones illuminated through the counter electrode. This can be obtained by using different widths of the cells or by matching the performance through optimizing the cell parameters. Han and co-workers have obtained certified module efficiencies of 8.2%<sup>906</sup> and 8.4%<sup>907</sup> for glass-based devices of size  $25\text{ cm}^2$  by using this design and the black dye as a sensitizer (dye 3, section 5.2.1.1). They have also demonstrated the possibility to scale-up the device size to  $625\text{ cm}^2$ , see Figure 23.<sup>908</sup>

### 7.1.3. Sandwich Current-Collecting Modules

This sandwich module design is based on increasing the cell size through the use of current collectors in the TCO glass to reduce the sheet resistance. One possibility is to place the current collectors underneath the TCO layer to obtain a protection layer between the metal grid and the electrolyte solution. Another possibility is to use an inert combination of conductors and electrolyte. However, the most common solution in literature has been to place silver current collectors on top of the TCO layer, Figure 21c. Since silver corrodes in contact with the conventional iodide/triiodide redox couple in the DSC, the silver lines must be thoroughly insulated. Dai et al. have used this concept for their DSC panel of  $45 \times 80\text{ cm}^2$  consisting of 12 sandwich current-collecting

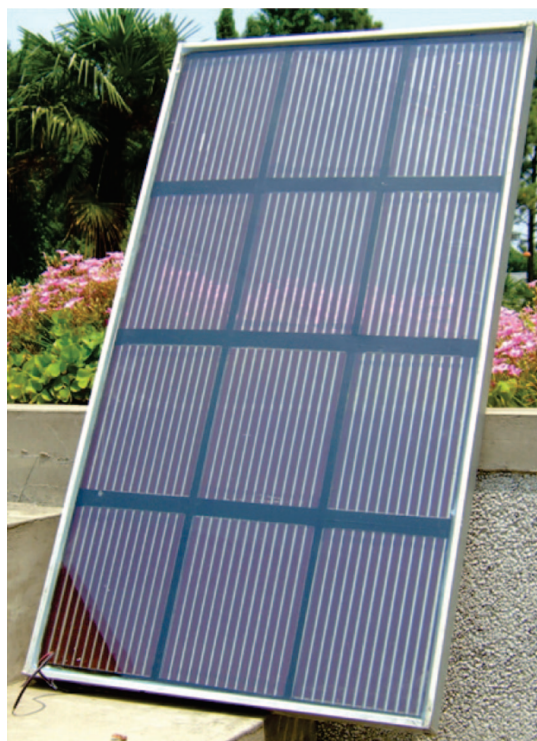


**Figure 24.** The  $3600\text{ cm}^2$  panel consisting of 12 serial-connected current-collecting glass-based sandwich DSC modules. Reprinted with permission from the Institute of Plasma Physics in Hefei, China.



**Figure 25.** The  $900\text{ cm}^2$  glass-based sandwich module. The device consists of six serial-connected so-called meander-type current-collecting parts. Reprinted with permission from Fraunhofer ISE, Germany.

devices of size  $300\text{ cm}^2$ , Figure 24.<sup>909</sup> Module efficiencies up to 5.9% were obtained. Arakawa et al. have used protected silver grids in their  $100\text{ cm}^2$  glass modules.<sup>337</sup> Three different patterns with different geometries were investigated for the current collectors. Module efficiencies of 8.7% (active area efficiency 9.4%) were obtained at  $1000\text{ W/m}^2$  using the black dye.

Sastrawan et al. have introduced an alternative design for current collection in a DSC sandwich module, the so-called meander-type.<sup>910</sup> The driving force behind this solution was to have fewer holes in the glass substrate for electrolyte filling in relation to the Z-interconnection, where each cell required individual holes. Their glass-based devices of size  $30 \times 30\text{ cm}^2$  consisted of six meander-type serial-connected parts, Figure 25. An active area efficiency of approximately 3% was obtained at  $1000\text{ W/m}^2$ . Han et al. have also used glass

frits to protect the silver current collectors from the electrolyte.<sup>908</sup> They obtained a module efficiency of 7.5% on a 102 cm<sup>2</sup> device. Späth et al. used polymers to protect the silver current collectors,<sup>911</sup> obtaining active area efficiencies up to 4.6% for devices of size 100 cm<sup>2</sup>. Okada et al. tried out a large number of metals as candidates for the current collectors of their glass-based devices.<sup>912</sup> By using nickel, they obtained a module efficiency of 4.3% (active area 5.1%) at 1000 W/m<sup>2</sup> on a 100 cm<sup>2</sup> device.

Matsui et al. have used a TCO substrate for the working electrode and a Pt-coated Ti foil for the counter electrode as substrates for their current-collecting sandwich devices.<sup>913</sup> The silver grid was covered with a protective layer consisting of sintered glass frit and a thermostable polymer to prevent direct contact with the electrolyte. Module efficiencies of 3.6% and 3.2% were obtained for device sizes of 5 × 5 cm<sup>2</sup> and 5.5 × 30 cm<sup>2</sup>, respectively.

#### 7.1.4. Monolithic Serial-Connection Modules

Kay et al. introduced the single-substrate serial-connected, the so-called monolithic, dye-sensitized solar module concept as an alternative to the one using two substrates.<sup>850</sup> The catalytic and conducting properties of the counter electrode were obtained through the combination of conducting graphite and catalyzing carbon black powders. Moreover, since the carbon layer could be used to connect adjacent cells, a single-substrate serial-connected module was realized, see Figure 21d. Using a module size of 21 cm<sup>2</sup> consisting of six serial-connected elements, a total area module efficiency of 5.3% was obtained at a light intensity of 1000 W/m<sup>2</sup> (5.6% with respect to the active surface). This corresponds to 94% active area/device. This high value could be realized since no encapsulation was used between adjacent cells. Later studies have shown that this is required for stability reasons to avoid unwanted mass transport between adjacent cells. Following the ideas from Kay et al., Burnside et al. used this concept for minimodules designed for low-power indoor applications.<sup>914</sup> During this work, screen printing was introduced as a deposition method for the monolithic electrodes. Moreover, Pettersson et al. developed an encapsulation method to efficiently separate adjacent cells electrolytically from each other in monolithic low-power modules.<sup>915</sup> Sano et al. have developed monolithic modules for outdoor applications and significantly scaled-up the module size.<sup>916</sup> The devices were of size 24 × 24 cm<sup>2</sup> and consisted of 22 serial-connected cells. Additionally, DSC panels consisting of 30 such modules have been realized. The active area efficiencies of the modules were found to be almost the same as those for small-size cells. However, no efficiency values for cells or modules were presented. Meyer et al. developed monolithic serial-connected devices with an active area of 55.2 cm<sup>2</sup>.<sup>917</sup> Active area efficiencies up to 5.8% (corresponding to approximately 4% module area efficiency using a module area of 9 × 9 cm<sup>2</sup>) were obtained at 1000 W/m<sup>2</sup> on non-encapsulated devices. However, the module performance decreased significantly after encapsulation of the modules. Takeda et al. have presented a transparent monolithic serial-connected device, see Figure 26.<sup>918</sup> They have used Pt-loaded In<sub>2</sub>O<sub>3</sub>:Sn nanoparticles and an insulator composed of SiO<sub>2</sub> particles instead of the conventional nontransparent monolithic materials.

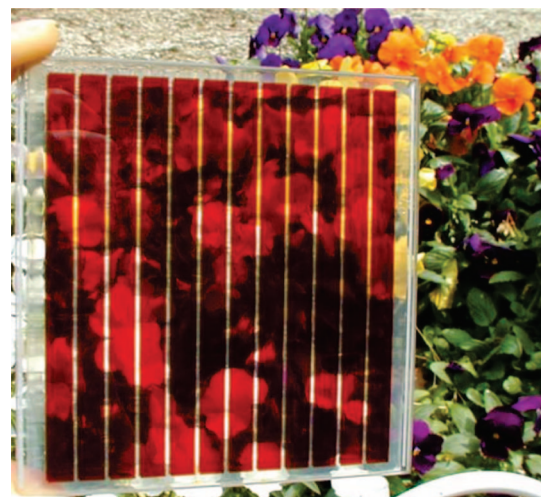


**Figure 26.** The 90 cm<sup>2</sup> transparent serial-connected monolithic DSC module from Toyota Central R&D Laboratories., Inc. and AISIN SEIKI CO., LTD., Japan. Reprinted from ref 918, copyright 2009, with permission from Elsevier.

#### 7.1.5. Monolithic Current-Collecting Modules

The past few years, current-collecting versions of the monolithic concept have been introduced. Hinsch et al. have applied the above-mentioned meander-type current collection on the monolithic cell geometry.<sup>919</sup> However, no module performance is included. Goldstein et al. have proposed another solution for current collection of monolithic devices.<sup>920</sup> This design is based upon using a current-collecting material that can be in contact with the device electrolyte. A module efficiency of 5.4% has been reported on a 225 cm<sup>2</sup> device under one sun conditions. Pettersson et al. have developed 17 cm<sup>2</sup> modules consisting of four parallel-connected monolithic cells.<sup>921</sup> The four cells are two sets of mirror-inverted cells allowing the use of one current collector strip between each set of two cells, Figure 21e. Each cell is insulated to the silver current collectors by a polymer. Total area module efficiencies of 5% have been obtained at 200 W/m<sup>2</sup> (around 4% at 1000 W/m<sup>2</sup>) using a Ru-complex dye coded as K77.<sup>921</sup>

Gonda et al. have proposed another monolithic DSC design based on current collectors with high tolerance to iodide/triiodide-containing electrolytes.<sup>922</sup> This design differs from most others because the devices are made on ceramic substrates carrying the working and counter electrodes next to each other instead of the conventional case in which the two electrodes face each other. Tungsten could be used as current collector since the ceramic substrate allows for higher temperatures than the glass substrates. No device efficiency is presented.

### 7.2. Accelerated and Outdoor Module Testing

The stability of a DSC module is strongly related to the device encapsulation. For outdoor applications, the sealing material must, for example, be mechanically and thermally stable, stable under UV exposure, and chemically inert to the electrolyte. Moreover, it should prevent mass transport between adjacent cells. All of this should preferably be realized on small distances to avoid significant surface losses and thus reduced module performance. The difficulties involved in this are illustrated by the fact that there have historically been few published results containing module efficiencies in combination with data from accelerated or

outdoors testing of DSC modules. An interesting trend is that the publications dealing with module stability generally have lower module efficiencies than the publications where stability is not mentioned. This is a commonplace experience within the field of dye-sensitized solar cells and modules, namely, that the devices offering the best long-term stability are different from those exhibiting the highest device efficiencies. For modules, this may be due to the composition of the device components or due to the design, that is, large distances for encapsulation between cells.

Kato et al. have published results from 2.5 years of outdoor tests of monolithic modules of size  $10 \times 11 \text{ cm}^2$ , with an electrolyte using  $\gamma$ -butyrolactone as the solvent.<sup>923</sup> Even if the efficiencies are not explicitly stated, they can be roughly calculated from the *IV* characteristics. Using a device area of  $9 \times 10 \text{ cm}^2$ , they obtained module efficiencies below 3% at the light-intensities 320 and  $710 \text{ W/m}^2$ . This resulted in approximately 20% degradation of the initial device performance, caused by a decrease of fill factor and open-circuit voltage. By comparing the outdoor module aging results to accelerated illumination tests on the single cell level, the acceleration factor of the light-soaking test was estimated at 11. Dai et al. have performed one year outdoor testing of their panel consisting of 12 current-collecting sandwich devices with module efficiencies up to 5.9%.<sup>909</sup> The performance of the panel shows a minor decrease, which is not numerically stated in the publication. A mixture of 3-methoxypropionitrile and acetonitrile (50/50 by volume) was used as the solvent for their electrolyte. Both of these publications are very important since they show outdoor feasibility of the DSC modules.

Hinsch et al. have highlighted an important aspect of module testing, because they performed outdoor measurements under various illumination intensities and angles and under partial shading.<sup>924</sup> They have used glass-based meander-type modules designed for building integration of DSCs, with typical active area efficiencies of 4.6% (module area efficiencies of 3.6%). The results have been compared with commercial a-Si and CIGS thin film modules installed at the same test site. At light intensities below  $200 \text{ W/m}^2$ , an advantage for the DSC modules has been observed during morning and evening hours. Toyoda et al. have also compared outdoor DSC module data to conventional crystalline-Si modules.<sup>925</sup> They highlighted that the module efficiencies obtained by certified measurements under full sun conditions do not coincide with the electricity generated in real outdoor use, that is, the total generated output throughout a year. The reasons behind this were that the DSC modules in contrast to Si devices have higher module efficiencies at lower light intensities. In addition, the DSC modules maintain performance relatively well at increased operating temperatures and absorb light efficiently from different angles. Outdoor tests were performed for half a year on modules composed of 64 serial-connected current-collecting sandwich devices of size  $100 \text{ cm}^2$  each. The results showed that the DSC devices, in comparison to the crystalline-Si modules of the same rated output, generated more electrical power over the testing period. However, since the module efficiency of the DSC modules was lower, a larger surface was required to obtain the same peak power, especially under certified measurement conditions. Tulloch has during one day compared the instantaneous power outputs of a DSC and a Si module rated to similar peak-watt power.<sup>926</sup> For façade applications, the results showed higher total energy output

from the DSC modules in the morning and in the afternoon (see Figure 2 in ref 926).

With regards to accelerated stability testing of modules, Pettersson et al. in an early publication presented results of monolithic serial-connected minimodules for low-power application.<sup>927</sup> The module performance degraded by 4% after half a year of illumination with fluorescent light (5000 lx), and by 6% after around 1000 h illumination at a light intensity around  $1000 \text{ W/m}^2$ . The device performance was defined by the maximum power at low light intensities using fluorescent light, and no efficiency values at full-sun conditions were thus presented. Yun et al. illuminated Z-interconnected modules of size  $100 \text{ cm}^2$  with active area efficiencies of 6.3% (module area efficiencies estimated to 3.7%, see section 7.1.1) under full-sun conditions and around  $50^\circ\text{C}$  for 1500 h. This only caused minor changes in the device performance; however, these changes are not numerically presented.<sup>902</sup> Pettersson et al. have performed light-soaking and high-temperature storage testing of parallel-connected monolithic modules.<sup>921</sup> Module efficiencies of 5% have been obtained at a light intensity of  $200 \text{ W/m}^2$  after 2200 h of light soaking at  $1000 \text{ W/m}^2$  and  $50^\circ\text{C}$  (degradation factor of  $1.36 \times 10^{-4}$  percent/h). However, the module stability after storage of devices in darkness at  $80^\circ\text{C}$  for 1000 h was poor with a degradation factor of the module efficiency of  $1.82 \times 10^{-3}$  percent/h. Regarding high-temperature storage tests, Matsui et al. obtained excellent module stability over 1000 h storage in darkness at  $85^\circ\text{C}$  and 85% relative humidity.<sup>913</sup> They used glass-based sandwich current-collecting modules of the size  $25 \text{ cm}^2$ , with module efficiencies of 3.1%. Additionally, 200 cycles of a cycle test in a range of  $-40$  to  $90^\circ\text{C}$  were carried out with maintained device performance. They highlight the importance of having an excellent encapsulation to avoid the degradation of the cell due to moisture penetration. Arakawa et al. performed 200 dry-heat cycles (from  $-40^\circ\text{C}$  to  $90^\circ\text{C}$  for 10 min) and 10 heat-humidity cycles (from  $-40^\circ\text{C}$  to  $90^\circ\text{C}$  at 85% humidity) on their glass-based current collecting sandwich devices of the size  $100 \text{ cm}^2$ .<sup>928</sup> The ratio of the efficiency decrease after the 200 cycles was 20%, whereas the heat-humidity cycles only lead to an efficiency decrease by 0.3%. The heat-humidity stability was obtained at 5.7% device efficiency.

Ikegami et al. report on results from accelerated testing using the previously mentioned Z-interconnected devices on plastic substrates designed for consumer electronics.<sup>905</sup> After 880 h of continuous illumination ( $1000 \text{ W/m}^2$ ), the devices had been reduced to half of the initial efficiency. The device performance was preserved after 220 h in the dark at  $55^\circ\text{C}$  and 95% relative humidity.

### 7.3. Manufacturing Processes

The challenge of the development of manufacturing technology for DSC modules is to develop processes allowing reliable production of modules with good performance and stability without renouncing the idea of a low-cost PV technology. Moreover, in order to have high module efficiency, the highest possible ratio of active area per device is sought. However, this has to be weighed against smaller tolerances, for example, for insulation between adjacent cells or protection of current collectors that may cause defects in the devices causing reduced performance or stability.

The processes for DSC modules can be divided into the ones used for batch-wise production of glass-based devices

and the ones used for roll-to-roll production of flexible devices. The number of publications dealing with processes for module manufacturing is low, especially for flexible DSC devices. Moreover, the details for the manufacturing processes of DSC modules are often left out in the literature. All of this is obviously due to the direct relevance for development of commercial products.

For the glass-based batch-wise production of DSC modules, there is a fundamental difference between the difficulties involved in processing the sandwich and the monolithic constructions. For the sandwich design, the main processing challenges are related to the flatness of the glass substrates, homogeneous distance between the two substrates over a large area, and to position the two substrates against each other at small tolerance levels. For the monolithic construction, the challenges are rather related to the deposition of the monolithic layers with high precision. However, both module categories share the same requirements for a functional encapsulation technology.

The process technology for both the sandwich and the monolithic glass-based DSC module is conventionally based on screen printing the electrodes followed by one or several sintering processes to fuse the particles. The choice of encapsulation method further influences the processes for dye and electrolyte application. Various encapsulation materials and related process methods are used for encapsulating the devices; most common are so-called glass frits or polymer-based foils. Different methods for application of the light-absorbing dye and the redox couple containing electrolyte are used.

An example of the processes for making a glass-frit-sealed module is given by Sastrawan et al.<sup>910</sup> The glass-frit powder is turned into a screen-printable paste and printed on both the working and counter electrode substrates. After the two substrates were mounted together, they were sintered and thus sealed together at the same time as the working and counter electrodes were sintered. Thereafter, the dye and the electrolyte solutions were introduced through openings in the glass substrate. Finally, these openings were closed by using a polymer as encapsulation material. Späth et al. describe the processes in a semiautomated baseline for production of current-collecting sandwich modules sealed by polymers,<sup>911</sup> using various specially designed pieces of equipment for DSC devices. The dye was adsorbed either before or after a first encapsulation of the substrates. The electrolyte was introduced through openings in the substrate before closing them by using a polymer. Dai et al. discuss the different processes involved in making glass-based Z-interconnected modules and current-collecting ones.<sup>929</sup> Tulloch discusses processing advantages and disadvantages of different module designs.<sup>926</sup> Pettersson et al. describe the manufacturing techniques for low-power monolithic mini-modules, demonstrating the possibility to introduce the electrolyte before closing the devices and thus reduce the device encapsulation to one process.<sup>915</sup>

#### 7.4. Discussion: Future Outlook for the Different DSC Module Designs

As described above, there are many different DSC module designs, substrates, and manufacturing combinations. According to us, it is still too early to identify a winning combination. Clearly, the monolithic concept offers a cost advantage because only one substrate is used. Likewise, the use of flexible substrates, polymers or metal foils, allow for

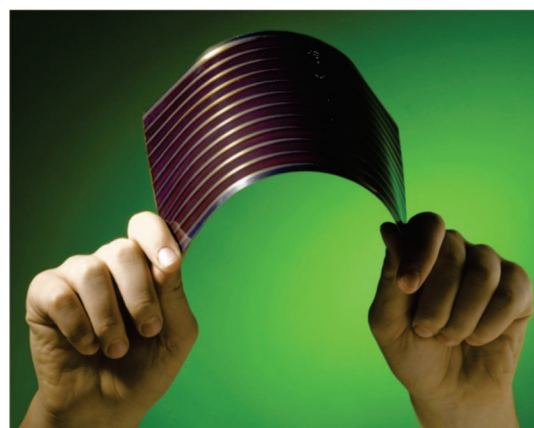


**Figure 27.** Sandwich Z-interconnected flexible DSC module. Reprinted with permission from G24i Innovations Ltd., UK.

rapid manufacturing using, for example, roll-to-toll processes. However, the highest module efficiencies have been obtained on glass-based sandwich modules. The performance of the described DSC module designs may be increased by improved device components, for example, TCO glass and dye, or closer packaging of cells, that is, less inactive area. The latter can, for the designs utilizing current collectors or interconnects, be obtained by using an inert combination of electrical conductor and electrolyte. Various companies have in the last years reported such DSC systems. Unfortunately, the DSC technology is not so trivial that the highest module efficiency, the fastest production methods, or the lowest materials cost necessarily provides the best module solution. The big challenge is to produce reliable devices that are long-term stable to fulfill the requirements of the designed application. It may thus be that a winning combination springs from the most functional encapsulation method.

Regarding stability of DSC modules, the conditions for accelerated testing have not yet been standardized. Until now, 1000 h light-soaking and 1000 h high-temperature storage tests have mainly been performed to compare materials and to show feasibility of the technology. As the technology advances, the outcome of accelerated testing will also be used to start calculating acceleration factors and estimating product life. Since this is not straightforward, intensified research and development to define the procedures for relevant accelerated testing of dye-sensitized solar devices is urgently required. Especially important is to collect outdoor test results from different locations and application-relevant conditions. The outcome needs to be related to results from accelerated testing to define the key tests for accelerated testing of DSC modules.

The DSC technology is in a stage where various pilot plants for module production are being built. As an example, G24i in Wales has initiated a commercial production of DSC modules using Z-interconnected devices with working electrodes on titanium foil and counter electrodes on a plastic substrate, Figure 27. Such initiatives will lead to technology leaps such as the creation of supplier chains and the development of methods for quality control of materials and processes. Many module manufacturers have already shown DSC demonstrators larger than 1 m<sup>2</sup>. Examples from the Institute of Plasma Physics in Hefei, 3GSolar, AISIN SEIKI and Toyota Central R&D, and Dyesol are shown in Figures 28–31. However, it seems like these devices always consisted of connecting many smaller devices up to the size 30 × 30 cm<sup>2</sup>. A remaining challenge for the DSC module



**Figure 28.** DSC demonstrator from the Institute of Plasma Physics. Reprinted with permission from the Institute of Plasma Physics, China.



**Figure 29.** DSC demonstrator from 3GSolar. Reprinted with permission from 3GSolar Ltd., Israel.

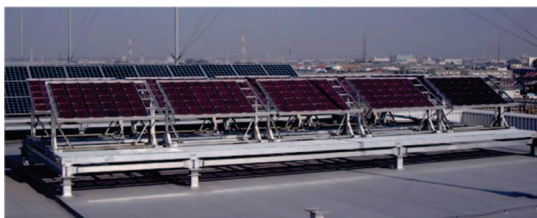


**Figure 30.** DSC demonstrator from AISIN SEIKI CO., LTD. and Toyota Central R&D Laboratories., Inc., Japan. Reprinted with permission from ref 916.



**Figure 31.** Building-integrated DSC demonstrator from Dyesol (Photo by Thomas Bloch). Copyright Dyesol Ltd. 2009, reprinted with permission.

technology is thus to scale-up the device size to production of square-meter-sized substrates.

## 8. Future Outlook

After more than 15 years of intense research, still the physical chemistry of several of the basic operations in the

DSC device remains far from fully understood. For specific model and reference systems and controlled conditions, there is a rather detailed description in terms of energetics and kinetics. It is, however, still not possible to predict accurately how a small change to the system, that is, replacing one component or changing the electrolyte composition, will affect the DSC performance. With time, the chemical complexity of DSCs has become clear, and the main challenge for future research is to understand and master this complexity in particular at the oxide/dye/electrolyte interface. Thus, for future research, it will be important to carefully select several reference systems that emphasize different key aspects of the device and characterize these systems in-depth with all the different techniques we have at hand. From comparisons and modeling, we may then find a better generality of our fundamental understanding.

A challenging but realizable goal for the present DSC technology is to achieve efficiencies above 15%. We know where the main losses in the state-of-the-art DSC device are, that is, the potential drop in the regeneration process and the recombination loss between electrons in the  $\text{TiO}_2$  and acceptor species in the electrolyte, reactions 3 and 6 in Figure 5. Decreasing the  $>0.6$  V of the potential drop to about 0.3 V would give efficiencies of 15%. The challenge is to develop dye–electrolyte systems that give efficient regeneration of the oxidized dye at a driving force of 0.2–0.4 V. Such systems must probably be combined with efficient blocking layers of the mesoporous oxide film and TCO substrate. The *potential* of dye-sensitized solar cells lies in the fact that components with better individual characteristics than the ones used in the state-of-the-art device have been developed. The *problem* is that it has not been possible yet to adapt these components to each other and optimize them to their full potential range in a complete DSC device. We can summarize our current lack of understanding in five fundamental questions for further research on DSC.

1. **What is the *injection* time required for high injection yields in a complete DSC?** The discrepancy between measurements of dye/oxide systems with ultrafast injection on the femtosecond time scale using normally transient absorption spectroscopy and the subnanosecond injection times measured on complete devices with the single photon counting method needs to be understood. The injection yield will depend on driving force for injection, electronic coupling between the chromophore and the oxide, and the number of accessible states to which to inject in the oxide. Knowledge on how energy levels of the excited state of the dye and the electronic states in the oxide depend on the interfacial environment, and how the excited state lifetime of the dye is affected, will be critical for detailed understanding of complete devices under relevant conditions.

2. **What is the mechanism of electron transport?** The electrons move in the mesoporous film between trap states. But is it through a lateral hopping between the traps or does it involve the conduction band? Does the mechanism depend on the type of semiconductor or the morphology of the nanostructure? What is the precise nature of the traps? How can we understand the nonideality observed, for example, in a simple measurement of the dependence of  $V_{oc}$  on light intensity? What factors define the diffusion length of the electrons in the mesoporous electrode and what methods should be used for accurate measurements? What are the influence of the ionic

strength in the electrolyte and the electrostatic screening of the electrons in the oxide by cations?

3. **What are the roles of the dyes for the recombination reaction of electrons with electrolyte species?** At first it is reasonable to assume that the dye layer blocks electrons in the metal oxide from reacting with acceptor species in the electrolyte. This is quite often the case, but lately the studies of O'Regan and co-workers have pointed out that some sensitizers facilitate the recombination reaction, probably through an association between the dye and "iodine" species in the electrolyte. These kinds of dye/electrolyte species interactions will be highly important to understand and will lead to design of dye/electrolyte structures that will improve the DSC performance by hopefully both decreasing the rate of recombination and increasing the rate of the regeneration of the oxidized dye.
4. **What is the minimum driving force needed for the regeneration of the oxidized dye to obtain high efficiencies and long-term stability?** Little attention has so far been paid to the detailed mechanisms of this process, which is one of the most central electron transfer processes for the overall DSC performance in terms of both efficiency and stability. It is a two-electron transfer process and involves intermediate species in the overall reaction of the oxidation of  $I^-$  to  $I_3^-$ . The energetics, kinetics, and chemical nature of the intermediate species remain to be determined, in particular at the oxide/dye/electrolyte interface. Ultimately, the question is: How much more photocurrent can we take out from the state-of-the-art DSC device by increasing the HOMO level of the dye without causing regeneration problems? And at what level are we forced to change the redox system to achieve higher efficiencies.

5. **What are relevant accelerated lifetime tests for DSC?** So far, the accelerated test procedures have been adapted from silicon solar cells. It is interesting to note that even in the research of silicon PV, there are discussions of how accurate the rather old standardized procedures are in determining acceleration factors and product life. Research and development to define the procedures for relevant accelerated testing of DSCs is thus urgently required.

The answers to these questions will lead to development of powerful design guidelines for the preparation of new material components with optimal structure/function relationships.

The DSC is more than a solar cell technology. We would like to finish this review by generalizing the impact of the DSC field for future chemical research with regards to developments of (i) third-generation solar cell technologies, (ii) optoelectronic devices based on functional molecular materials, and (iii) fundamental science of complex molecular systems (systems chemistry).

The *generalization* of DSCs as a photovoltaic technology is based on the notion that most of the development of third-generation PV systems will be based on nanotechnology, utilizing, for example, properties in the quantum-size domains. Hence, the nanoaspect of the DSC technology provides an interesting launching pad. The advantages of the DSC technology for fabrication of tandem devices were outlined in section 5.6. Moreover, the concept of a dye-sensitized nanostructured oxide film can be generalized into mesoscopic injection solar cells (MISC). With a mesoscopic electrode, we can utilize a very large internal surface area

for heterogeneous electron transfer reactions to produce electricity or even chemical fuels. Moreover, a mesoscopic electrode provides a simple way of contacting the electrode interface by an electrolyte. The sensitization of the mesoscopic electrode can be made by dye molecules, supramolecular complexes, or semiconductor quantum dots. A fundamental difference of MISC compared with conventional semiconductor solar cell technologies is also that we can control and play with the semiconductor/sensitizer/electrolyte interface, rather than the bulk, by designing and preparing well matched, energetically as well as kinetically, components that optimize the overall device performance.

The *generalization* of DSCs from a materials science point of view lies in the versatility of nanostructured and mesoporous materials, which can be surface modified for various properties and functions. Thus, different heterogeneous electron transfer processes can be amplified, controlled and monitored by external factors; light, electrical, chemical, etc. The DSC research field drives development of new materials such as nanostructured oxide particles and films, a large number of families of dyes, redox systems, ionic liquids, hole conductors, and efficient cathodes. For opto-electronic molecular devices, DSC has provided a material and device platform utilized in several applications, for example, displays,<sup>89,930</sup> batteries,<sup>90,91</sup> photoassisted electrocatalysis for organic synthesis,<sup>931</sup> mercury sensor,<sup>932</sup> biosensors,<sup>933</sup> and on-plate phosphopeptide enrichment.<sup>934,935</sup>

The *generalization* of DSCs from a basic scientific perspective is the understanding and handling of a complex chemical system. The DSC is a good example of a system where the function of the overall device is better than predicted from the sum of the properties of its components. The nanostructured  $TiO_2$  electrode does not conduct any electrical current; it is in itself a very good insulator. The conventional N3 dye dissolved in a dye solution degrades after a few hours under light. But when these are brought together in a well-working device, the solar cell conducts electrical currents up to  $20\text{ mA/cm}^2$ , and accelerated tests demonstrate that the dye will be stable for more than 15 years in outdoor solar irradiation. To use the language of complex systems, the sensitizer, oxide, and electrolyte species are the individual entities, and the photovoltaic function is the *emergent* property of the device. The continuous development of DSCs, either through clever design of new materials or by statistical trial-and-error approaches, may therefore be an example in the context of understanding and developing chemistry as an evolutionary science.<sup>936,937</sup>

## 9. Acknowledgments

This work was a cooperation within the Center for Molecular Devices, KTH, Stockholm, Sweden. We thank our colleagues within the Center for Molecular Devices for excellent collaborations and stimulating work. Dr. Elizabeth Gibson, Dr. Kazutero Nonomura, and Dr. Erik Johansson are gratefully acknowledged for collecting some of the materials for this review. We would like to thank Dr. Haining Tian for help with preparing the dye section of the manuscript. The herculean task to bring all the bits and pieces together has been wonderfully done by Ulrika Jansson. The Center for Molecular Devices is supported by the Swedish Energy Agency, Vinnova, the Swedish Research Council, Knut and Alice Wallenberg Foundation, BASF SE (Ludwigshafen, Germany), and The German Federal Ministry of Education and Research (BMBF, Berlin, Germany).























